THESIS REPORT
Master's Degree
Institute for Systems Research

Modeling and Analysis of the Grinding Process

by S. Ghosh
Advisor: G.M. Zhang

The Institute for Systems Research is supported by the National Science Foundation Engineering Research Center Program (NSFD CD 8803012), Industry and the University

M.S. 93-3

Abstract

Title of Thesis:	Modeling and Analysis of the Grinding Process
Name of degree candidate:	Shuvanker Ghosh
Degree and Year:	Master of Science, 1993
Thesis directed by:	Dr. Guangming Zhang, Assistant Professor, Department of Mechanical Engineering, and Institute for Systems Research

Product quality assurance is a very important concern in industries these days. Surface quality is an important constituent of the overall product quality. Although the desired surface quality of a product is dependent on the functional requirements of the product, the actual surface quality of the finished product depends mainly on the chosen manufacturing processes. In the case of machining, it depends mostly on the finishing process. One of the commonly used finishing processes is grinding. And therefore, it is important to understand the surface quality produced during a grinding process.

In grinding, surface quality depends on the grain geometry, the kinematics of the grinding process and the dynamics of the grinding system. In this thesis work, a grinding model is formulated taking the random wheel topography into consideration. An analytical representation of the ideal ground surface is developed.

To include the effect of grinding wheel vibration on ground surface topography generation, a grinding force model and a mathematical model representing the grinding system are developed.

The above three models are implemented in a simulation package which can predict the behaviour of the surface grinding process. With the help of this package, surfaces ground at different cutting conditions can be compared quantitatively and qualitatively. The simulation package facilitates the selection of a proper grinding wheel and cutting conditions to achieve the desired surface quality.

MODELING AND ANALYSIS OF THE GRINDING PROCESS

by

Shuvanker Ghosh

Thesis submitted to the Faculty of the Graduate School
of The University of Maryland in partial fulfillment
of the requirements for the degree of
Master of Science
1993

Advisory Committee:

Assistant Professor Guangming Zhang, Chairman/Advisor
Professor Patrick F. Cunniff
Associate Professor Dana S. Nau

Dedication

To My Parents

Acknowledgments

First, I want to thank Prof. Guangming Zhang for his constant guidance and advice during my graduate studies and thesis work. I also sincerely thank Prof. P. F. Cunniff and Prof. Dana S. Nau for serving on the committee and for their valuable comments.

I would like to acknowledge Graduate School, Department of Mechanical Engineering and Institute for Systems Research for providing me continuous financial support during my graduate studies and research.

I also want to acknowledge Stone Industrial, College Park and in particular, Mr. Venkatesh Ketty for helping me in performing the grinding experiments for this work. I want to thank Mr. J. F. Song of the Precision Engineering Division at the National Institute of Standards and Technology, Gaithersburg, MD for helping me in taking the surface roughness measurements. I also appreciate the help provided by Mr. Myron E. Taylor Jr. and Helaleh Maghsoudlou of Central Facility for Microanalysis in taking SEM pictures. I would also like to acknowledge Dr. Tsuwei Hwang, G. Raju Khanchustambham, Rajesh Ratnakar, K. G. Satish, Don L. DeVoe, Goutam Chatterjee and R. Jayant for their valuable support and suggestions during my thesis work. Finally, I want to thank my apartment mates Debanjan Saha, Pravin Bhagwat, Satyandra K. Gupta and Shailendra Verma and my friends Sarit Mukherjee and Praveen Kamath for their continuous support and assistance without which it would have been impossible to complete my thesis work.

Contents

List of Tables

List of Figures

Chapter 1

Introduction

1.1 Background

Grinding is a common manufacturing process that utilizes abrasive particles as cutting medium. It is a commonly used abrasive machining process. In fact, removal of metal utilizing abrasive action is an ancient practice. Prehistoric man found that he could sharpen his tools by rubbing against the rocks. Also there are a plenty of abrasive phenomena occurring very often in nature. A typical example would be sand on a riverbed that is formed by abrasive action of water and rocks. During the twentieth century grinding has developed as a rapid, efficient and accurate process of metal removal. Now-a-days, grinding is one of the widely used manufacturing processes.

Grinding process uses a grinding wheel fabricated by cementing abrasive particles with a suitable bonding agent similar to natural sandstone - prehistoric

man's abrasive tool - which contains grains of sand in silicate bond matrix. The abrasive grains on the grinding wheel act as cutting tools. In the grinding process the rotating grinding wheel is brought into contact with the surface of the workpiece. And as each abrasive grain on the periphery of the wheel contacts the workpiece, it removes a tiny chip of metal as depicted in Fig. 1.1 .

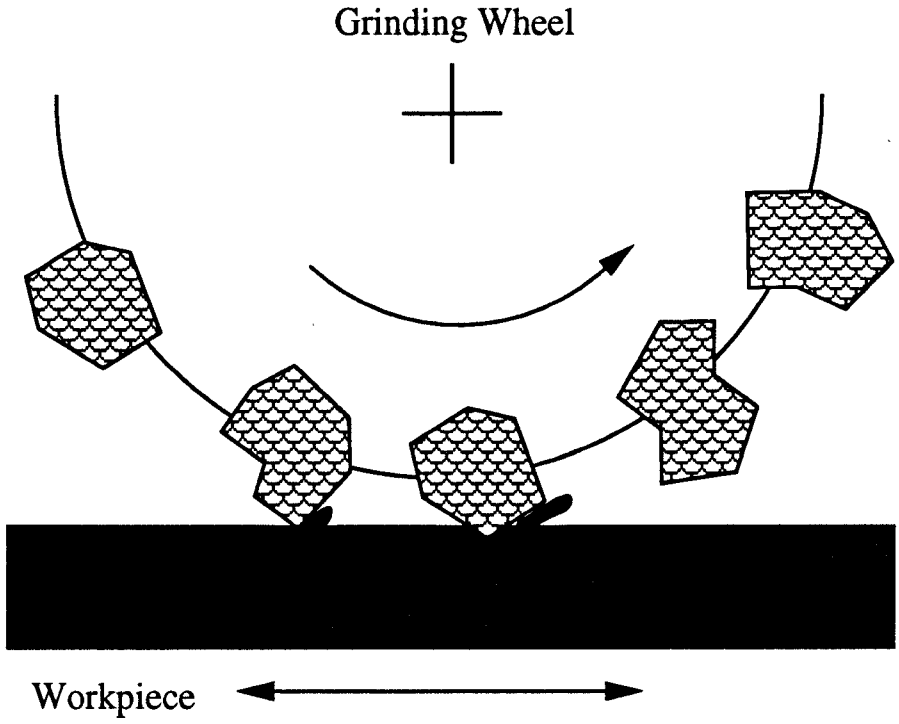

Figure 1.1: The Cutting Action of the Abrasive Grains

A grinding process differs from other traditional machining processes with respect to cutting tools. Unlike other traditional machining processes the grinding process uses tens, hundreds or more of abrasive grains removing material simultaneously. There are various types of grinding operations which vary depending on the shape of the surface to be machined and on the kinematics of the workpiece and the grinding wheel motions. On the basis of the shape of the surface

to be machined, the grinding process can be classified as:

- *Surface Grinding,* for producing flat surfaces.
- *Cylindrical Grinding,* for machining cylindrical workpieces with internal and external cylindrical surfaces.

Cylindrical grinding is further subdivided in two subclasses, namely, *Centertype* and *Centerless* cylindrical grinding. The subdivision is based on the supporting mechanism to hold the workpiece. In centertype cylindrical grinding the workpiece is supported between the centers or in a chuck or fixture. In centerless cylindrical grinding a regulating wheel guides the workpiece motion against the rotating grinding wheel. On the basis of the number of kinematic motions, the grinding process can be classified as :

- *Plunge Grinding :* It has two kinematic motions - rotation of the grinding wheel and the table speed in the case of surface grinding and rotations of the grinding wheel and the workpiece in the case of cylindrical grinding.
- *Traverse Grinding :* It has an additional kinematic motion - crossfeed, which is relative motion of the grinding wheel and the workpiece in the direction perpendicular to the plane of the wheel rotation.

Some of the common grinding processes for machining flat and cylindrical surfaces are illustrated in Fig. 1.2 .

Among the various traditional machining processes the grinding process is commonly regarded as a finishing machining process because it can provide

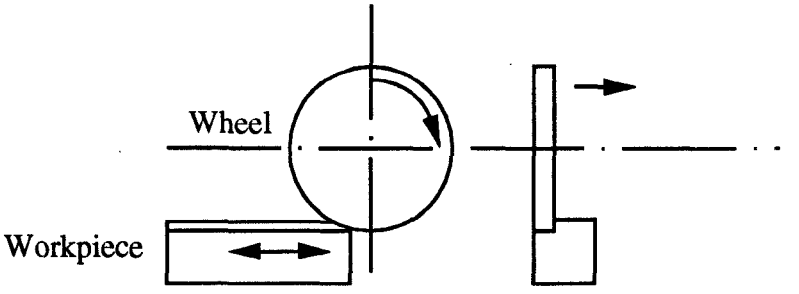

a) Surface Grinder- Traverse Grinding

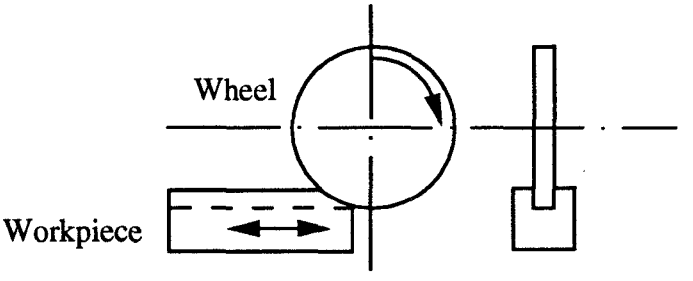

b) Surface Grinder- Plunge Grinding

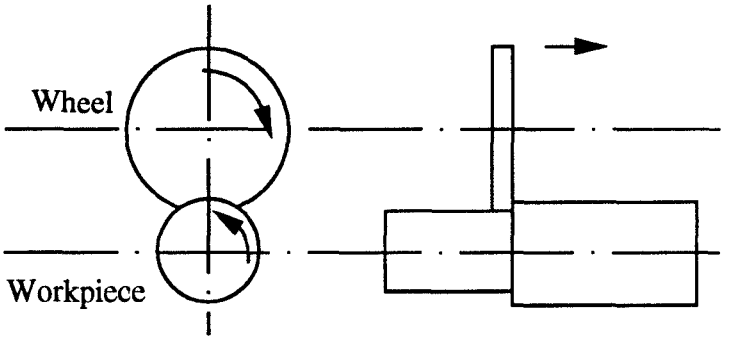

c) Cylindrical Grinder - Traverse Grinding (Centertype)

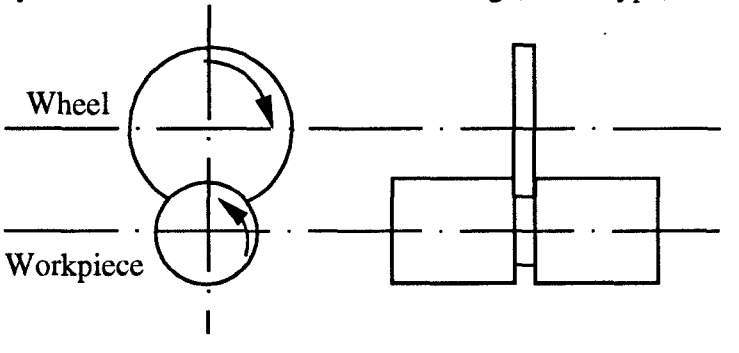

d) Cylindrical Grinder - Plunge Grinding (Centertype)

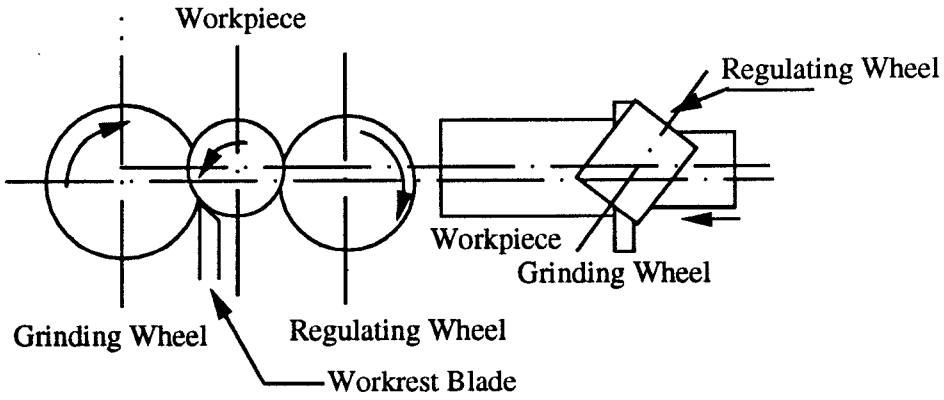

e) Cylindrical Grinder - Traverse Grinding (Centerless)

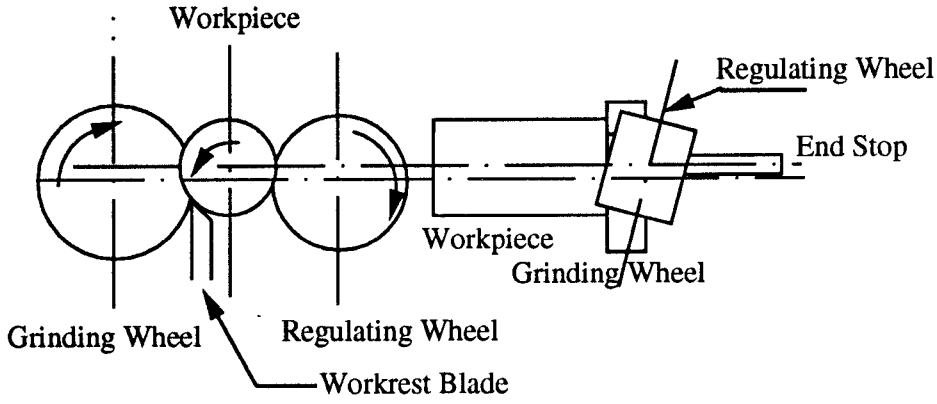

f) Cylindrical Grinder - Plunge Grinding (Centerless)

Figure 1.2: Schematic Illustration of Some of the Grinding Processes

smooth surfaces with fine tolerances. It is also extensively used for high precision machining. Now-a-days grinding is not limited to metal machining. In recent years the grinding process has been used to machine superalloys and extremely hard and brittle materials. Components like cutting tools and roller bearing rings made of hardened steel are produced by grinding processes. Machining of non-metallic brittle materials including ceramics, cemented carbides is exclusively done by the grinding process. Unlike metal machining where grinding is predominantly performed as a finishing operation, in machining of ceramics and superalloys the grinding process is the only effective machining process which can be performed with comparable ease.

1.2 Literature Review

In the past few decades, there has been an increase in research on grinding due to its ever increasing application in manufacturing industry. Also the complexity of the grinding process demands more and more attention to understand the grinding process better. In this section relevant research work done on grinding is reviewed. The review covers three areas in grinding, namely, ground surface topography generation, modeling of the grinding system and dynamic analysis of the grinding process.

In the past, several statistical models have been developed to account for the random behaviour of the grinding process. In a simple random model built by

Baul [1], the emphasis was placed on grit heights and on spacing between the grits along the wheel periphery. The peaks or asperities of the grinding wheel surface was represented by rods of varying height. The effect of variation in spacing between successive grits along the periphery was not taken into account in the model. The individual grit geometry was also neglected. In another model postulated by Yoshikawa [2], random numbers were used to determine the coordinates of the locations of the grains on the grinding wheel. A Monte Carlo simulation of the grinding process was conducted assuming a three dimensional - axial, peripheral and radial - distribution of the grain positions. McAdams [3] analyzed the profiles of abrasive surface of the grinding wheel by means of Markov chain theory. The Chapman-Kolmogorov equations together with recurrent event theory were used to deduce theoretical distributions for spacing between the active cutting points and the lengths of lands on a worn grinding surface . The profile heights were measured at intervals δx along the wheel periphery and values 1 or 0 were assigned accordingly as heights exceed or fail to exceed some fixed height. Thus the grinding wheel profile was regarded as a two state Markov chain. The entries of the transition matrix provided an approximation of the quantities like the spacing between the successive cutting points and the lengths of lands which develop on the grinding surface as a result of grinding wheel wear. In the model develop by Wu *et al* [4, 5], the geometry of the abrasive grains was taken into account. First a grinding model was postulated based on prior information about the grain distributions on the abrasive wheel and

kinematic conditions of the grinding process. Positions of the grit tips were described by a suitable coordinate system. There were two main parameters in the model - one describing the distribution of grit heights and another was tangent of semi-apex angle of the grits. Knowing these parameters, the transverse workpiece profiles were simulated assuming that the workpiece and the grinding wheel interact according to geometrical relationship only. The sample spectrum corresponding to the simulated workpiece profile was calculated. The sample spectrum for experimentally produced workpiece profile was also calculated. A computation of the sum of squares of the differences between the experimental and predicted spectral estimates was made. The process was repeated with appropriate modification of the two parameters until minimum sum of the squares was obtained, yielding the least square estimates of the two parameters. The grinding wheel was then characterized by its diameter, nominal grain size, a three dimensional distribution of the grain positions and grain semi-apex angle determined as mentioned above. The model was limited to single-pass surface grinding without crossfeed.

The pioneering work in the area of dynamic modeling of grinding system was done by Hahn [6] and Bartalucci *et al* [7]. Hahn [6] discussed the phenomenon of regenerative chatter in grinding. Regeneration effect due to the workpiece was only taken into consideration assuming the grinding wheel to be infinitely wear resistant. An analysis was made, based on the proportionality of the instantaneous wheel depth of cut to the instantaneous dynamic force existing between

the wheel and the workpiece , which yields two stability criteria from the Nyquist diagram. He found out that the grinding system will be unconditionally stable if the first stability criteria is satisfied. If this criteria is not satisfied, a second criteria for conditional stability may yet be satisfied by proper adjustment of the cycles of vibration per revolution of the workpiece. Bartalucci [7] considered the regeneration due to the workpiece and the grinding wheel both. The grinding wheel wear is the major cause of the regeneration effect due to the grinding wheel. Later on, Thompson [8] studied the conditional stability of the grinding process. The results of this analysis were presented in form of stability charts in terms of grinding wheel speed and the workpiece speed in the case of cylindrical grinding. Thompson [9] also studied the dynamic behaviour of the surface grinding process. The main feature of the model was that it took into account the reversing action of the workpiece, typical to surface grinding.

1.3 Scope of the Thesis

Surface quality is an ever increasing concern in industries now-a-days. Every industry cares to produce products with supposedly better surface finish. Of course, the importance of the surface quality of a product depends on its functional requirements. Prediction of the quality of the surface produced by a manufacturing process requires a deep understanding of the process itself and the various physical phenomena occurring during the manufacturing process.

Surface quality has two aspects. The first aspect is *Surface Topography* or *Surface Texture*. Surface topography describes the deviation of the surface from the intended nominal shape. It is associated with the fine irregularities and the 'lay' which refers to the dominant pattern of the texture on the surface produced by a machining process. The surface topography consists of two components, namely, *surface roughness and surface waviness*. Surface roughness consists of finer irregularities characteristic of the machining process itself like grit size of the grinding wheel or feed and tool shape in turning. Surface waviness are also fine irregularities but more widely spaced than the surface roughness. The major cause of the surface waviness is the machine tool vibration. Surface topography, surface texture and surface roughness are used interchangeably by the engineers.

The second aspect of surface quality is *Surface Integrity*. Surface integrity describes the mechanical and metallurgical alteration in surface and sub-surface layers. Surface integrity includes surface and sub-surface characteristics like cracks, residual stress, plastic deformation etc. For example, in grinding the surface integrity is associated with thermal damage caused by excessive grinding temperature.

As mentioned earlier, grinding is mainly used as a finishing process in metal machining. Hence, the surface quality obtained by the grinding process is more important than that obtained by any other conventional machining process.

Surface finish and tolerance are closely related. A finer tolerance on a component demands a smoother surface and lesser surface roughness. Mainly the

finishing process affects the surface quality and hence, achieving the imposed tolerance depends on the finishing process. And since, the grinding process is usually used as the finishing process in metal machining, it is absolutely necessary to study and understand the surface quality produced during a grinding process.

In industries, tolerance is decided during the design stage of a component depending upon its application. The required tolerance limits the maximum allowable roughness which in turn decides the machining process to be used to produce the component. The proper selection of a machining process in order to achieve the specified tolerance requires a large interaction between the design and the manufacturing departments in an industry. In recent years there has been an increase in the level of interaction between the two departments in industries. This new philosophy of having intensive interaction between the design and the manufacturing departments throughout the evolution process of a new component is called Design for Manufacturability. For the success of this new philosophy, it is necessary to predict the behaviour of the manufacturing process *a priori*. A specific example is to predict the surface quality in order to select a machining process to achieve the desired tolerance.

Therefore, in order to select a machining process which can provide the desired tolerance, some kind of tool is necessary to predict the surface quality produced during various machining processes. One such tool can be simulation packages to predict the surface topography generated during various machining processes.

For this reason it is necessary to develop a simulation program to predict the surface topography generated during the grinding process - the most common finishing process in metal machining.

And therefore, the ultimate objective of this thesis work is to understand the fundamentals behind the ground surface topography generation and to develop a simulation program for predicting the ground surface topography. To develop such a simulation program, following methodology is used :

1. Formulate a grinding model.

2. Develop a grinding force model.

3. Develop a mathematical model representing the grinding system.

Using these three models ideal ground surface topography and ground surface topography in the presence of machine tool chatter are generated. The results of this research work are presented in the form of three dimensional plots of the ground surface topography. Also, values of various surface characterization parameters like R_a, R_q and PTV are presented. The aforementioned surface characterization parameters are defined in Section 3.2.2 in Chapter 3.

In Section 1.1 various grinding processes are described. For this thesis work Traverse Surface Grinding Process is chosen for investigation. For the purpose of simulating the surface topography the cylindrical grinding process can be treated as a surface grinding process where the length of the workpiece in surface grinding will be the circumference of the workpiece in cylindrical grinding. And also, the

surface speed of the workpiece in cylindrical grinding can be treated as the table speed in surface grinding. As far as plunge grinding is concerned it is a special case of traverse grinding with no crossfeed. In brief, by using the simulation package developed to predict the ground surface topography based on the traverse surface grinding process, the surface topography generated during majority of the grinding processes can be predicted fairly well. The chosen grinding process is depicted in Fig. 1.3 .

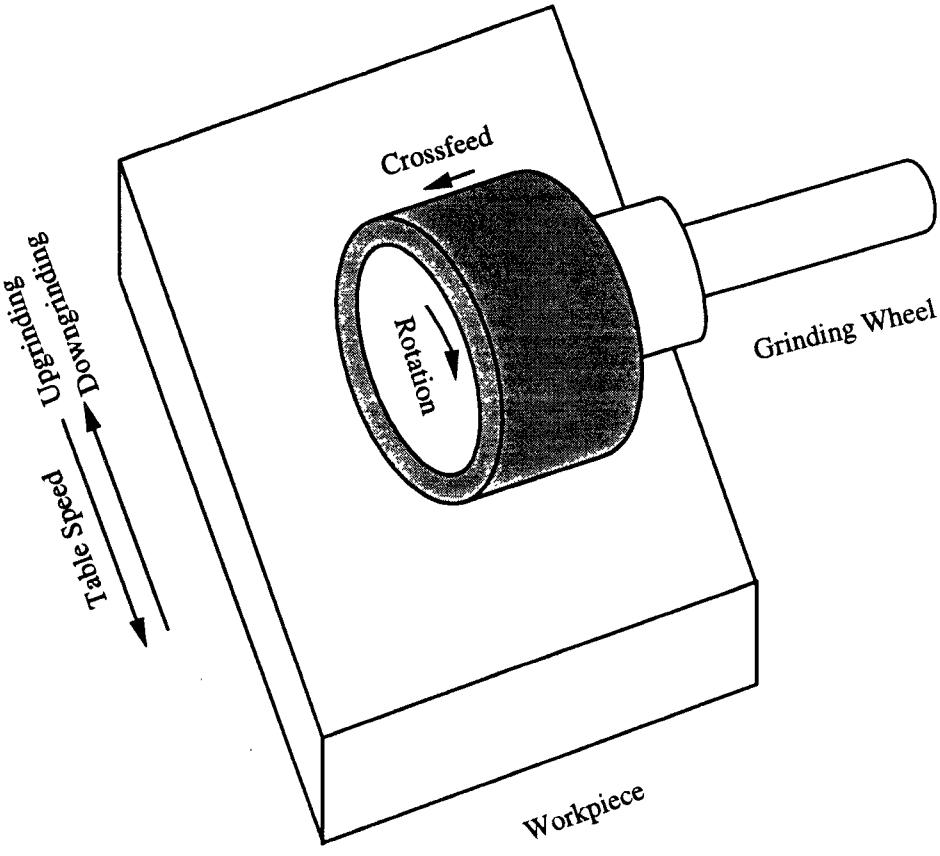

Figure 1.3: Traverse Surface Grinding Process

1.4 Outline of the Thesis

There are eight chapters in this thesis. Chapter 1 provides a brief introduction on the grinding process. In this chapter previous research work on the grinding process is reviewed. The review is mainly focused on ground surface topography generation, dynamic models for the grinding machining system and mechanics of the grinding processes such as grinding force models. The main objective of this work is also highlighted in this chapter.

In Chapter 2 fundamentals of grinding are briefly covered. Various important features of the grinding wheel and the grinding process are discussed in this chapter.

The methodology to simulate the surface topography generated during the grinding process consists of two major parts. First, a grinding model is developed to describe the ideal ground surface topography. The model describing the ideal surface topography is totally based on the geometry of the process such as grit sizes and grit location and on kinematic motions of the process such as rotation of the grinding wheel, table speed, crossfeed and downfeed. In Chapter 3 the grinding model predicting the ideal ground surface topography is formulated. Flow charts describing the simulation details are also listed.

Secondly, the effect of the grinding wheel vibration is superimposed on the ideal ground surface topography in order to get a more realistic picture of the surface topography generated during the grinding process. In order to determine

the effect of the grinding wheel vibration on the surface topography, a dynamic model for the grinding machining system and a grinding force model are required. The mathematical model estimating the grinding forces is formulated in Chapter 4. The mathematical model representing the grinding system is developed in Chapter 5.

These three models are then integrated in a simulation program to predict the surface topography generated during a grinding process in the presence of grinding wheel vibration. The simulation details regarding the generation of ground surface topography in the presence of the machine tool chatter are discussed in Chapter 6.

Experiments are carried out to verify the simulation results. In Chapter 7, experimental work performed in this thesis work is presented. Experimental arrangements are illustrated and experimental results are discussed and analyzed. A comparison between simulation and experimental results is made in this chapter.

In Chapter 8, conclusions of this thesis work are listed. Results of this thesis work are briefly summarized. Also, a few recommendations are made for future work in this area.

Chapter 2

Fundamentals of Grinding

In this chapter, some important issues of the grinding process are discussed. A brief discussion on grinding wheel components is presented. Standard marking systems for various kinds of grinding wheel are illustrated. The usual procedure followed to mount the grinding wheel on the machine tool structure is briefly explained. The two commonly used operations for grinding wheel preparation, namely, truing and dressing are discussed in this chapter. And in the last section of this chapter, the importance of grinding fluid is briefly explained.

2.1 Grinding Wheel Components

Grinding wheel is composed of two components, namely, abrasive grains and bonding materials. Abrasive grains on the grinding wheel act as cutting tools. There are two broad classifications of abrasives.

- Natural abrasive
- Artificial abrasive

Natural abrasives are those abrasives which have been produced by uncontrolled forces of nature. The most common natural abrasives are emery, corundum, crocus, quart, sandstone and diamond. Since natural abrasives are produced by uncontrolled forces of the nature, they contain varying amount of impurities and differ in quality too. The uncertainty in the quality of a natural abrasive resists its use in grinding.

Virtually, all the abrasive grains used in recent days are man-made. These artificial abrasives are synthesized by a variety of controlled industrial processes and hence have well defined shapes and sizes. There are four main types of man-made abrasives - Aluminium Oxide, Silicon Carbide, Cubic Boron Nitride(CBN) and Synthetic Diamond. Synthetic diamond is the hardest of all. But, aluminium oxide is the most commonly used to machine a vast array of materials from difficult to machine superalloys to high alloy steels and mild steel. There are certain properties which an abrasive must possess, namely, hardness, heat resistance, toughness and friability. Although toughness and friability are two opposing properties, but both of them are necessary for proper functioning. Friability helps in dressing. High toughness helps in resisting impact and pressure created during grinding there by decreasing the wheel usage. A tough but not friable abrasive gets dull but doesn't break away easily. In contrary, a friable but not tough grain will crack and fracture very rapidly increasing wheel usage.

Abrasives grains on a grinding wheel are held together by a bond. A standard grinding wheel uses one of the following bonds : vitrified(V), resinoid(B), rubber(R), shellac(E), silicate(S) and oxychloride(O).

There are two very important characteristics of a grinding wheel which greatly affect the performance of the grinding wheel. They are grade and structure. Grade quantifies the strength with which bond holds the abrasive grains together. It refers to hardness of the grinding wheel. The grade of a grinding wheel is indicated by letters ranging from 'A' (the weakest bond) to 'Z' (the strongest bond). The structure of a grinding wheel refers to the density of the abrasive grains on the grinding wheel. The structure quantifies the voids on a grinding wheel. These voids are necessary for chip disposal while grinding.

A grinding wheel is specified by a well accepted standard. Typical examples of the standard specification are illustrated in Tables 2.1 and 2.2 .

2.2 Grinding Wheel Mounting

The handling and mounting of grinding wheel have to be carried out with utmost care and attention to ensure safe and efficient operation. Carelessness in either handling or mounting can result in wheel breaking, damage to machine tool and workpiece and possibly a serious injury to the operator. Prior to mounting, it is therefore essential to inspect and ring test the wheel to ensure that the wheel hasn't been fractured during shipping and handling. Once the ring test is done

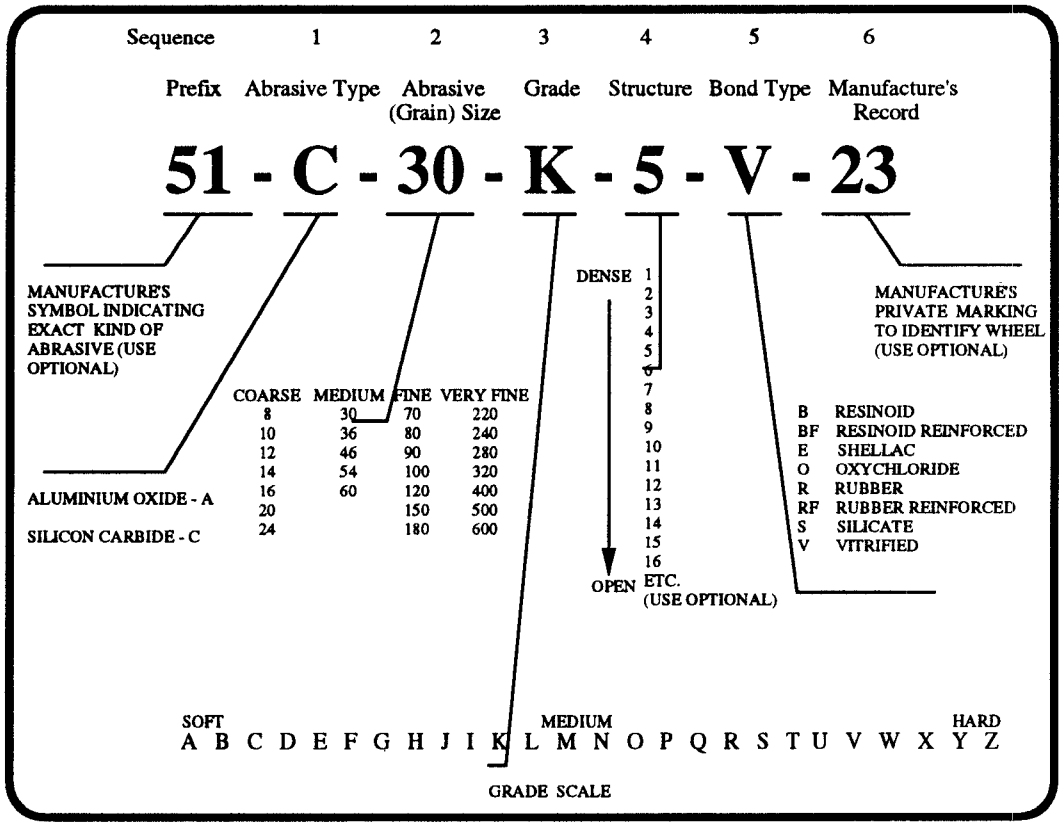

Table 2.1: Marking System for Aluminium Oxide and Silicon Carbide Wheel

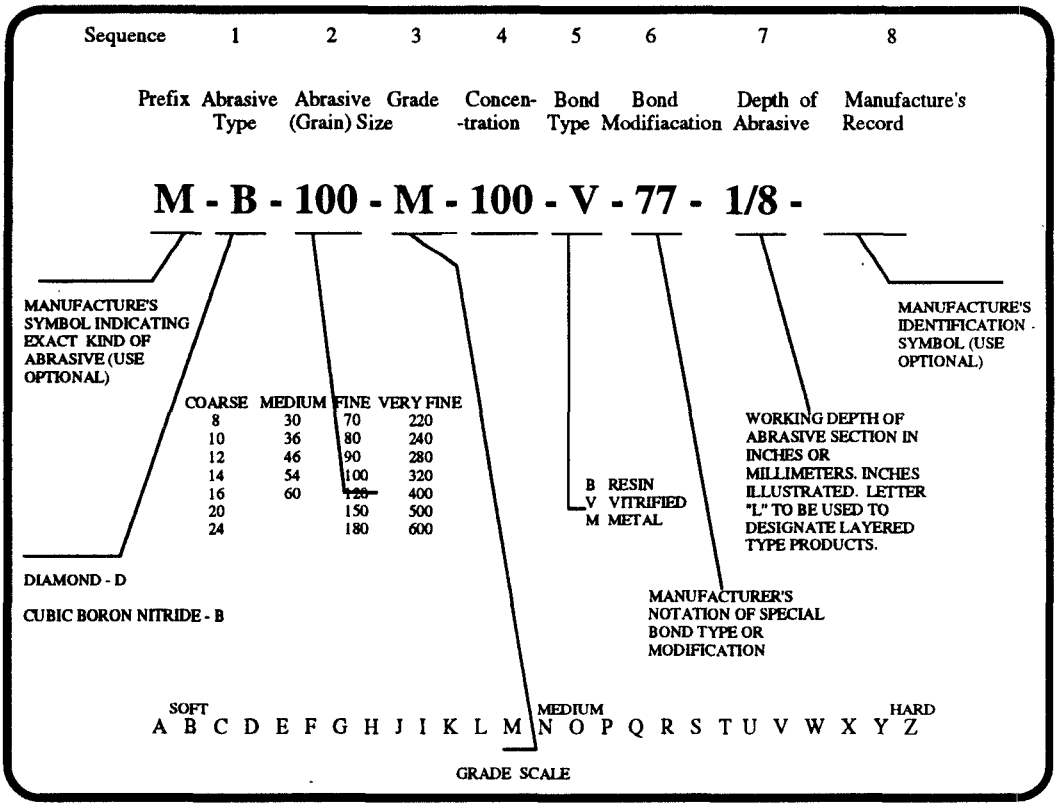

Table 2.2: Marking System for Diamond and Cubic Boron Nitride Wheel

and the wheel is inspected properly, the wheel is ready for mounting on the spindle.

There are two common types of grinder spindles on which the grinding wheel is mounted. They are *Straight Spindle* and *Tapered Spindle.* Sectional views of these two types of grinder spindles are shown in Figs. 2.1 and 2.2 . The straight spindle has a shoulder at one end against which a recessed flange is shrunk or keyed. The grinding wheel, which should easily slip on the spindle, is held in position by another flange and nut on the opposite end. Grinding wheels having small holes are generally mounted on a straight spindle. Wheel bolters made of paper or plastic are fitted between the grinding wheel and each flange to prevent the metal flanges from breaking into the sides of the grinding wheel and initiating a crack. The tapered spindle has a tapered section to fit the tapered wheel collet adapter and a threaded section with a nut at the other end for locking the adapter on the spindle. The grinding wheel is first mounted on the adapter and then the entire assembly is mounted on the grinder spindle. The adapter is generally used for mounting wheels with large holes such as those used on some cylindrical grinders and certain surface grinders. The adapters vary in design to accommodate various wheel and grinding factors. Their flanges are designed for the following:

- Various size grinding wheels.
- Dry or flood grinding applications.

- Through-the-wheel coolant.

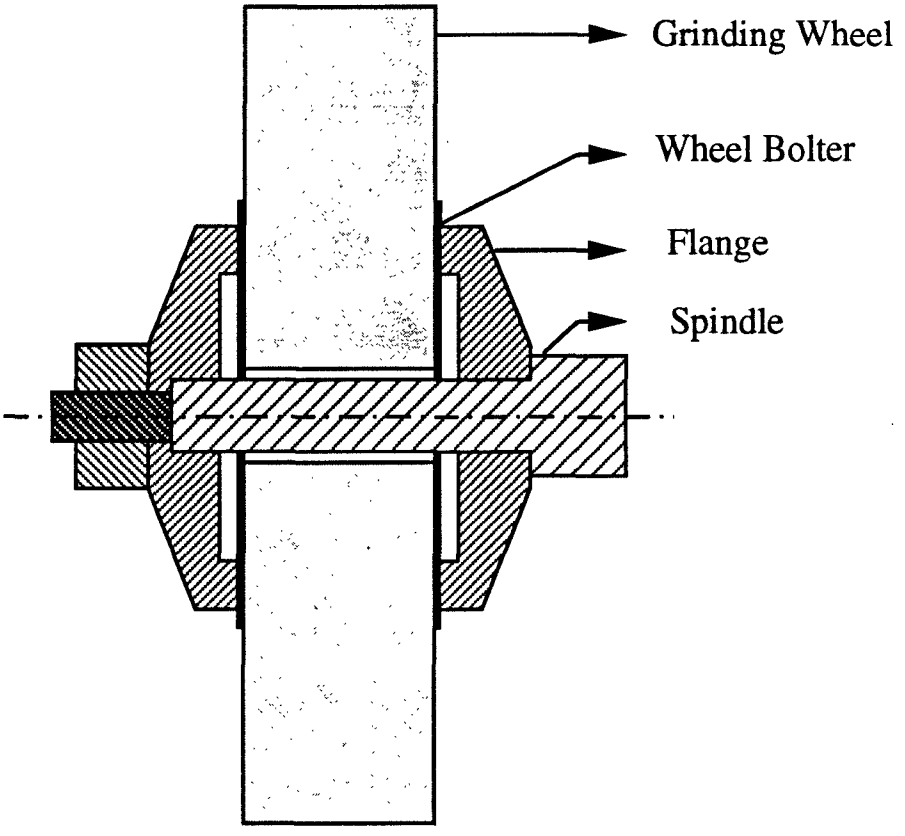

Figure 2.1: Sectional View of a Straight Grinder Spindle

Prior to use, a grinding wheel must be balanced to produce fine surface finishes, maintain close tolerances and avoid excessive wheel and bearing wear. Unbalanced wheels results in grinding wheel vibration which nullifies the advantages of proper wheel selection and a well maintained machine. Although the grinding wheels are balanced at the place of manufacture before shipping, it is usually necessary to balance them for the machine on which they are used because of the slight clearance between the grinding wheel and the wheel collet. Smaller wheels usually require little or no balancing, while larger wheels require

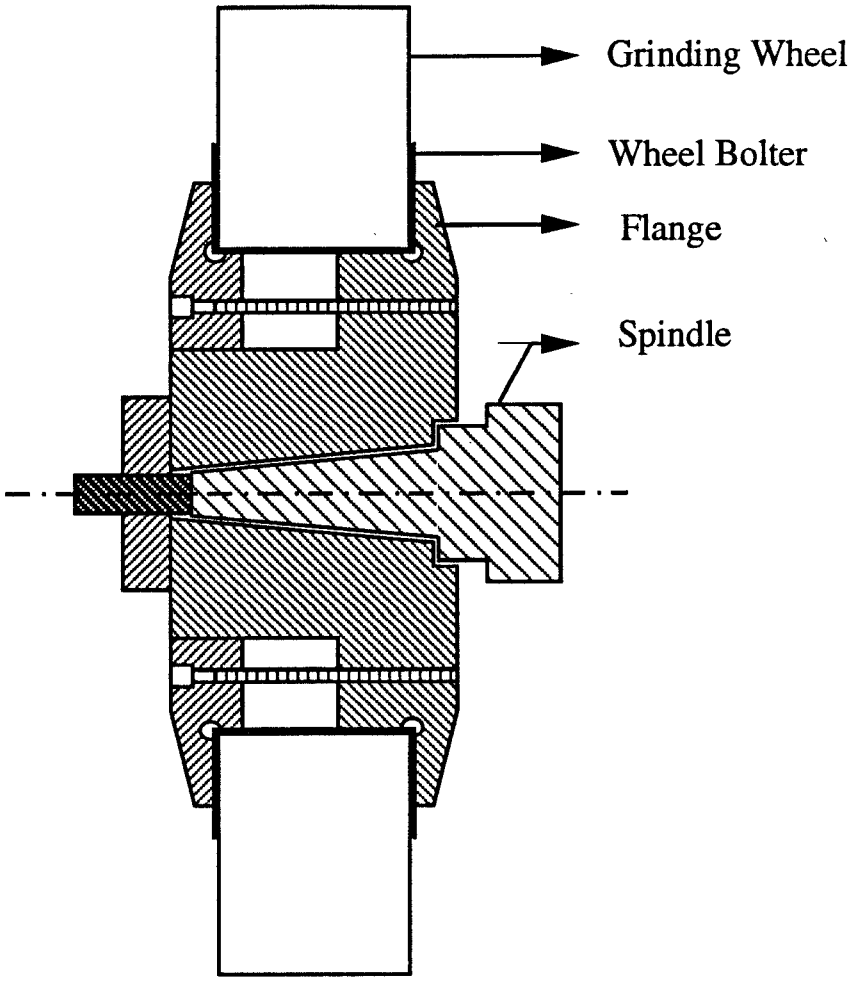

Figure 2.2: Sectional View of a Tapered Grinder Spindle

balancing frequently during their grinding life. Both static and dynamic methods are used to do balancing of the grinding wheels.

2.3 Grinding Wheel Preparation

For any grinding wheel to be fully effective, its grinding surface must be maintained at peak efficiency to maximize metal removal rate and still produce a satisfactory surface finish. Preparing the wheel prior to grinding or periodically

during the course of grinding is essential to obtain high production rates, maintain accurate size and form, and produce the desired surface finish. Wheel preparation generally includes truing and dressing. Truing usually refers to removal of material from the cutting surface of a grinding wheel so that the spinning wheels runs true with minimum run-out from its microscopic shape. Truing also includes profiling the wheel to a particular shape. Dressing is the process of conditioning the wheel surface so as to achieve a certain grinding behavior. During normal grinding action the sharp edges of the abrasive grains become worn and sometimes metal particles from the workpiece embed themselves in the wheel. Dressing removes the dulled grains and/or particles of metal embedded in the wheel. It restores the wheel face to maximum efficiency by exposing new sharp grains. The grinding surface of a wheel should be kept in good condition and dressed when any of the following occur.

- The wheel leaves load lines in the workpiece caused by metal particles in the wheel.
- Chatter lines appear on the work surface.
- The wheel undergoes excessive vibration when it is in contact with the workpiece.
- Excessive heat is generated during the grinding process.
- Black or brown burn marks appear on the work surface.

A variety of dressing methods are used to dress the grinding wheel. The type of dressing method employed depends on the desired surface quality of the ground surface. The most common types of grinding wheel dressers are hand dressers, abrasive wheel dressers, diamond dressers and crushing rolls.

2.4 Grinding Fluids

Like any other machining processes, grinding(cutting) fluid also aids in cooling, lubricating and cleaning. In a grinding process, enormous amount of heat is produced and hence cooling is the primary objective of using grinding fluids. The cutting fluid assists in dissipation of the grinding energy and thereby reduces the grinding temperature. There are three main types of grinding fluids - water soluble chemical, water soluble oils and straight oil fluids. The choice of grinding fluid depends on the workpiece material, the metal removal rate and the desired surface quality. There are three main ways of applying the grinding fluids - the flood system, the through-the-wheel-system and the mist cooling. The flood system is most widely used on shop floors. In the through-the-wheel system, the grinding fluid is discharged into a recess on the side of each wheel flange. Centrifugal force carries the fluid from these recesses through a series of holes to the wheel center and then through the porous wheel to its periphery and to the wheel-workpiece contact region. The mist cooling system uses the atomizer principle.

Chapter 3

Ideal Surface Topography Generation

3.1 Introduction

The necessity of predicting the ground surface topography has been discussed in Chapter 1. Research has been done in previous years to analyze the surface topography generated during various machining processes in general and during a grinding process in particular. For the machining processes with well defined tool geometry such as turning and milling, the analysis of the ideal surface topography is deterministic in nature. The ideal topography depends on the tool geometry and the kinematic motions of the process. The actual surface topography includes the effect of tool wear, build-up edge phenomenon, machine tool vibrations and other physical phenomena taking place during machining.

The ideal surface topography generated during a grinding process is difficult to model owing to random undefined topography of the grinding wheel surface and the individual grits - the cutting points. In the past, simplifying assumptions were introduced to model the ideal ground surface topography in the longitudinal direction - the grinding direction. An ideal wheel was considered with equal spacings between the two consecutive grits along the grinding wheel periphery and each grit protruding to the same height radially. The model was modified by assuming that grits protrude to varying heights radially. The variation of spacings between consecutive grits along the wheel periphery was also considered in the subsequent models developed [18]. To generate ideal surface topography along the transverse direction - across the grinding direction, a simple model was developed considering equal spacings between two neighbouring grits along the axial direction and each grit protruding to the same height [12]. The variation of radial heights of the grits was also taken into account in a subsequent analysis [12].

The grinding model developed in this thesis work to simulate the ground surface topography generation is described in this chapter. Simulation details are described mainly in the form of flow charts.

3.2 Formulation of the Grinding Model

The grinding process is inherently random in nature. At different instants, different sets of grits with varying individual geometry remove material from the workpiece. To consider the random behaviour of the grinding process one has to resort to statistical techniques.

A physical system can be represented by either a mechanistic model or empirical model or both. A mechanistic model is developed when the behaviour of the process is extensively known. An empirical representation is required when very little is known about a process. Both approaches can be integrated when the behaviour of the process is partially known. Due to the inherent random nature of the grinding process, it is difficult to develop a purely mechanistic model for the grinding process. An integrated approach is used to formulate the grinding process model.

3.2.1 Assumptions

The following assumptions are made to postulate a grinding process model in order to predict the surface topography generated during a traverse surface grinding process.

- The abrasive grains or the grits are cone shaped or cone like shaped. There are two basic grit shapes. Grits are either like an ordinary cone with a sharp tip or like a cone with rounded tip as shown in Fig. 3.1 . The cone

shaped grit with a sharp tip will be called type 1 grit from now onwards and the cone shaped grit with rounded tip will be called type 2 grit. These two type of grits are distributed uniformly on the grinding wheel surface.

- The grinding wheel is divided into a number of thinner discs called slices as shown in Fig. 3.2 .
- The number of grits on each slice follows a normal distribution.
- The angular spacings between two consecutive grits along a slice follow a normal distribution.
- The diameter of the grits also follows a normal distribution.
- The radial heights of the grits also follow a normal distribution.

Statistical models have been successfully used over the years to describe many naturally occurring phenomena. Both normal and uniform distributions have been used to represent these phenomena. Hence these two theoretical distributions are chosen to represent the variation of various physical quantities in the grinding process as discussed above. Fig. 3.12 at the end of this chapter validates the assumption that the abrasive grains are randomly located on the grinding wheel surface and Fig. 3.13 validates the assumption that the abrasive grains are cone shaped.

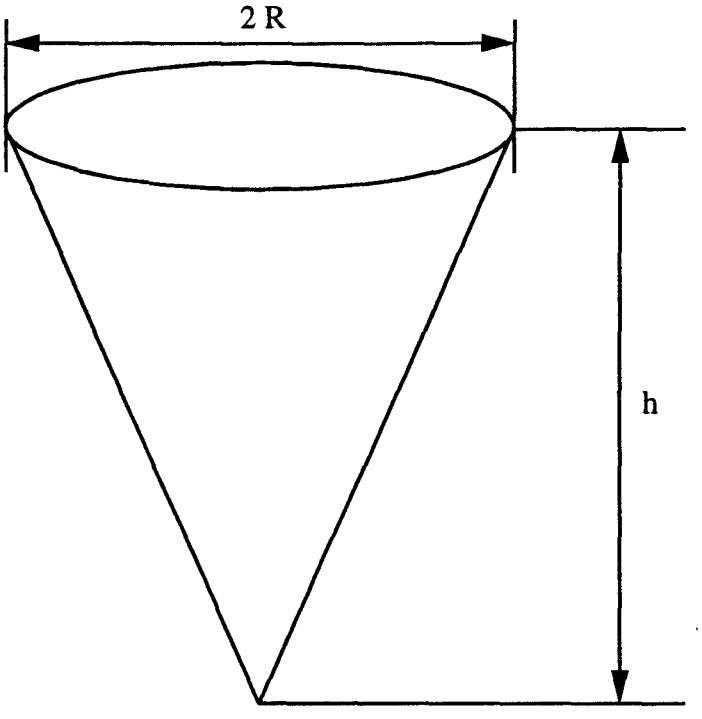

Type 1 Grit

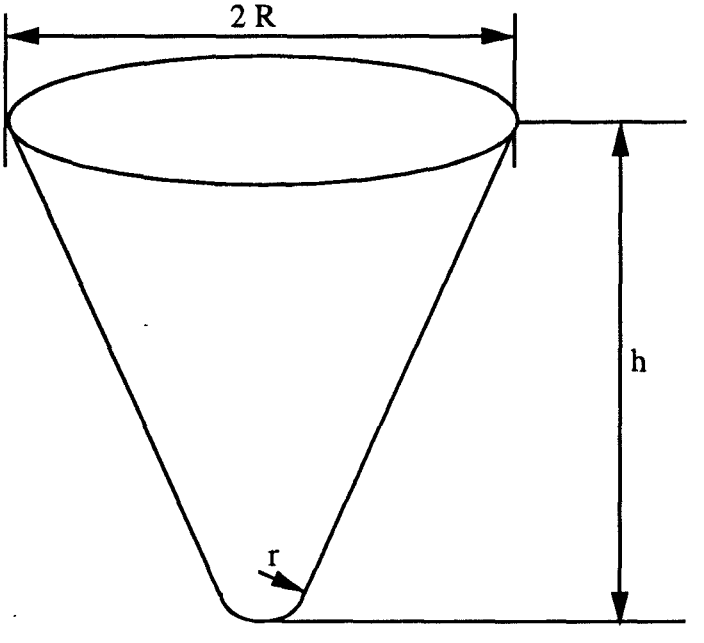

Type 2 Grit

Figure 3.1: Basic Shapes of the Abrasive Grains

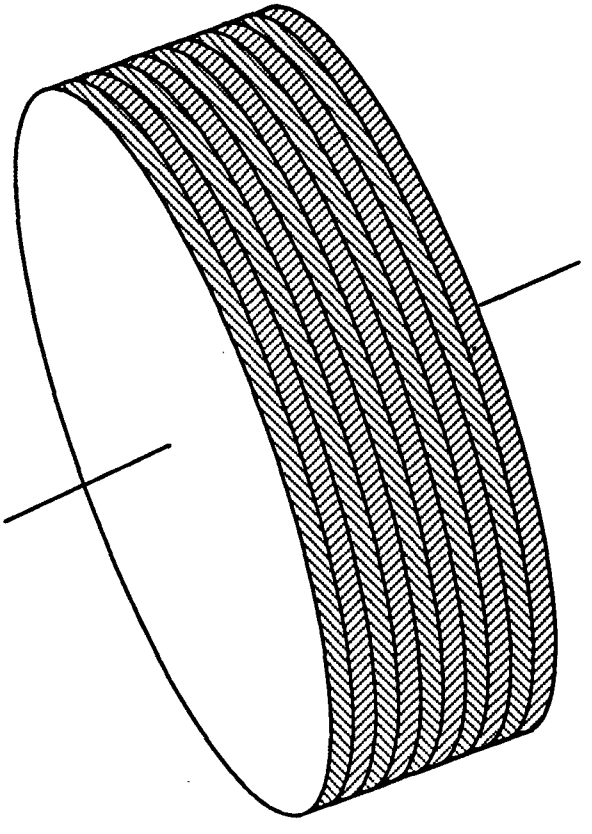

Figure 3.2: Slices on a Grinding Wheel

3.2.2 Basic Methodology

As mentioned earlier, the main objective of this thesis work is to develop a simulation package which can predict the the surface topography generated during the grinding process using a specified grinding wheel under given cutting conditions. This simulation package facilitates in selecting a grinding wheel and a set of cutting conditions to achieve the desired surface quality of a component. The desired surface quality of the component, in turn, depends on the application of the component and its tolerance specifications.

In order to develop such a simulation package, it is necessary to formulate a model describing the grinding process. In this subsection the basic methodology followed to develop the model describing the grinding process is discussed.

Wheel Topography Generation

It has been assumed that the abrasive grains of the grinding wheel have two basic shapes as mentioned in Section 3.2.1 . There are three main grit dimensions - grit diameter, grit height and semi-cone angle of the cone shaped grits. Also the nose radius for the type 2 grit has to be specified. It has been assumed that the grit diameter and the grit height follow normal distributions. To generate grits of randomly varying size, mean and standard deviation for grit diameter variation and for grit height variation are required. Average grit diameter is dependent on the grit size. It is approximated as 60 percent of the average spacing between the adjacent wires in a sieve whose mesh number equals the grit size number M

[18]. The empirical relationship between the average grit diameter and the grit size is given as

$$Mean\ grit\ diameter = \frac{0.6}{M}\ \ inch = \frac{15.2}{M}\ \ mm \tag{3.1}$$

The grit size is specified in the grinding wheel specification. Sieving is used to determine the grit size of the abrasive grains. The sieving method consists of passing abrasive grains through a stack of standard sieves from coarser sieve progressively to finer sieve. Since sieving method is used to determine the grit size, the mean grit diameter and the mean grit height should be more or less of the same order. And hence, mean grit height is equal to some factor of the mean grit diameter. If the mean semi cone angle $\phi_{0_{mean}}$ is known, then the $mean\ \ grit\ \ height = \frac{mean\ grit\ diameter/2}{\tan \phi_{0_{mean}}}$. Using photographs of the grinding wheel taken under scanning electron microscope, the standard deviation for grit diameter variation can be estimated. For simplicity, the standard deviation for grit height variation is assumed to be equal to the standard deviation for the grit diameter variation.

The grinding wheel is divided into many slices. The number of slices is decided based on the slice width. Number of slices necessary is given by

$$Number\ of\ slices = \frac{Grinding\ wheel\ width}{Slice\ width} \tag{3.2}$$

The slice width is chosen to be equal to a factor of the mean grit diameter.

Assumptions regarding the nature of the distributions for the number of grits in each slice and for the spacing between two consecutive grits along the periphery

of the grinding wheel are made earlier. These two variations along with the number of slices into which the grinding wheel is divided specify the location of the grit along the circumferential and axial directions of the grinding wheel. Mean and standard deviation for the variation of the number of grits on each slice can be decided based on the photographs of the grinding wheel taken under SEM. Once the number of slices and number of grits on each slice are known, then the mean for the variation of spacing between two consecutives grits along a slice is an angular distance of 360° divided by the number of grits on that particular slice i.e.

$$Mean\ for\ i^{th}\ slice = \frac{360^{o}}{Number\ of\ grits\ on\ i^{th}\ slice} \tag{3.3}$$

The standard deviation for this variation can be estimated from the photographs of the grinding wheel mentioned above. Various important parameters necessary to describe the wheel topography of the grinding wheel used during the grinding experiments performed as a part of this thesis work are listed in Section 7.2 .

Once the grinding wheel is divided into slices and the mean and standard deviation for various aforementioned variations are known, the wheel topography can be generated. A set of random integers with specified mean and standard deviation is generated to determine the number of grits on each slice. Let n_i be the number of grits on the i^{th} slice. Then another set of random real numbers is generated for the i^{th} slice with mean $360^0/n_i$ and specified standard deviation to determine the grit locations on the i^{th} slice. Thus the location of the grits on the wheel surface is decided.

So far the average grit dimensions are known. In order to generate individual grit geometry, a set of random real numbers with mean equal to average grit diameter and specified standard deviation is generated to get the grit diameter distribution. Another set of random real numbers is generated with mean equal to average grit height and specified standard deviation in order to determine the grit height distribution. Using these two variations, grit dimensions - grit diameter and grit height - are decided for all the grits. Also integer 1 or 2 is generated randomly to decide the type of the grits. If a particular grit is type 1 grit then the semi-cone angle ϕ_0 of the grit is given by (Refer Fig. 3.3)

$$\phi_0 = tan^{-1}(\frac{R}{h}) \tag{3.4}$$

where,

R is grit radius of the grit.

h is grit height of the grit.

If the grit is type 2 grit then

$$(h - r + r\,sin\,\phi_0)\,tan\,\phi_0 + r\,cos\,\phi_0 = R \tag{3.5}$$

or,

$$(h - r)\,tan\,\phi_0 + r\,sec\,\phi_0 = R \tag{3.6}$$

or,

$$r\,sec\,\phi_0 = R - (h - r)\,tan\,\phi_0 \tag{3.7}$$

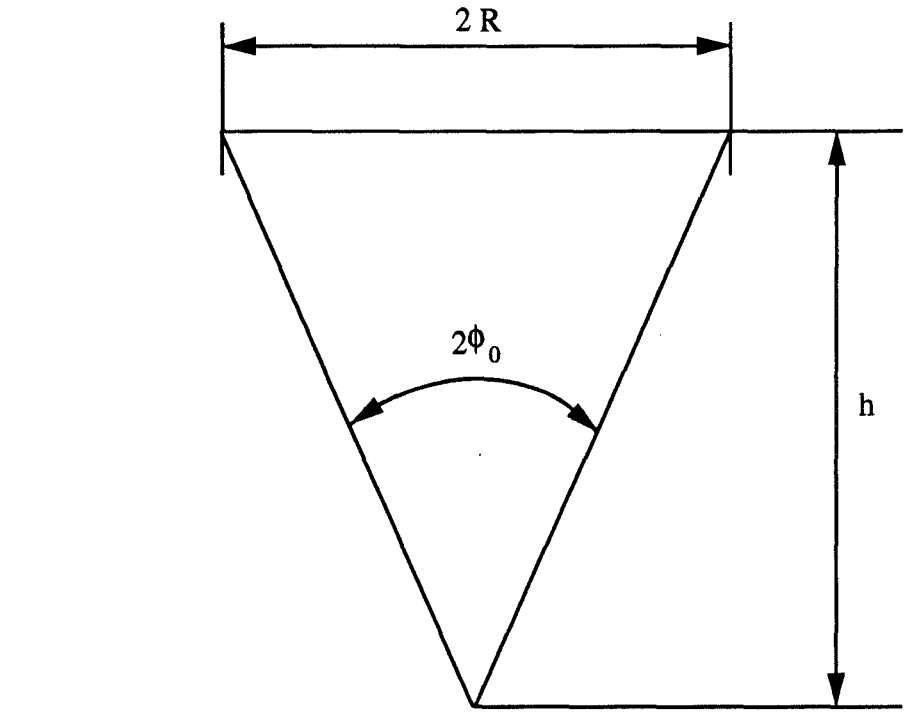

Type 1 Grit

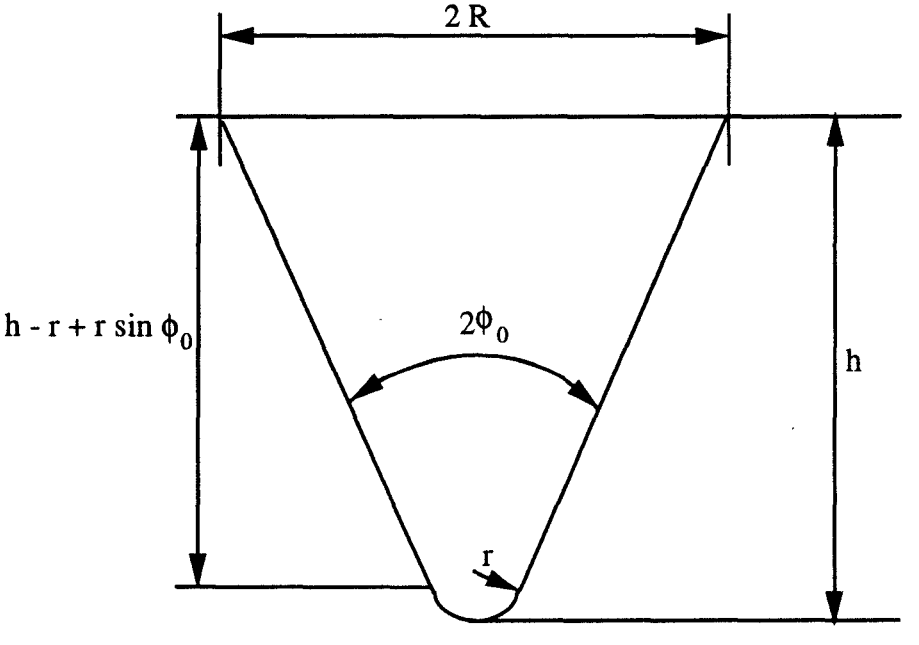

Type 2 Grit

Figure 3.3: Outlines of the Two Types of the Abrasive Grains

Squaring both sides and simplifying

$$h\,(h-2r)\,tan^2\phi_0 - 2\,R\,(h-r)\,tan\,\phi_0 + R^2 - r^2 = 0 \tag{3.8}$$

Solving the quadratic equation in $tan\,\phi_0$

$$tan\,\phi_0 = \frac{R\,(h-r) \pm \sqrt{R^2\,r^2 + r^2\,h^2 - 2\,r^3 h}}{h\,(h-2r)} \tag{3.9}$$

ϕ_0 determined by taking - sign only satisfies the Eqn. 3.5 . Hence,

$$\phi_0 = tan^{-1}\left(\frac{R\,(h-r) - \sqrt{R^2\,r^2 + r^2\,h^2 - 2\,r^3 h}}{h\,(h-2r)}\right) \tag{3.10}$$

where,

r is the nose radius for type 2 grit.

Workpiece Representation

In order to use available graphics software like Matlab or Mathematica, the top unmachined surface of the workpiece is divided into equally spaced divisions in both X and Y directions. As illustrated in Fig. 3.4, the coordinate system XYZ is fixed to the workpiece at point Q. Let the workpiece be divided into n equally spaced divisions along the X direction and m equally spaced divisions along the Y direction. Then, there are m x n representative points on the top surface of the workpiece. An array Z stores the depth at all these points. For example, $Z(i,j)$ stores the depth at point (i,j) . Array Z is initialized to 0 representing the unmachined surface. The X direction is along the grinding direction and the dimension of the workpiece along the X direction is called length of the

workpiece. The Y direction is along the crossfeed direction and the dimension of the workpiece along the Y direction is called width of the workpiece. Let ΔX be the equal spacing along the X direction and ΔY be the equal spacing along the Y direction. ΔX and ΔY are determined based on the geometry and the kinematic conditions of the particular grinding process.

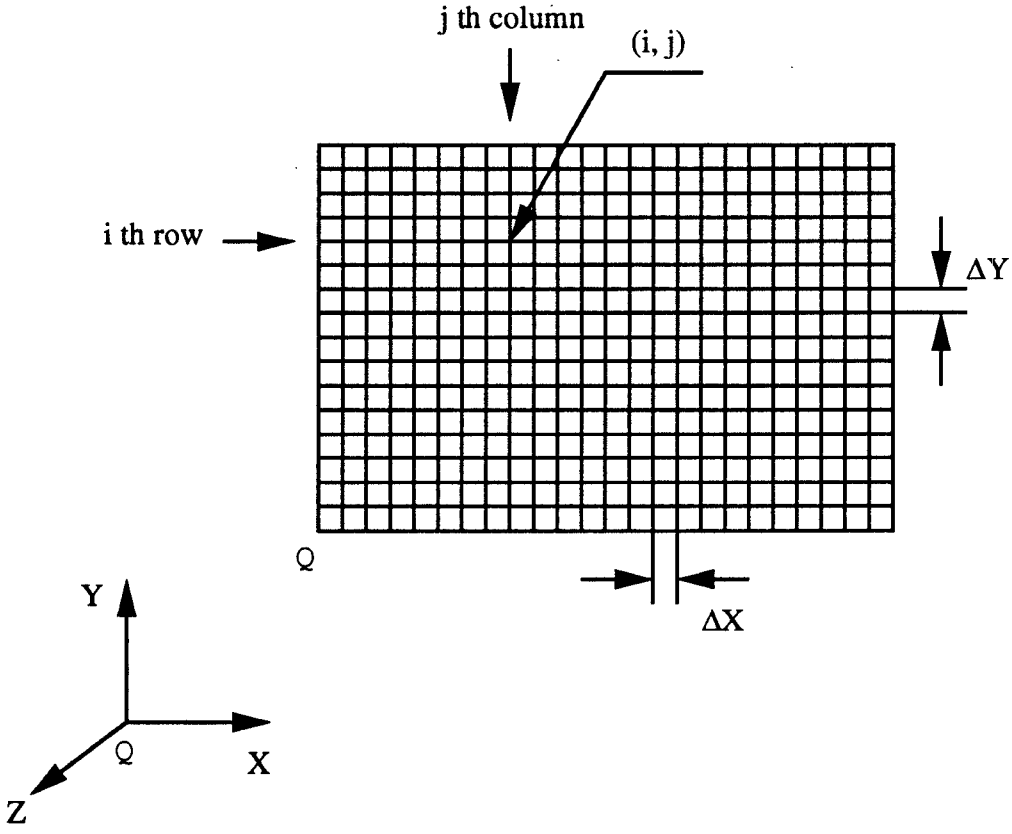

Figure 3.4: Workpiece Representation

Surface Topography Generation

For the purpose of surface topography generation only the outline of a grit is needed not the complete 3-D configuration of the grits. This is because the

symmetric nature of the assumed grit shapes and the kinematic conditions of the grinding process. The outline of a grit is the center plane of the cone shaped grit as shown in Fig. 3.3 . An enlarged view of the grinding wheel - workpiece contact region is depicted in Fig. 3.5 . A cavity is formed on the workpiece when

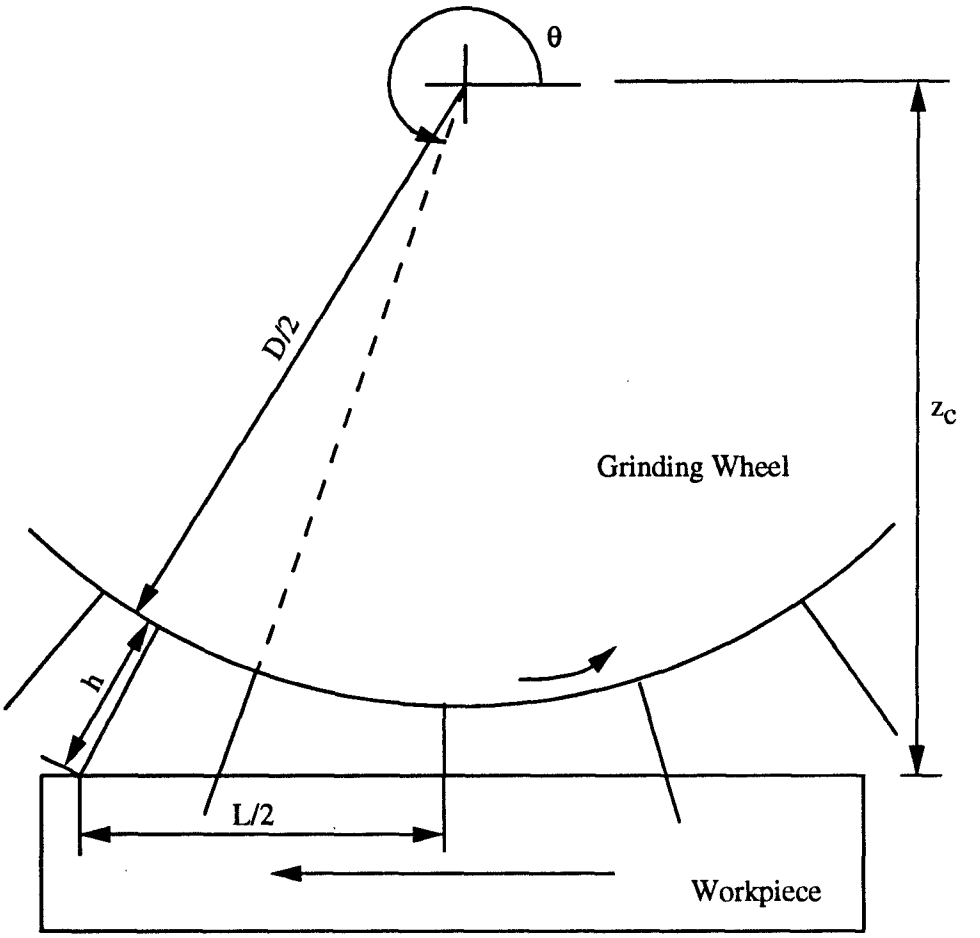

Figure 3.5: Enlarged View of the Workpiece - Grinding Wheel Contact Region

a grit removes material from the workpiece. The typical shape of the cavity so formed is shown in Fig. 3.6.

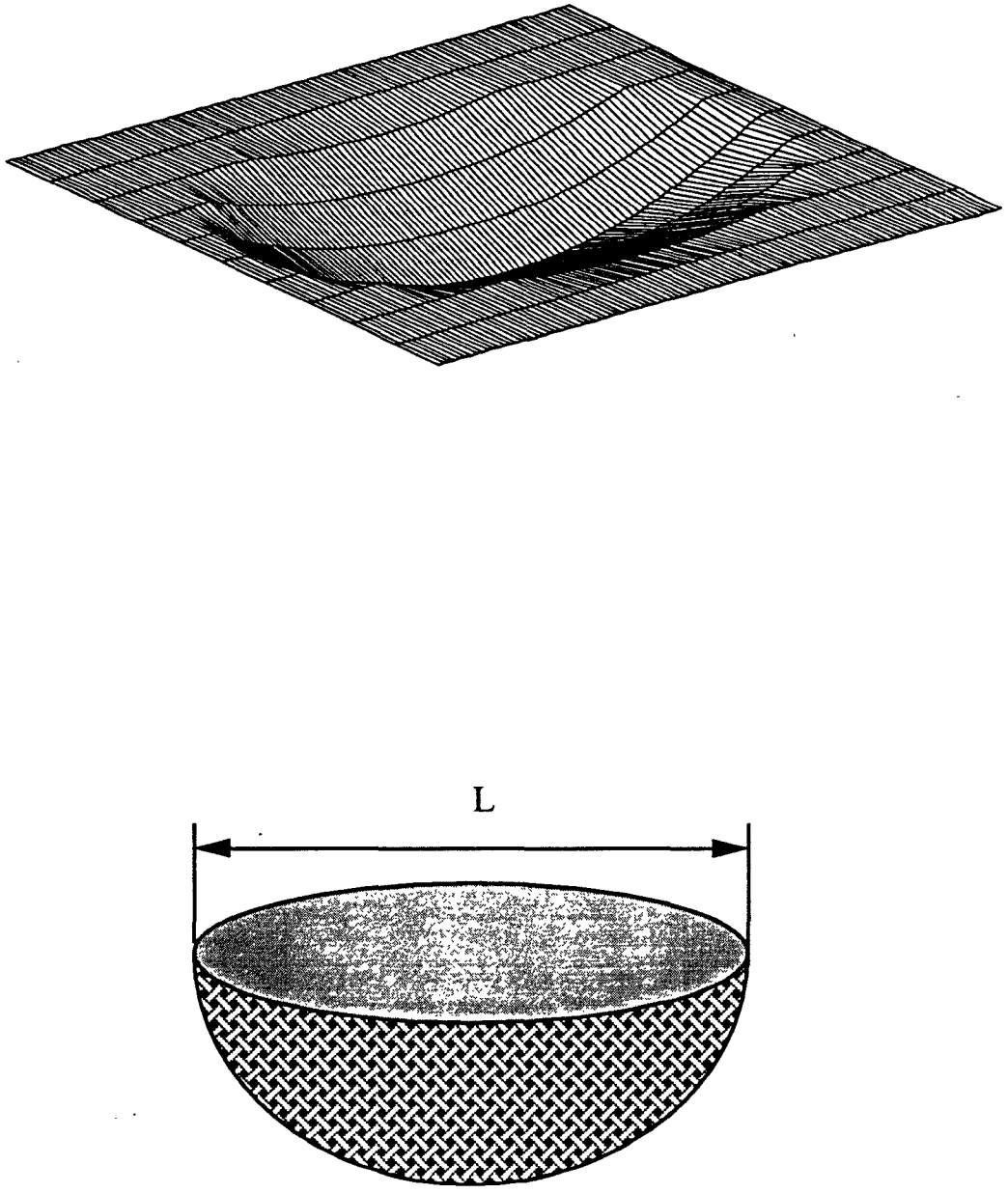

Figure 3.6: Cavity formed on the Workpiece by a Grit

In Fig. 3.6, assuming a zero table speed, we have

$$L = 2\sqrt{(h + D/2)^2 - z_c^2} \tag{3.11}$$

where,

h is the grit height.

D is grinding wheel diameter.

z_c is the distance between center of the grinding wheel and top of the unmachined surface.

But, the actual length L of the cavity made by a grit is given as

$$L = 2\sqrt{(h + D/2)^2 - z_c^2} + v\,t_1 \tag{3.12}$$

where,

t_1 is the time required to rotate the grinding wheel by angle 2δ and $t_1 = 60\,\frac{2\delta}{N\,2\pi}$

δ is the angle in radians as shown in Fig. 3.9 and $\delta = cos^{-1}(\frac{z_c}{h + D/2})$.

N is the rpm of the grinding wheel.

v is the table speed.

Therefore,

$$L = 2\sqrt{(h + D/2)^2 - z_c^2} \; + \; 60\,(\frac{\delta}{\pi})\,(\frac{v}{N}) \tag{3.13}$$

Depending on the desired number of points to create the cavity of length L, ΔX is decided. If k_1 number of points are desired along the length L, then $\Delta X = \frac{L}{k_1}$. In reality, the grit dimensions are randomly varying. So average grit dimensions can be used to determine ΔX, i.e.

$$L_{mean} = 2\sqrt{(h_{mean} + D/2)^2 - z_c^2} \; + \; 60\,(\frac{\delta_{mean}}{\pi})\,(\frac{v}{N}) \tag{3.14}$$

And therefore,

$$\Delta X = \frac{L_{mean}}{k_1} \tag{3.15}$$

where,

$\delta_{mean} = cos^{-1}\left(\frac{z_c}{h_{mean}+D/2}\right)$

h_{mean} is the mean grit height.

ΔY is a function of depth of cut which varies with grits and time. But, mean depth of cut can be used to determine ΔY. Refering to Fig. 3.7,

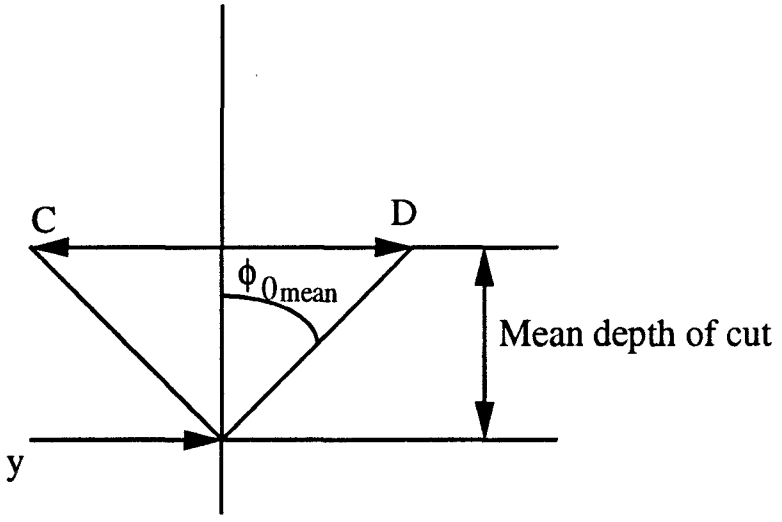

Figure 3.7: Outline of a Grit inside the Workpiece

$$CD = 2\,(mean\ depth\ of\ cut) \times tan\,(\phi_{0_{mean}}) \tag{3.16}$$

where,

$\phi_{0_{mean}}$ is the mean semi-cone angle of the grits and $\phi_{0_{mean}} = tan^{-1}\left(\frac{R_{mean}}{h_{mean}}\right)$.

R_{mean} is the mean grit radius.

Depending on the desired number of points k_2 along CD to create the topography, ΔY can be determined as

$$\Delta Y = 2\,\frac{(mean\ depth\ of\ cut)\ \times\ tan\ (\phi_{0_{mean}})}{k_2} \tag{3.17}$$

The cavity formed on the workpiece due to the kinematic interaction of a grit and the workpiece is a pile of infinitesimally thick elliptical sections with varying lengths of major and minor axes. One such elliptical section is shown in Fig. 3.8 which is at distance z from the center of the grinding wheel. In Fig. 3.8 xyz represents a coordinate system fixed to the axis of the grinding wheel just above the center of the cavity formed by a grit on the workpiece. The equation defining the elliptical section at a distance z from the center of the grinding wheel is given as

$$\frac{x^2}{a^2} + \frac{y^2}{b^2} = 1 \tag{3.18}$$

where,

a and b are half the lengths of the major and the minor axes of the ellipse as shown in Fig. 3.8 and are functions of z.

Let us consider a section of the cavity parallel to x-axis and at $y = 0$ as shown in Fig. 3.9 . The length of half of the major axis, a is given as

$$a = \sqrt{(h + D/2)^2 - z^2}\ +\ 60\,(\frac{\delta'}{2\,\pi})\,(\frac{v}{N}) \tag{3.19}$$

where,

$\delta' = cos^{-1}(\frac{z}{h+D/2})$

But, the second term $60\,(\frac{\delta'}{2\,\pi})\,(\frac{v}{N})$ is very small compare to the first term. In fact,

the second term is close to ΔX or even smaller than ΔX. Therefore, neglecting the second term, a as a function of z is given as

$$a = \sqrt{(h + D/2)^2 - z^2} \tag{3.20}$$

The outlines of the two types of grits when they are vertical are shown in Fig. 3.10 . The length of half of the minor axis, b is given as (Refer Fig. 3.10(a))

$$b = (h + D/2 - z)\, tan\, \phi_0 \tag{3.21}$$

Therefore, the equation representing the elliptical section of the cavity at a distance z from the center of the grinding wheel is given as

$$\frac{x^2}{(h + D/2)^2 - z^2} + \frac{y^2}{(h + D/2 - z)^2\, tan^2\, \phi_0} = 1 \tag{3.22}$$

The above derivation of the equation representing the elliptical section at a distance z from the center of the grinding wheel is only true for type 1 grit. For type 2 grit the expression for a as a function of z remains the same as in the case of type 1 grit. But, the expression for b as a function of z is different. From Fig. 3.10(b) we have,

$$b = (h + D/2 - r + r\, sin\, \phi_0 - z)\, tan\, \phi_0 + r\, cos\, \phi_0 \tag{3.23}$$

or,

$$b = (h + \frac{D}{2} + \frac{r\, cos\, \phi_0}{tan\, \phi_0} - r + r\, sin\, \phi_0 - z)\, tan\, \phi_0 \tag{3.24}$$

Let $d = r\,(\frac{cos\, \phi_0}{tan\, \phi_0} - 1 + sin\, \phi_0) = r\, g$

where,

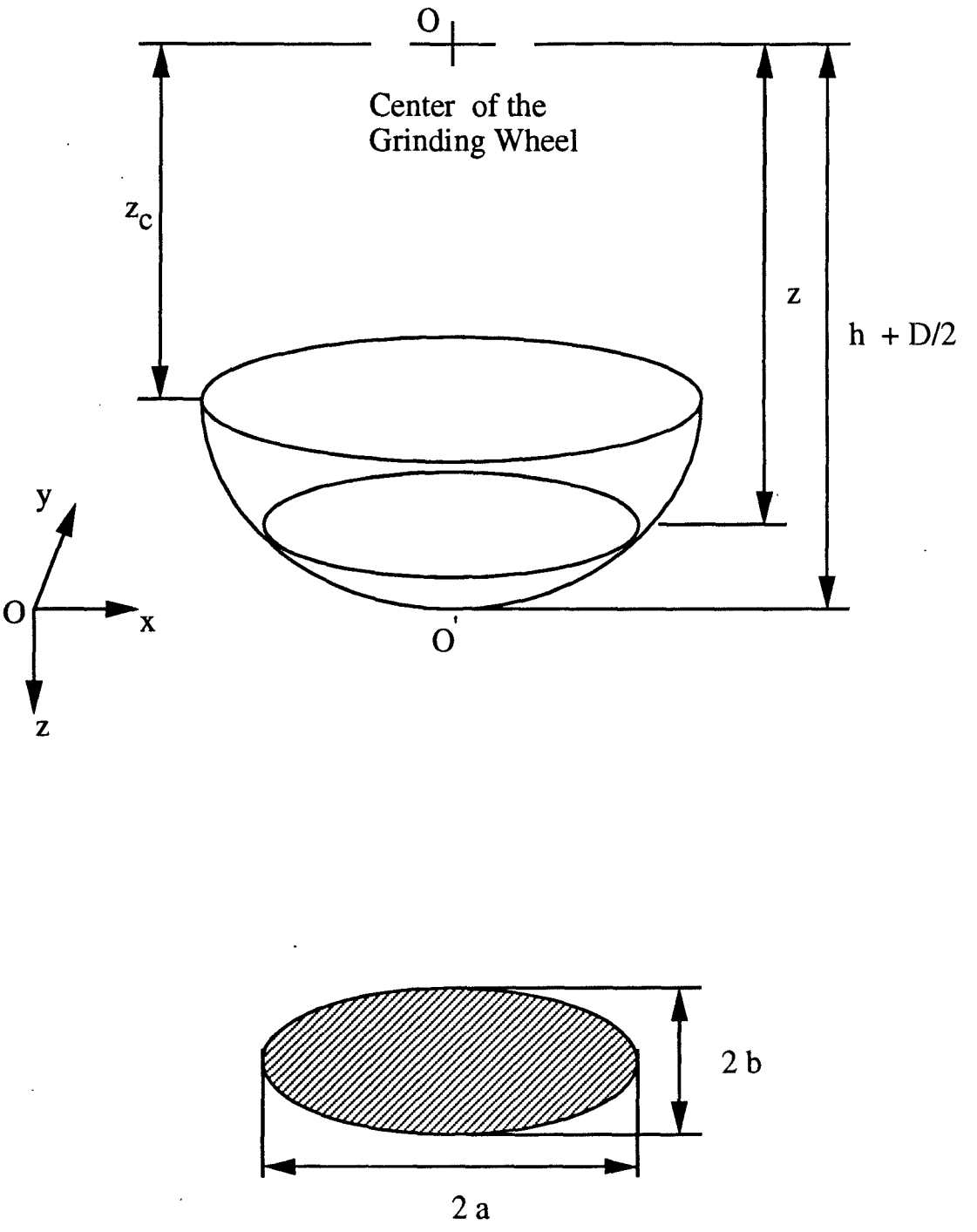

Figure 3.8: An Elliptical Section of the Cavity formed by a Grit

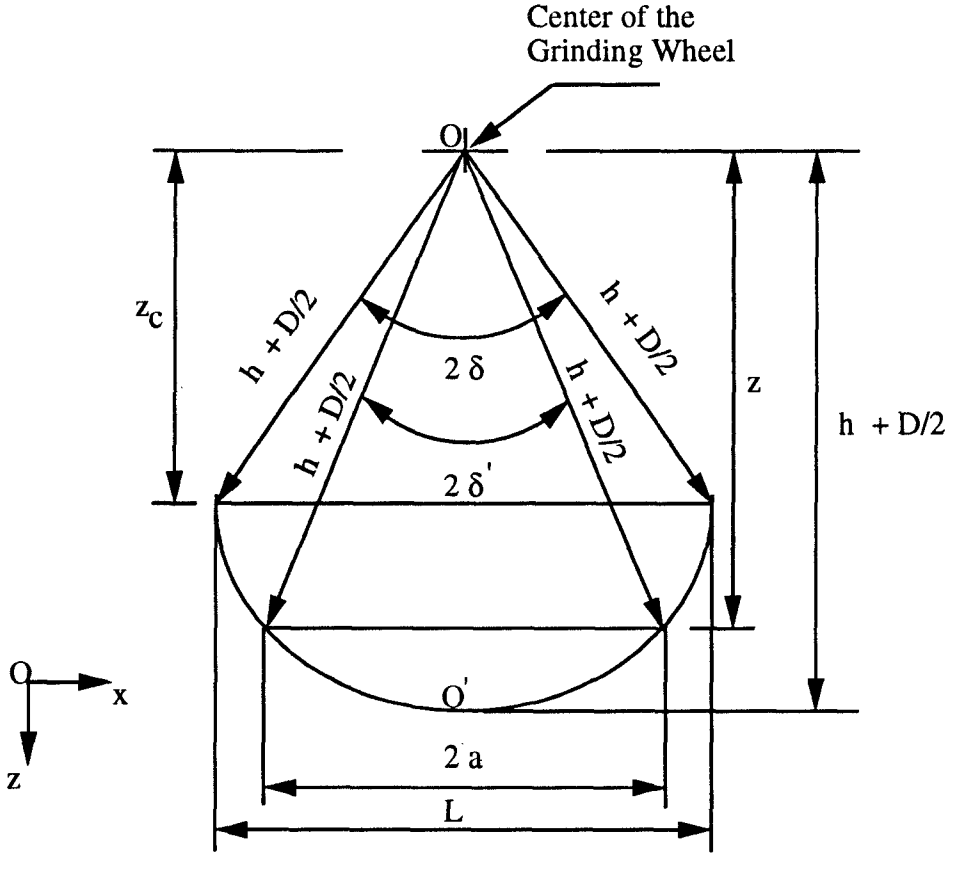

Figure 3.9: A Longitudinal Section of the Cavity formed by a Grit

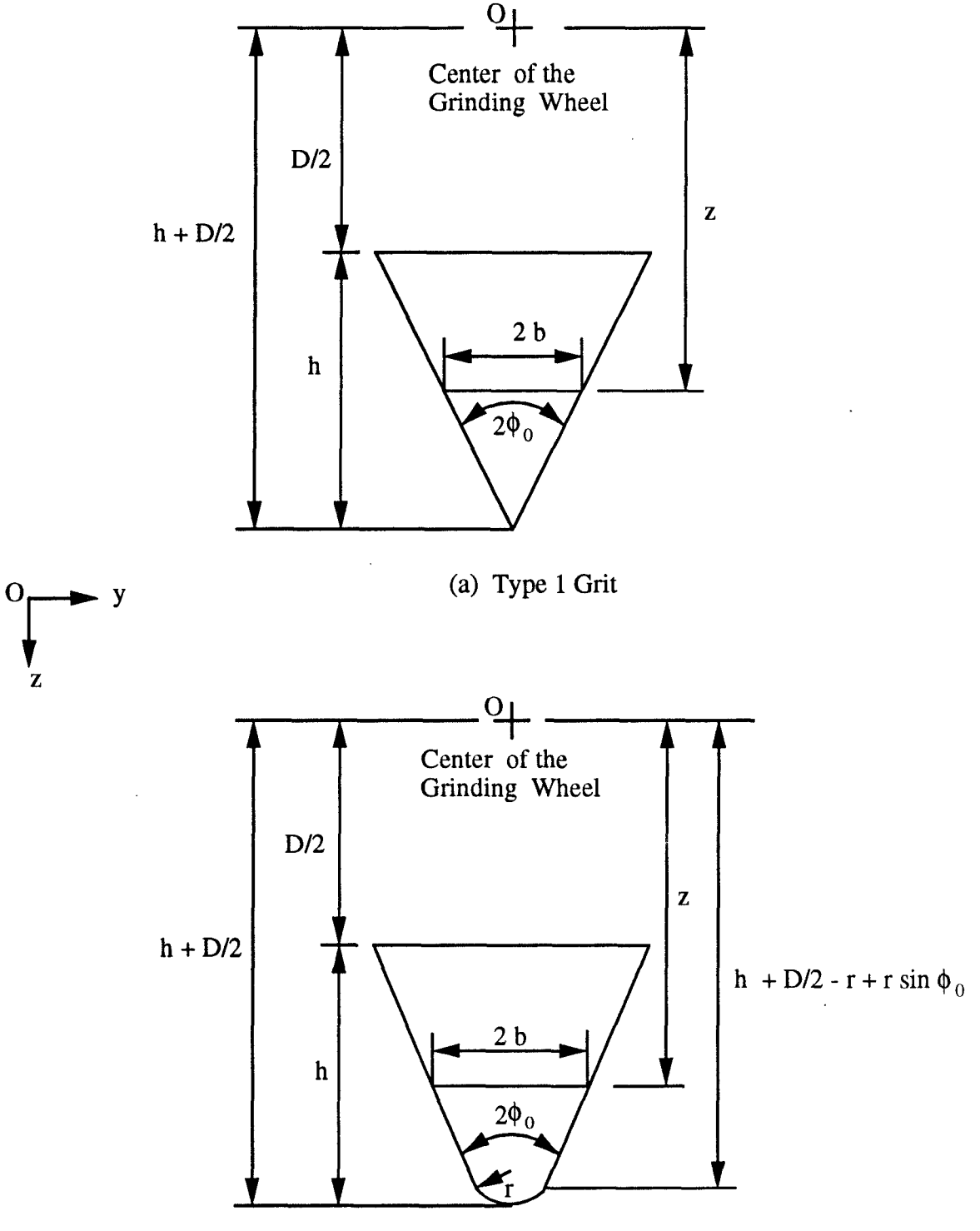

Figure 3.10: Grits as Viewed from the Grinding Direction

$g = \frac{cos\,\phi_0}{tan\,\phi_0} - 1 + sin\,\phi_0$

or,

$$b = (h + D/2 + d - z)\,tan\,\phi_0 \tag{3.25}$$

$$b = (h + D/2)\,(1 + \frac{d}{h + D/2} - \frac{z}{h + D/2})\,tan\,\phi_0 \tag{3.26}$$

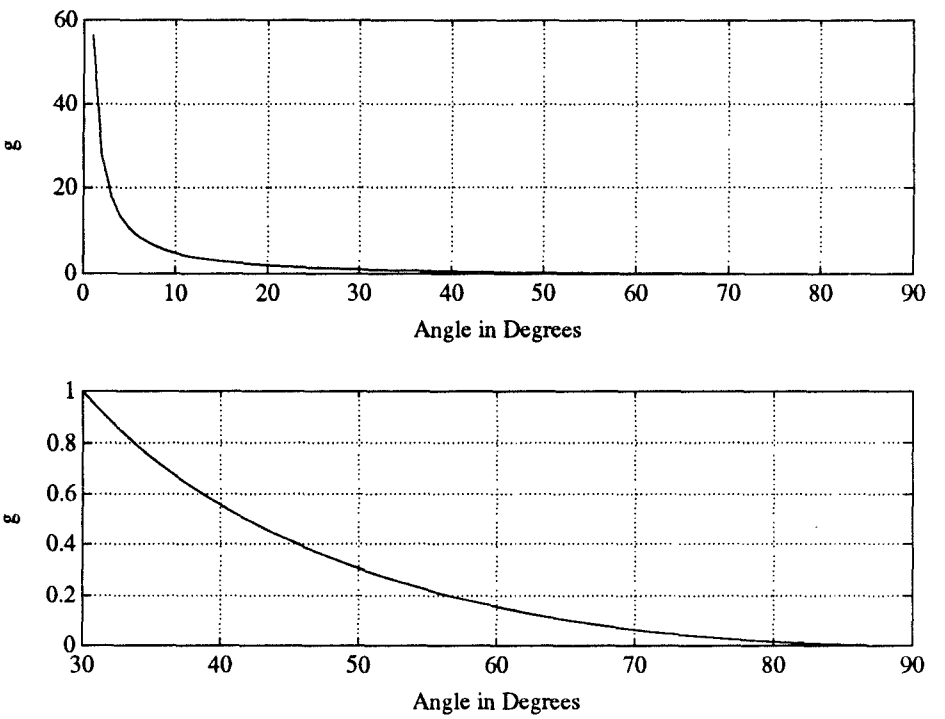

Figure 3.11: Plot of Factor g vs. Angle ϕ_0

Factor g is plotted for various values of ϕ_0 in Fig. 3.11 . It can be observed from the plot that the factor g has a value less than 1 when ϕ_0 is greater than 30°. The cone angles of the grits are usually obtuse or so to say semi-cone angle is usually greater than 45° . Moreover, nose radius of the type 2 grits is also very very small compare to the radius of the grinding wheel ($D/2$). Therefore,

$\frac{d}{h+D/2} \ll 1$ and can be neglected. Hence, the expression for b as a function of z for type 2 grit becomes

$$b = (h + D/2)\,(1 - \frac{z}{h + D/2})\,tan\,\phi_0 \tag{3.27}$$

or,

$$b = (h + D/2 - z)\,tan\,\phi_0 \tag{3.28}$$

Therefore, with the above approximation, the expression for b for type 2 grit becomes the same as in the case of type 1 grit. Hence, the equation representing the elliptical section at a distance z from the center of the grinding wheel for type 2 grit is also given as

$$\frac{x^2}{(h + D/2)^2 - z^2} + \frac{y^2}{(h + D/2 - z)^2\,tan^2\,\phi_0} = 1 \tag{3.29}$$

Let $\rho = h + D/2$ and hence,

$$\frac{(\frac{x}{\rho})^2}{1 - (\frac{z}{\rho})^2} + \frac{(\frac{y}{\rho\,tan\,\phi_0})^2}{(1 - \frac{z}{\rho})^2} = 1 \tag{3.30}$$

Let $x_1 = \frac{x}{\rho}$, $y_1 = \frac{y}{\rho\,tan\,\phi_0}$, $z_1 = \frac{z}{\rho}$

$$\frac{x_1^2}{1 - z_1^2} + \frac{y_1^2}{(1 - z_1)^2} = 1 \tag{3.31}$$

or,

$$(1 - z_1)^2\,x_1^2 + (1 - z_1^2)\,y_1^2 = (1 - z_1)^2\,(1 - z_1^2) \tag{3.32}$$

Cancelling $1 - z_1$ from both sides, we get

$$(1 - z_1)\,x_1^2 + (1 + z_1)\,y_1^2 = (1 - z_1)\,(1 - z_1^2) \tag{3.33}$$

or, by simplifying

$$z_1^3 - z_1^2 + z_1(-1 + x_1^2 - y_1^2) + (1 - x_1^2 - y_1^2) = 0 \tag{3.34}$$

In Eqn. 3.29, x and y lie within or on the uppermost elliptical section of the cavity formed by the grit on the workpiece. For the values of x and y satisfying the constraint

$$\frac{x^2}{(h + D/2)^2 - z_c^2} + \frac{y^2}{(h + D/2 - z_c)^2 \, tan^2 \, \phi_0} \leq 1, \tag{3.35}$$

the above cubic equation in z_1 has three real roots of the following nature. The roots are

1. $z_1 > 0$ and $z_1 \leq 1$ (close to 1)

2. $z_1 < 0$ and $z_1 > -1$

3. $z_1 \geq 1$

But, $z_1 = z/\rho$ and $z_c \leq z \leq \rho$ or $\frac{z_c}{\rho} \leq z_1 \leq 1$. Therefore, only the first solution is acceptable such that (x, y, z) represents a point on the surface of the cavity formed by a grit on the workpiece. This particular solution of the cubic equation is determined by Newton Raphson method in the simulation program.

The following methodology is followed to generate the ideal surface topography. First, time t_o is determined using the equations given below. t_o represents the different instants of time when the individual grits are oriented vertically downward with respect to the center of the grinding wheel. If θ_0 is the initial

orientation of a grit with respect to positive X-axis then

for $\theta_0 \leq \frac{3}{2}\pi$,

$$t_o = (\frac{3}{2}\pi - \theta_0)\frac{60}{2\pi N} + \frac{60\,n}{N} \tag{3.36}$$

for $\theta_0 > \frac{3}{2}\pi$,

$$t_o = (2\pi - \theta_0 + \frac{3}{2}\pi)\frac{60}{2\pi N} + \frac{60\,n}{N} \tag{3.37}$$

where,

n is the number of revolution and $n \geq 0$.

Then, the location of the center of the cavities formed by different grits at different instants of time are determined in terms of workpiece coordinate system as

$$X_o = X_{c_0} \pm v\,t_o \tag{3.38}$$

(+ is used in case of upgrinding and − is used in case of downgrinding.)

$$Y_o = Y_{c_0} + m\,(crossfeed) + j\,(slice\ width) \tag{3.39}$$

where,

X_o is X-coordinate of the center of the cavity formed by a grit at a particular time t_o during a particular pass of the grinding wheel.

X_{c_0} is the initial X-position of the center of the grinding wheel in terms of workpiece coordinate system and its value depends on whether grinding is upgrinding

or downgrinding.

Y_o is Y-coordinate of the center of the cavity formed by a grit during a particular pass of the grinding wheel.

Y_{c_0} is the initial Y-position of the center of the grinding wheel in terms of workpiece of coordinate system.

m is the number of pass and $m \geq 0$.

j is the slice number of a slice on which the particular grit lies.

Then, the cavities formed by different grits are generated by solving the cubic equation in z_1 (Eqn. 3.34) for different values of x, y satisfying the constraint (Eqn. 3.35) . The solution of the cubic equation in z_1 can then be transformed to workpiece Z coordinate by the following transformation rule.

$$Z = -(\rho z_1 - z_c) \tag{3.40}$$

The cavities formed by different grits are then embedded on the workpiece surface such that center of the cavities coincide with X_o and Y_o calculated above. Another important aspect of surface topography generation is the consideration of the overlapping among cavities formed by different grits at different instants of time during different passes of the grinding wheel. The top unmachined surface of the workpiece is divided into m x n representing points as mentioned earlier. For any point (i, j) on the workpiece surface only the maximum negative value of the Z - coordinate is stored in $Z(i, j)$ and thus the overlapping among cavities is taken into account.

Surface Characterization Parameters

In order to compare the surface textures, surface characterization parameters are needed. Using these parameters the surface texture can be quantified. A surface profile is most often characterized numerically by following parameters.

- Peak to Value (PTV)

  The peak-to-value is the height differential between a peak and valley.

- Roughness Average Value (R_a)

  This parameter characterizes the average deviation of the profile from the center line. Mathematically,

$$R_a = \frac{1}{N} \sum_{i=1}^{N} |z(i) - \bar{z}| \tag{3.41}$$

- Root Mean Square (R_q)

  This parameter also characterizes the average deviation of the profile from the center line. Mathematically,

$$R_q = \sqrt{\frac{1}{N} \sum_{i=1}^{N} (z(i) - \bar{z})^2} \tag{3.42}$$

where,

$\bar{z} = \frac{1}{N} \sum_{i=1}^{N} z(i)$

$z(i)$ is the height or depth of the profile at the sample point i.

N is the total number of sample points.

3.3 Simulation Details

The set of cutting parameters to be used later during actual grinding operation is an important set of input parameters necessary to predict the ground surface topography. The cutting parameters like the rpm of the grinding wheel, cross-feed, downfeed and table speed are specified. Important grit parameters like grit size, nose radius of type 2 grit etc. are also specified. The standard deviations and means for various distributions mentioned in Section 3.2 are entered. Major dimensions like grinding wheel diameter and grinding wheel width are also specified.

After data entry, wheel topography is generated as discussed earlier. A flow chart explaining the wheel topography generation is listed in Table 3.1 . Ideal ground surface topography is then generated. Flow chart explaining the basic methodology followed to generate the ideal ground surface topography is listed in Table 3.2 . The final results are stored. Using available software like Matlab or Mathematica 3-D ground surface topography is plotted. The surface characterization parameters like R_a, R_q and PTV are then calculated. Table 3.3 lists the flow chart depicting the overall methodology adopted to develop the simulation package to generate the ideal ground surface topography.

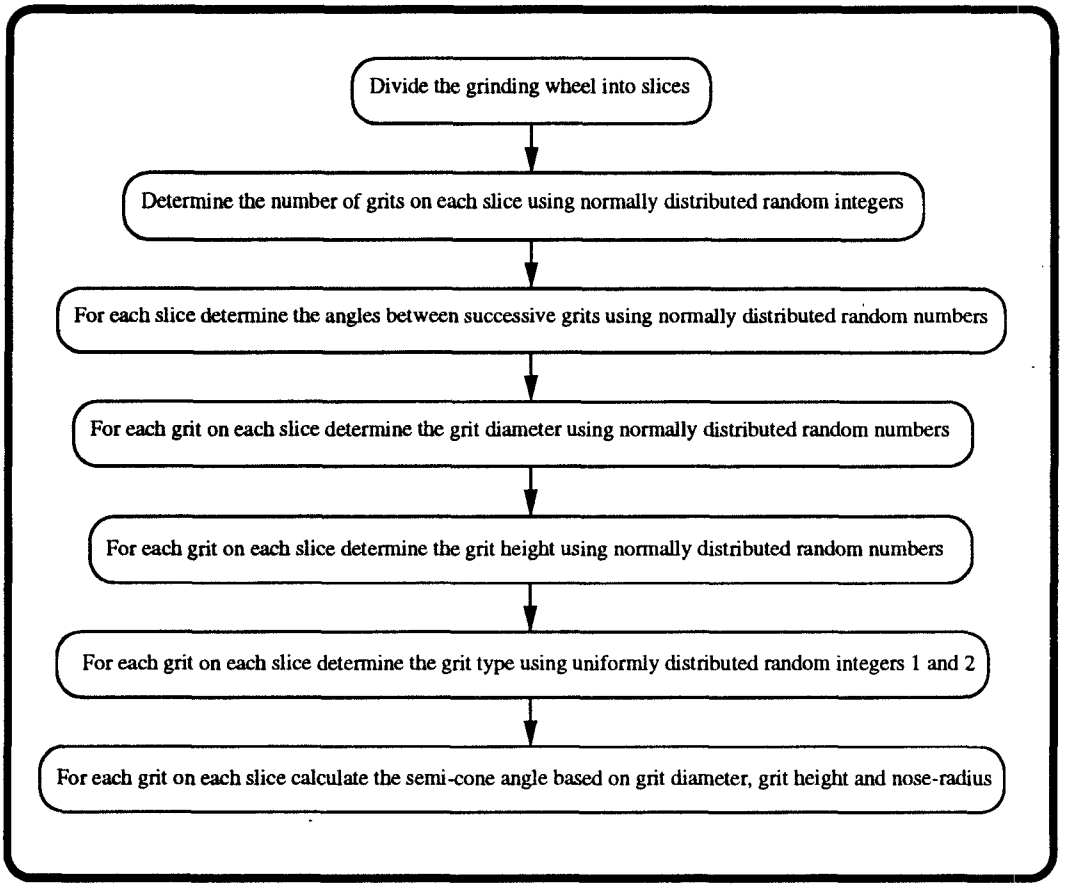

Table 3.1: Flow Chart for Wheel Topography Generation

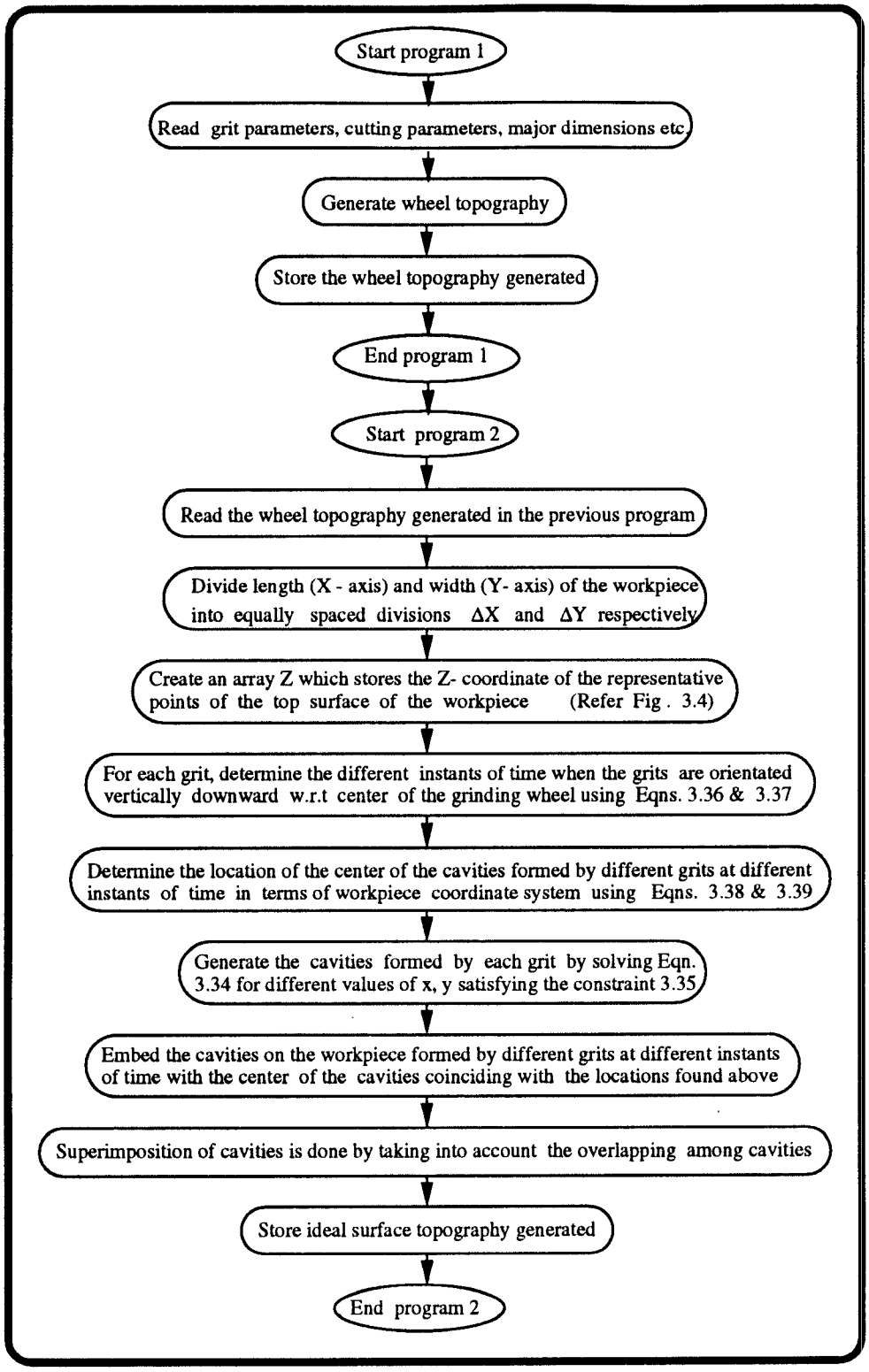

Table 3.2: Flow Chart for Ideal Surface Topography Generation

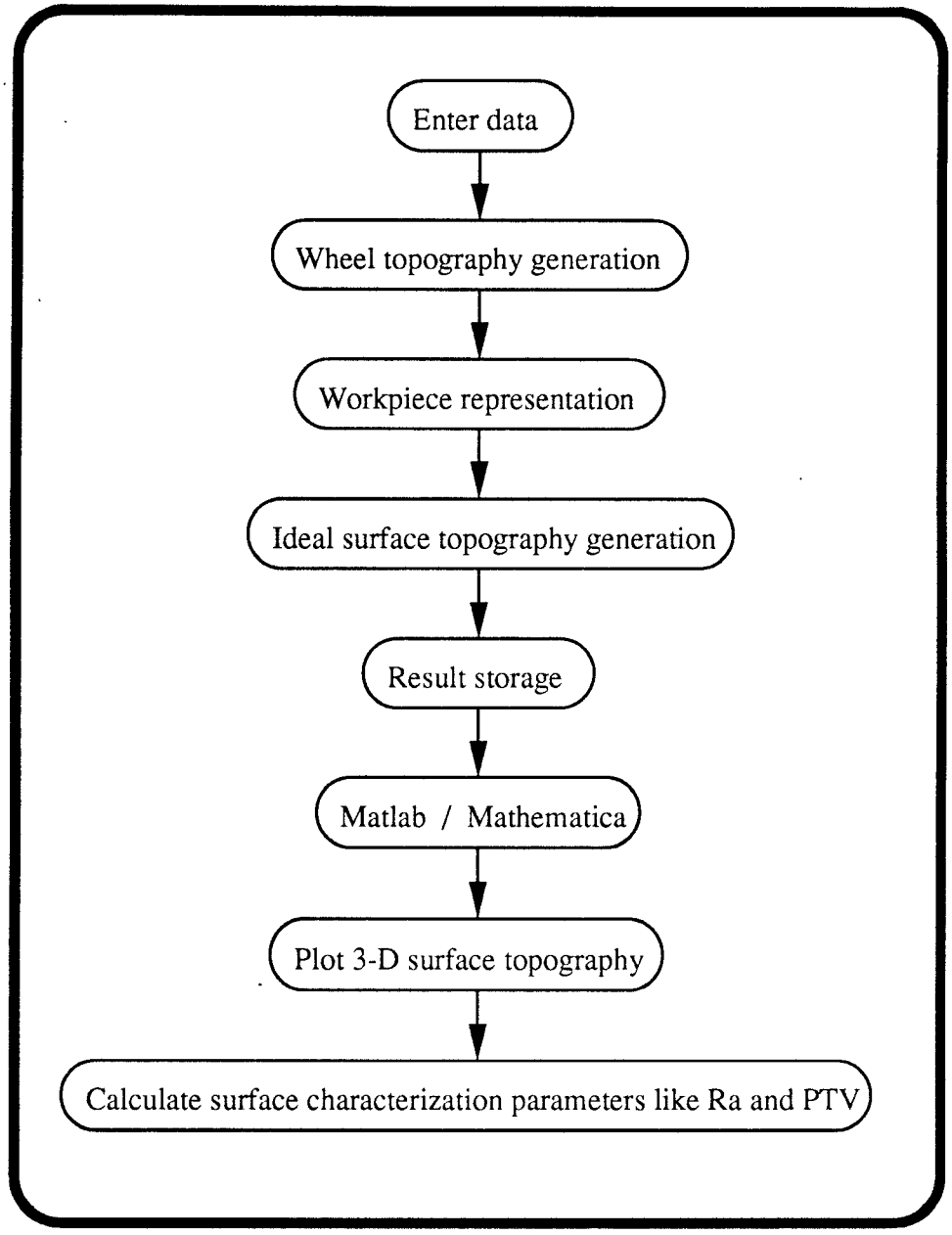

Table 3.3: Overall Plan for Ideal Surface Topography Generation

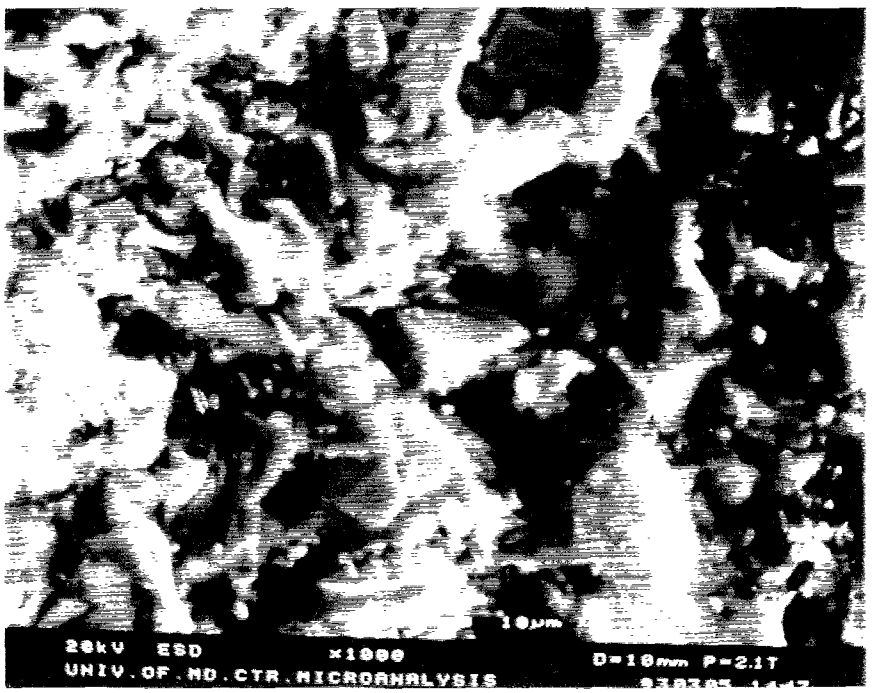

Figure 3.12: SEM picture of the Grinding Wheel Surface

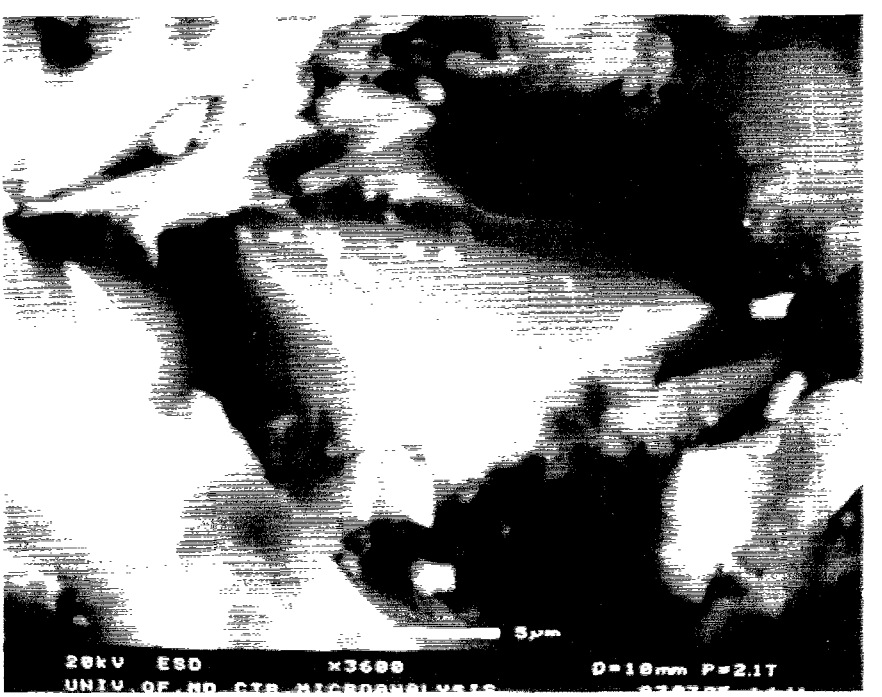

Figure 3.13: SEM picture of an Abrasive Grain

Chapter 4

Force Model for the Grinding Process

A model to describe the cutting forces generated during grinding is necessary for the development of a mathematical model of the grinding machining system. A cutting force model for the grinding process developed in this thesis work is presented in this chapter.

4.1 Coordinate Systems

The traverse surface grinding process is chosen for this work. It is schematically shown in Fig. 4.1 where a fixed reference system xyz is defined for the mathematical derivations. The origin of the coordinate system is fixed at point O.

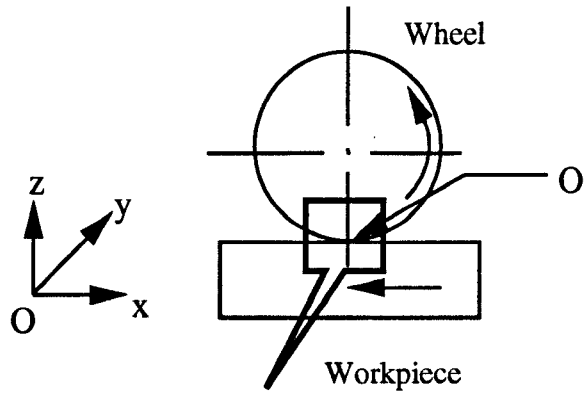

Figure 4.1: Schematic Illustration of Traverse Surface Grinding Process

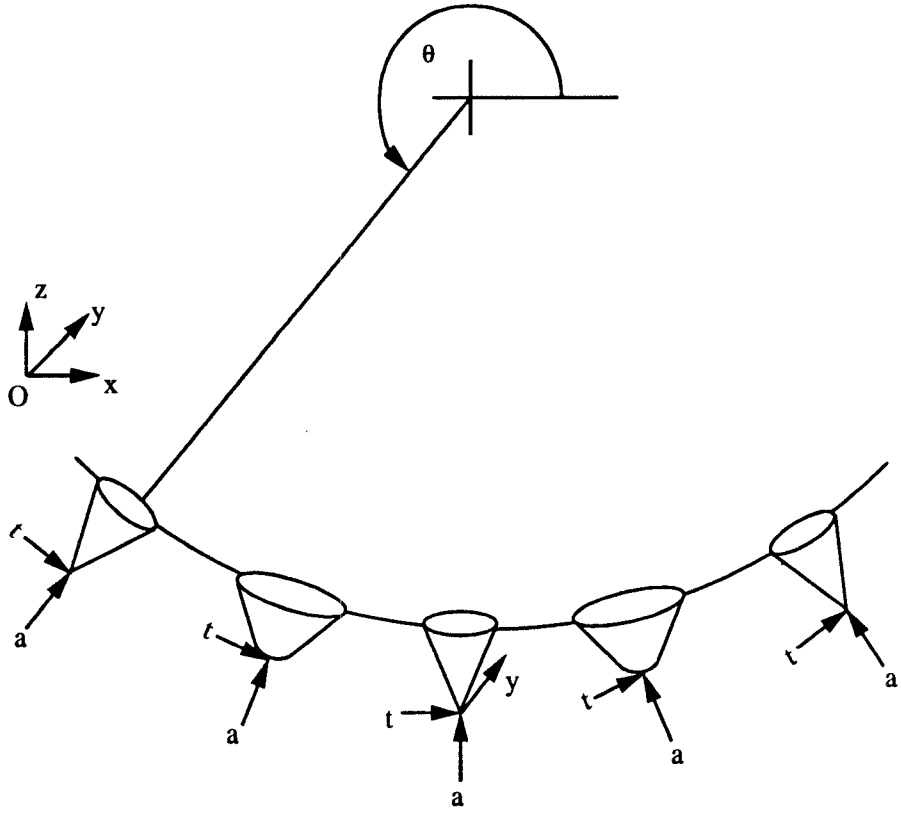

Figure 4.2: Enlarged View of the Workpiece - Grinding Wheel Contact Region

Each grit has its local rotating coordinate system. The local coordinate system tya is fixed to the individual grits as shown in Fig. 4.2 . The origin of this coordinate system is fixed at the tip of the individual grits. t is the tangential direction of the individual grits and a is the axial direction of the individual grits. The direction y of the rotating coordinate system is the same as the direction y of the fixed reference system.

4.2 Grit Dimensions

The important grit dimensions are shown in Figs. 4.3 and 4.4 . Important parameters are

ϕ_0 is the semi cone angle;

r is the nose radius for the type 2 grit;

h is the height of the part of the cone shaped grit which is inside the workpiece and $h = \frac{z_{tip}}{sin\,\theta}$;

R is the radius of the circular cross-section of the cone shaped grits at a height h from the tip and $R = h\,tan\phi_0$ for type 1 grit and $R = r\,cos\,\phi_0 + h_1\,tan\,\phi_0$ for type 2 grit;

l is the corresponding slant height of the cone for type 1 grit or extended cone for type 2 grit and $l = \frac{R}{sin\,\phi_0}$; and

l_1, h_1 are the dimensions as shown in Fig. 4.4 .

where,

$h_1 = h - r + r\,sin\,\phi_0$.

$l_1 = \frac{r\,cos\,\phi_0}{sin\,\phi_0} = \frac{r}{tan\,\phi_0}$.

z_{tip} is the z-coordinate of the tip of the grit and is a function of of the z-coordinate of the center of the grinding wheel (z_c), the grit height and the angle θ and

$z_{tip} = z_c + (D/2 + grit\ \ height)\,sin\,\theta$.

θ is the angular position of the grit with respect to positive x-axis as shown in Fig. 4.2 .

D is diameter of the grinding wheel.

Therefore, the dimensions l and R for a particular grit can be determined in terms of known grit dimensions such as h, r and ϕ_0.

4.3 Cutting Mechanism

From the viewpoint of the kinematics of the grinding process, only one-half of the assumed cone shaped grit is involved in the cutting operation at any instant. To facilitate the development of mathematical expressions for the grinding force, each grit is divided into triangular elements as shown in Figs. 4.5 and 4.6 . For each of the triangular elements, the cutting action can be treated as the cutting action of the single-point cutting process such as turning. By summing up the cutting action of these individual elements, a mathematical model for the grinding force can be derived.

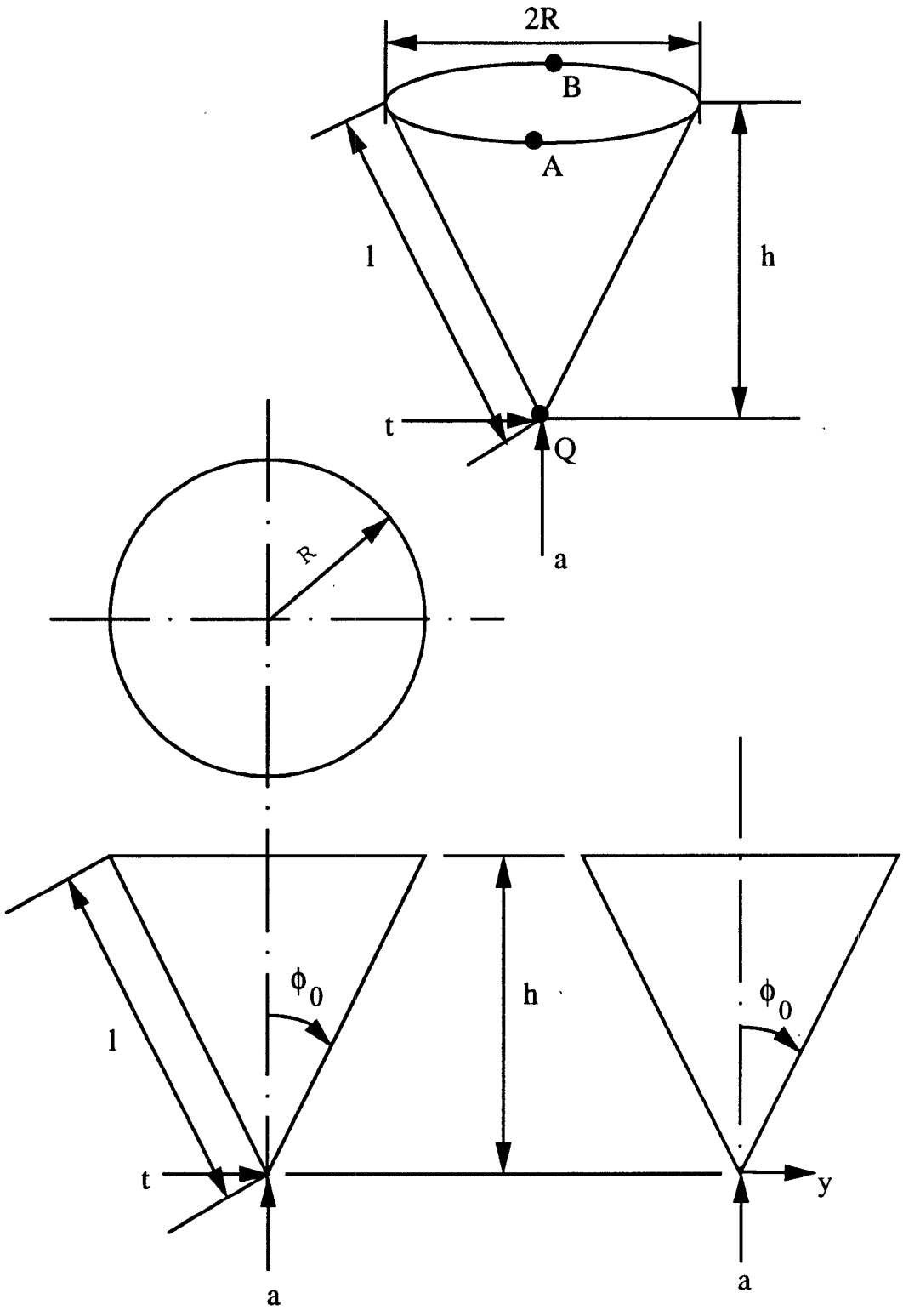

Figure 4.3: Grit Dimensions for Type 1 Grit

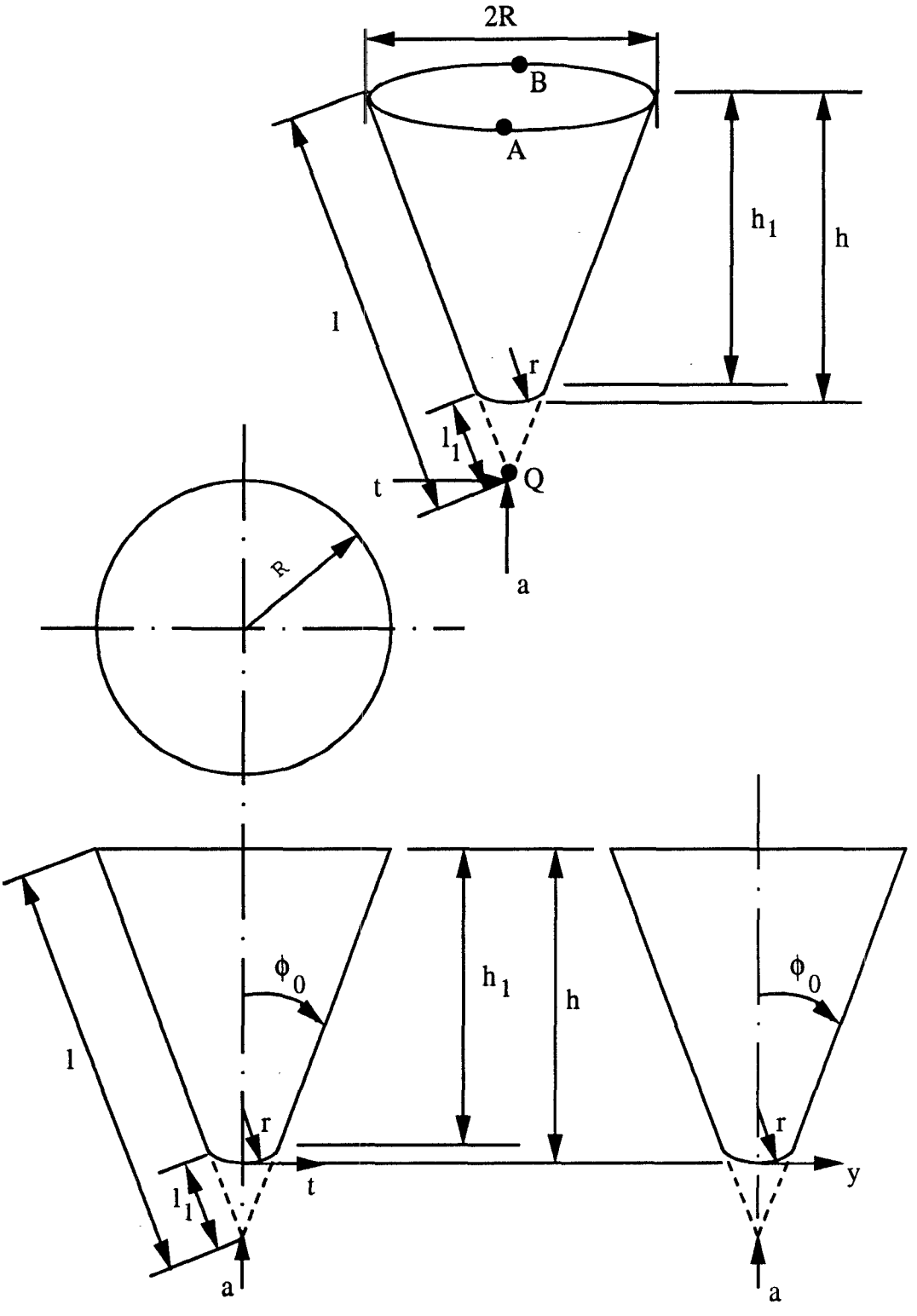

Figure 4.4: Grit Dimensions for Type 2 Grit

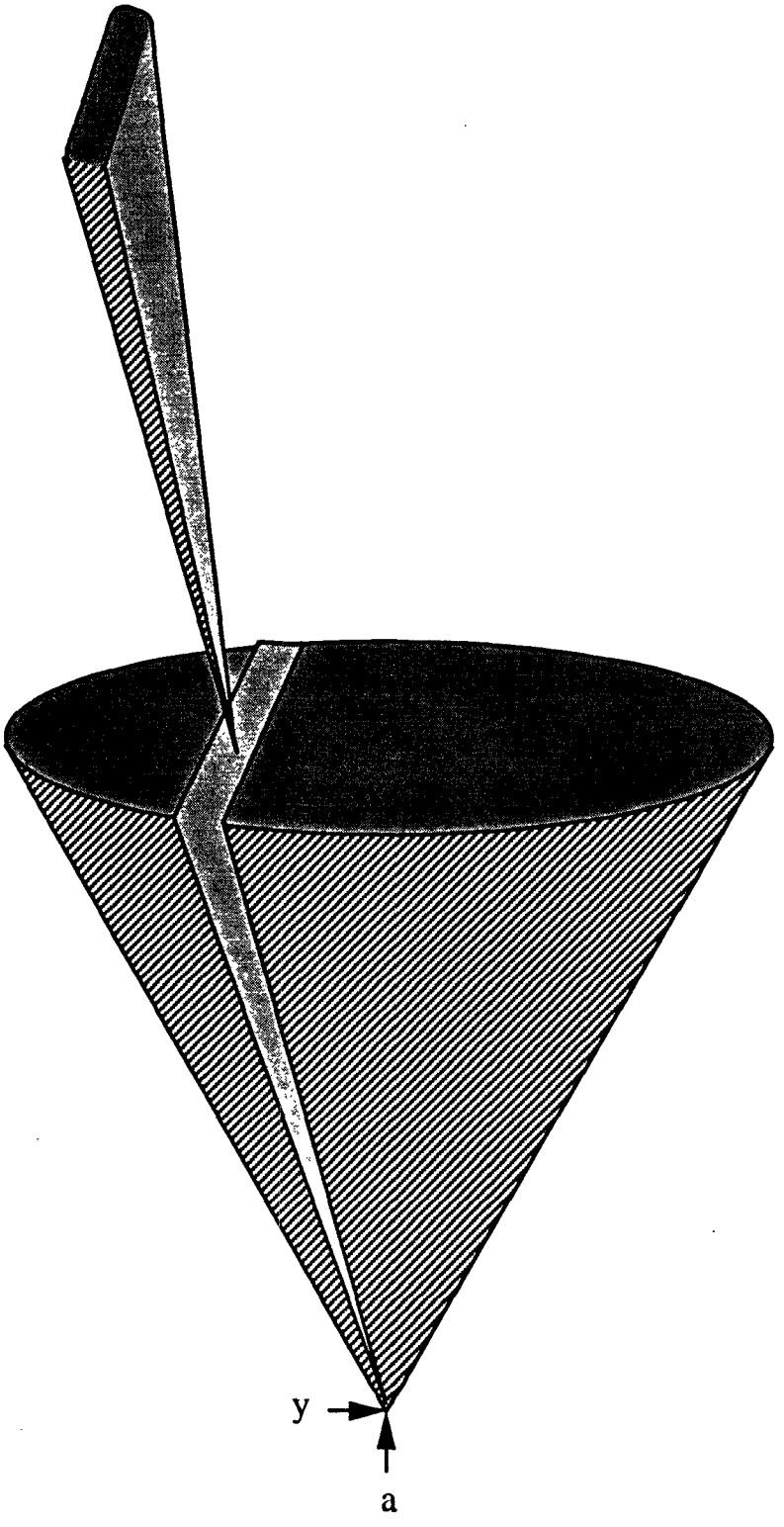

Figure 4.5: A Triangular Element for Grinding Force Analysis

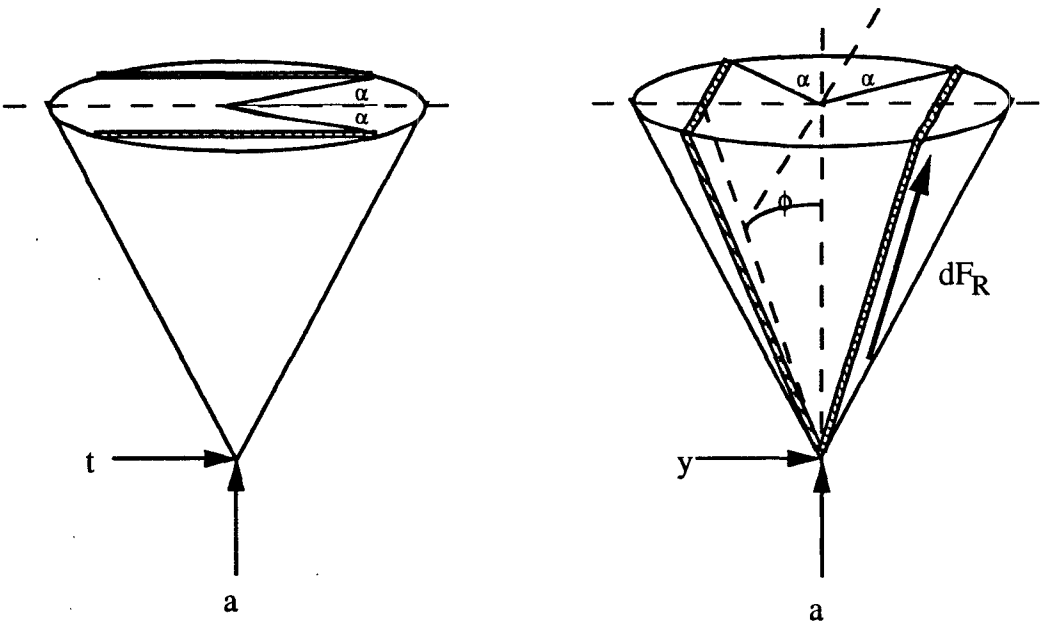

(a)

Type 1 Grit

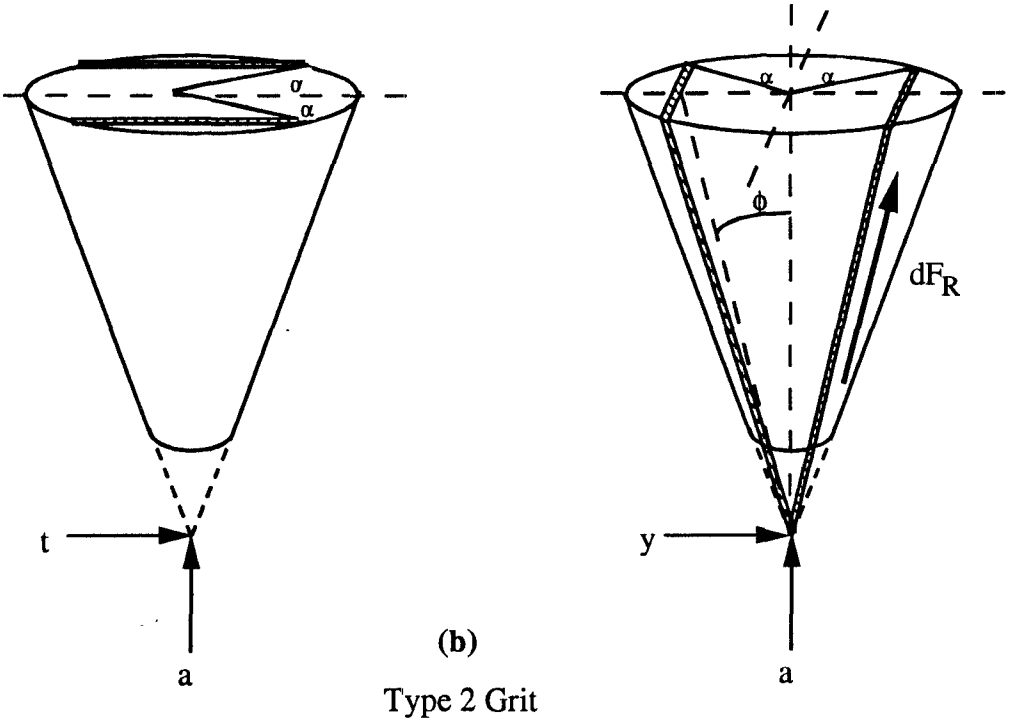

(b)

Type 2 Grit

Figure 4.6: Orientation of Triangular Elements on the Grits

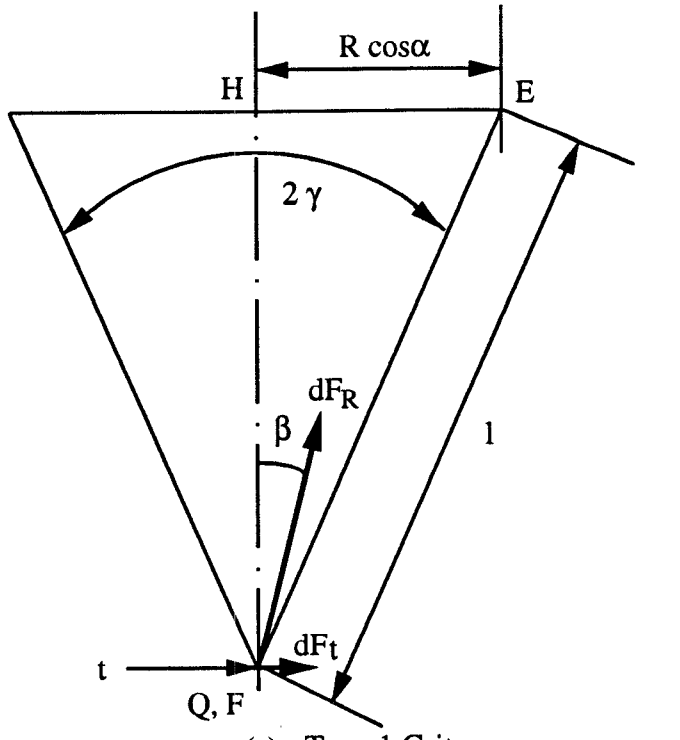

(a) Type 1 Grit

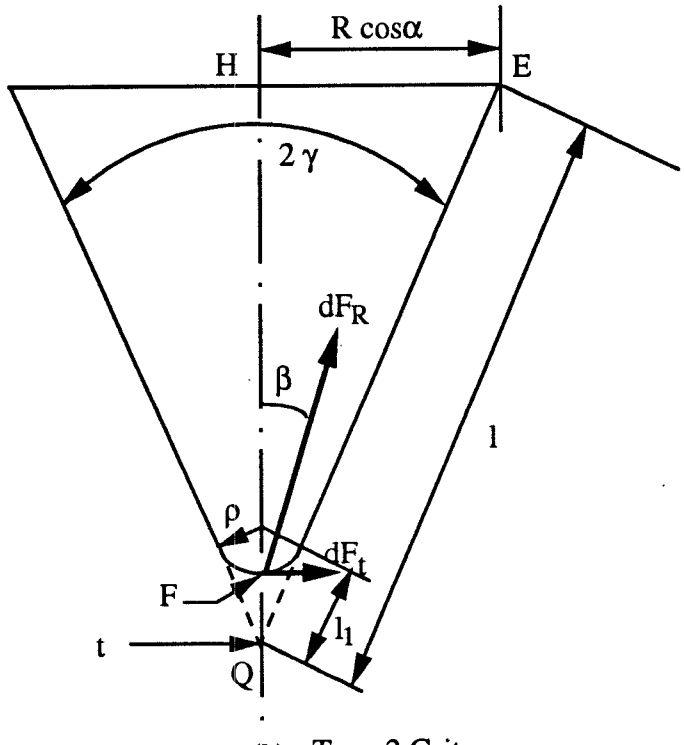

(b) Type 2 Grit

Figure 4.7: Triangular Elements of the Two Types of Grits

4.3.1 Determination of the Rake Angle for the Elements

Rake surface for a cutting tool is defined as a surface over which chips flow. Hence, the rake surface for the cone-shaped grits is the curved surface of the cone. Rake angle for a cutting tool is defined as the actual slope of the rake face with respect to the preferred reference plane through the axis of the rotating body (cutter or workpiece) passing through the tool nose as shown by the vertical dotted lines in Fig. 4.10 . The sign convention for the rake angle in case of single-point cutting is also shown in Fig. 4.10 .

The center plane AQB (See Figs. 4.3 and 4.4) of the cone shaped grit is the reference plane for the cone shaped grits with triangular elements. Triangular elements from each of the two types of grits are shown in Fig. 4.7 . The side EF in Fig. 4.7 is the cutting edge of the particular element. The center line QH of the each element as shown in Fig. 4.7 lies in the aforementioned center plane AQB shown in Figs. 4.3 and 4.4 . Therefore angle γ in Fig. 4.7 is the rake angle.

$$sin\,\gamma = \frac{R\,cos\,\alpha}{l} \tag{4.1}$$

We have, $sin\,\phi_0 = \frac{R}{l}$ with reference to Figs. 4.3 and 4.4 and therefore,

$$sin\,\gamma = sin\,\phi_0\,cos\,\alpha \tag{4.2}$$

Fig.4.8 presents the plot of γ vs. α where semi-cone angle ϕ_0 is equal to 45^o.

For a type 1 grit element, the rake angle is constant and is equal to γ and is negative following the sign convention as illustrated in Fig. 4.10 . But for a type 2 grit element the rake angle varies from -90^o to $-\gamma$ where γ is given by Eqn.

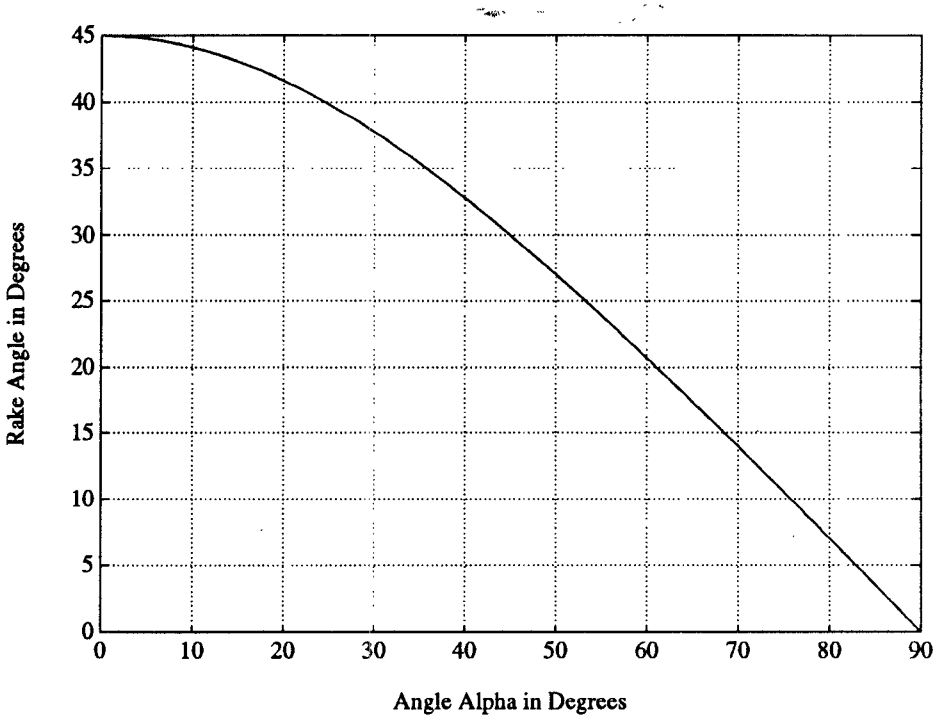

Figure 4.8: Plot of γ vs. α for $\phi_0 = 45^o$

4.2 . For this reason, an effective rake is defined for the type 2 grit. It is defined as the average of $\gamma(\xi)$ which is a function of ξ. Angle ξ is shown in Fig. 4.9 . Angle ξ varies from 0 to ξ_{max} where $\xi_{max} = \frac{\pi}{2} - \gamma$ and $\gamma(\xi) = \frac{\pi}{2} - \xi$.

$$\gamma_{effective} = \frac{1}{\xi_{max}} \int_0^{\xi_{max}} \gamma(\xi)\, d\xi = \frac{\pi}{2} - \frac{\xi_{max}}{2} \tag{4.3}$$

But, $\xi_{max} = \frac{\pi}{2} - \gamma$ and therefore,

$$\gamma_{effective} = \frac{\pi}{4} + \frac{\gamma}{2} \tag{4.4}$$

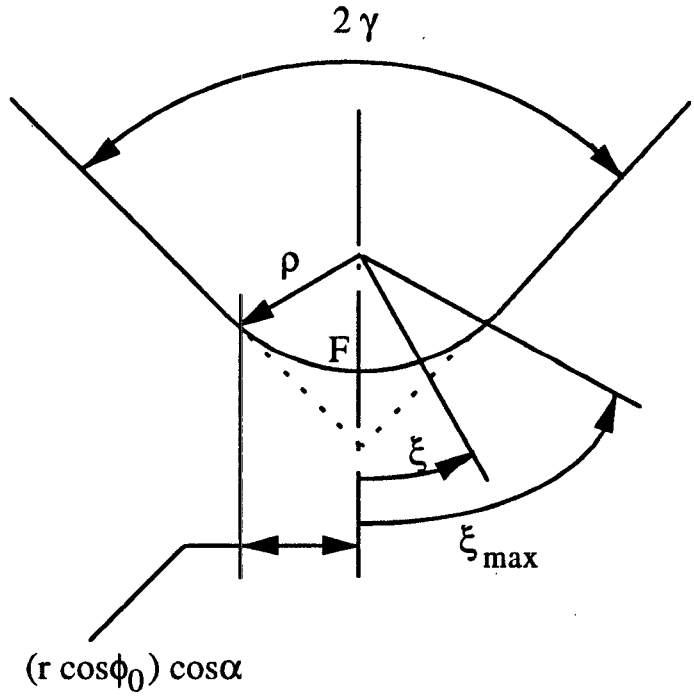

Figure 4.9: Enlarged View of the Tip Region of Type 2 Grit

4.3.2 Determination of the Cutting Area for the Elements

The elemental cutting area for an element of type 1 grit is given as :

$$dA = \frac{1}{2} l R \, d\alpha \tag{4.5}$$

where,

$-\frac{\pi}{2} \leq \alpha \leq \frac{\pi}{2}$ or, $|\alpha| \leq \frac{\pi}{2}$

The definition of angle α is shown in Fig. 4.6 .

l and R can be determined from known grit parameters as described in Section

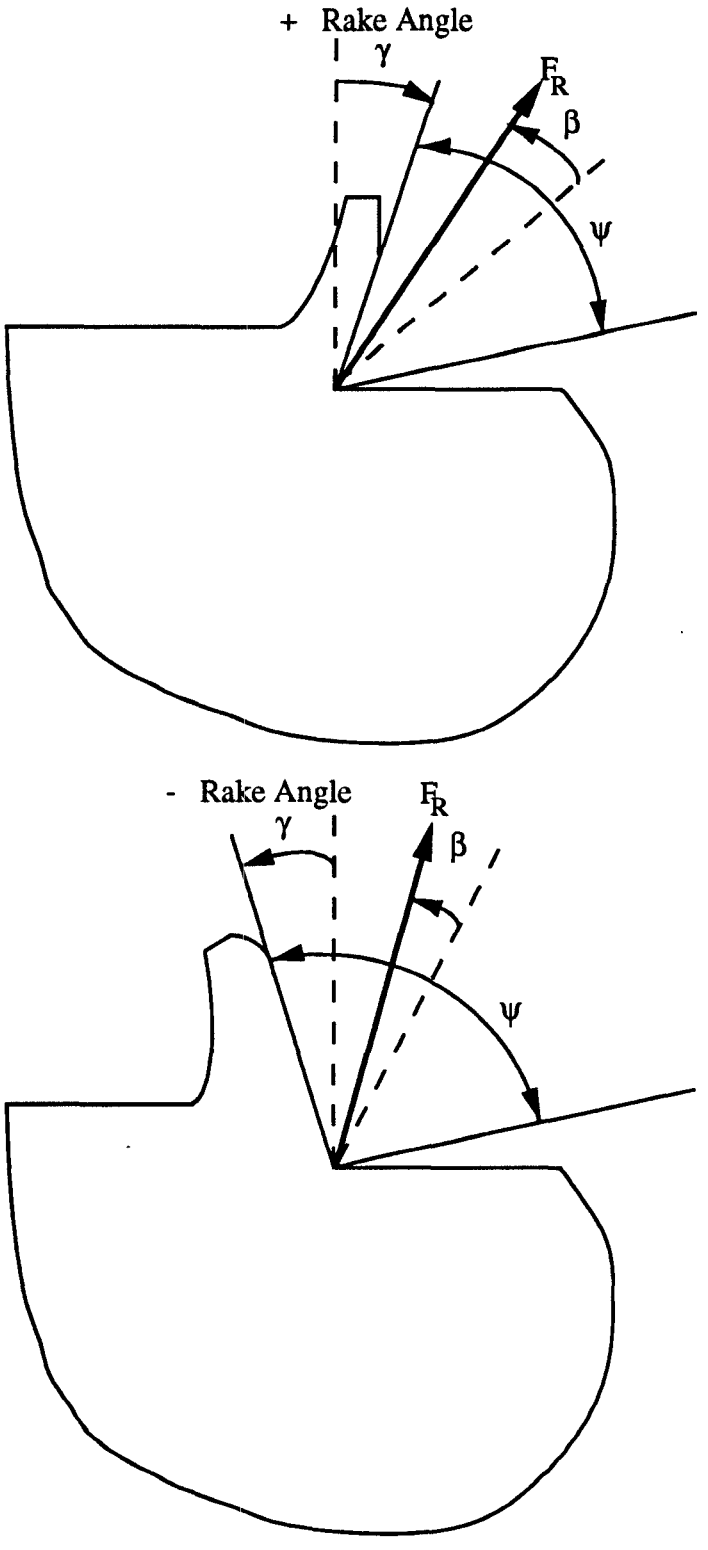

Figure 4.10: Sign Convention for Rake Angle in Single Point Tool

4.2 .

The curved part of an element of the type 2 grit is a part of an ellipse. For the purpose of estimating the elemental cutting area, the curved part of the element of a type 2 grit is assumed to be a part of a circle of radius ρ and tangent to the edges as shown in Fig. 4.7(b). From Figs. 4.4, 4.7(b) and 4.9, we have

$$\rho cos\gamma = (r\, cos\, \phi_0)\, cos\, \alpha \tag{4.6}$$

or,

$$\rho = \frac{r\, cos\, \alpha\, cos\, \phi_0}{cos\, \gamma} \tag{4.7}$$

Since, $sin\, \gamma = sin\, \phi_0\, cos\, \alpha$ or, $cos\, \alpha = \frac{sin\, \gamma}{sin\, \phi_0}$, and therefore we have,

$$\rho = \frac{r\, cos\, \phi_0\, sin\, \gamma}{cos\, \gamma\, sin\, \phi_0} = \frac{r\, tan\, \gamma}{tan\, \phi_0} \tag{4.8}$$

This equation satisfies the boundary conditions, i.e.,

@ $\alpha = 0 \Leftrightarrow \gamma = \phi_0 : \quad \rho = r$

@ $\alpha = \frac{\pi}{2} \Leftrightarrow \gamma = 0 : \quad \rho = 0$

Therefore, the elemental cutting area for type 2 grit is estimated as:

$$dA = \frac{1}{2}\, l\, R\, d\alpha - \frac{1}{2}\, l_1\, r\, cos\, \phi_0\, d\alpha + \frac{1}{2}\, \rho\, (\frac{\pi}{2} - \gamma)\, r\, cos\, \phi_0\, d\alpha \tag{4.9}$$

where,

$-\frac{\pi}{2} \leq \alpha \leq \frac{\pi}{2}$ or, $|\alpha| \leq \frac{\pi}{2}$

The parameter l_1 is illustrated in Fig. 4.4 and 4.7(b) and its expression is derived in Section 4.2 .

4.4 Grinding Force Model

4.4.1 Forces due to the Individual Elements

The resultant cutting force for the turning process F_R is given by

$$F_R = k_s A \tag{4.10}$$

where,

k_s is the unit cutting force which mainly depends on the workpiece material.

A is cutting area and given by

$A = (feed/rev)(depth\ of\ cut) = (thickness\ of\ uncut\ chip)(width\ of\ uncut\ chip)$

The resultant cutting force that would cause zero stress in the tool face acts at an angle β from the center line for the wedge shaped tool. The angle β is given by (Refer [17])

$$tan\,\beta = -(cot\,\frac{\psi}{2})\,\frac{\psi - sin\,\psi}{\psi + sin\,\psi} \tag{4.11}$$

where,

ψ is the lip angle of the cutting tool as shown in Fig. 4.10 .

Similarly, the elemental cutting force for the triangular element, dF_R is given by

$$dF_R = k_s\,dA \tag{4.12}$$

And for zero stress in the triangular element, dF_R should act at an angle β (See Fig. 4.7) from the center line of the triangular element as mentioned above. For the triangular elements of the cone shaped grits, the lip angle is equal to twice

the rake angle γ. Therefore, the expression for angle β can be written in terms of angle γ as

$$\tan \beta = -(cot\,\gamma)\,\frac{2\gamma - sin\,2\gamma}{2\gamma + sin\,2\gamma} \tag{4.13}$$

For type 2 grit, instead of γ, $\gamma_{effective}$ is used to determine the angle β.

The elemental force dF_R can be broken into three components, namely, dF_t, dF_a and dF_y (See Fig. 4.7).

where,

$$dF_t = k_s\,dA\,sin\,\beta \tag{4.14}$$

$$dF_a = k_s\,dA\,cos\,\beta\,cos\,\phi \tag{4.15}$$

where,

ϕ is as shown in Fig. 4.6 .

But, $tan\,\phi = \frac{R\,sin\,\alpha}{h}$ and $tan\,\phi_0 = \frac{R}{h}$ and therefore, $tan\,\phi = tan\,\phi_0\,sin\,\alpha$

And hence,

$cos\,\phi = \frac{1}{\sqrt{1 + tan^2\phi_0\,sin^2\alpha}}$

Based on the above relations,

$$dF_a = \frac{k_s\,dA\,cos\beta}{\sqrt{1 + tan^2\phi_0\,sin^2\alpha}} \tag{4.16}$$

And,

$$dF_y = k_s\,dA\,cos\beta\,sin\phi \tag{4.17}$$

Therefore, forces due to the individual elements can be written as follows.

$$F_{x_{element}} = -dF_t\,sin\,\theta - dF_a\,cos\,\theta \tag{4.18}$$

$$F_{y_{element}} = dF_y \tag{4.19}$$

$$F_{z_{element}} = dF_t \cos\theta - dF_a \sin\theta \tag{4.20}$$

where,

θ is the angular position of the grit with respect to positive $x-$axis as shown in Fig. 4.2.

4.4.2 Forces due to a Single Grit

The total grinding forces due to a single grit can be determined by integrating the expressions for $F_{x_{element}}, F_{y_{element}}, F_{z_{element}}$ from $\alpha = -\frac{\pi}{2}$ to $\alpha = \frac{\pi}{2}$. The y component of the total grinding force due to a single grit is equal to zero since the elements are symmetric about the ta plane. In other words, $F_{y_{element}}$ due to the element at $\alpha = \alpha_0$ is equal and opposite to $F_{y_{element}}$ due to the element at $\alpha = -\alpha_0$ where α_0 is any suitable value of α.

The expressions for $F_{x_{grit}}$ and $F_{z_{grit}}$ are given below.

$$F_{x_{grit}} = -2\sin\theta \int_{\alpha=0}^{\alpha=\frac{\pi}{2}} dF_t - 2\cos\theta \int_{\alpha=0}^{\alpha=\frac{\pi}{2}} dF_a \tag{4.21}$$

$$F_{z_{grit}} = 2\cos\theta \int_{\alpha=0}^{\alpha=\frac{\pi}{2}} dF_t - 2\sin\theta \int_{\alpha=0}^{\alpha=\frac{\pi}{2}} dF_a \tag{4.22}$$

$$F_{y_{grit}} = 0 \tag{4.23}$$

where,

$$\int_{\alpha=0}^{\alpha=\frac{\pi}{2}} dF_t = k_s \int_{\alpha=0}^{\alpha=\frac{\pi}{2}} \sin\beta \, dA \tag{4.24}$$

$$\int_{\alpha=0}^{\alpha=\frac{\pi}{2}} dF_a = k_s \int_{\alpha=0}^{\alpha=\frac{\pi}{2}} \frac{\cos\beta \, dA}{\sqrt{1 + tan^2\phi_0 \sin^2\alpha}} \tag{4.25}$$

dA is a function of angles α and γ as expressed in Eqns. 4.5 and 4.9 . Also, angle β is a function of rake angle γ as expressed in Eqn. 4.13 . But rake angle γ is a function of angle α only as shown in Eqn. 4.2 . Hence, the integrands in Eqns. 4.24 and 4.25 are the functions of angle α only. The grinding forces F_x and F_z due to single grit are listed in the following two tables for both the types of grits for three different values of θ.

It is clear from Eqns. 4.5 and 4.9 that dA is dependent on l, R, l_1, r, ϕ_0, γ, ρ etc. But quantities like l_1, r, ϕ_0, γ, ρ are fixed for a grit and are not dependent on the coordinates of the center of the grinding wheel which undergoes vibration as discussed in the next chapter. Hence, dA is a function of l, R and fixed grit parameters. l is a function of R and ϕ_0 as shown in Section 4.2 . In turn, R is a function of h and other fixed grit parameters as also explained in Section 4.2 . And hence, dA is a function of h^2 and other fixed grit parameters. h is dependent on z_{tip} and θ. But, z_{tip} is dependent on z-coordinate of the center of the grinding wheel (z_c) which varies with time, grit height and θ as mentioned in Section 4.2 . And therefore, dA is a function of z_c^2, z_c, θ and fixed grit parameters. Consequently, dF_t and dF_x and hence, F_{xgrit} and F_{xgrit} are functions of z_c^2, z_c, θ and fixed grit parameters.

4.4.3 Total Forces in the Grinding Process

The total cutting force in the grinding process is the summation of cutting forces due to individual grits engaged in material removal at a given instant of time.

ϕ_0 $= 45^o$

Nose radius for type 2 grit $= 0.005$ mm

For Downfeed = 0.0508 mm :

θ	Grit type	F_{xgrit} in N	F_{zgrit} in N
268.5°	Type 1 grit	-0.181	1.122
	Type 2 grit	-0.343	1.389
270.0°	Type 1 grit	-2.002	10.59
	Type 2 grit	-3.113	11.33
271.5°	Type 1 grit	-0.240	1.111
	Type 2 grit	-0.414	1.369

For Downfeed = 0.0762 mm :

θ	Grit type	F_{xgrit} in N	F_{zgrit} in N
268.5°	Type 1 grit	-1.173	7.243
	Type 2 grit	-1.946	7.884
270.0°	Type 1 grit	-4.505	23.84
	Type 2 grit	-6.829	24.85
271.5°	Type 1 grit	-1.551	7.172
	Type 2 grit	-2.356	7.771

Mathematically,

$$F_{x_{total}} = \sum_{i=1}^{N} F_{x_{grit_i}} \tag{4.26}$$

$$F_{z_{total}} = \sum_{i=1}^{N} F_{z_{grit_i}} \tag{4.27}$$

where,

N is number of grits in contact with the workpiece at a particular instant.

It has been mentioned that F_{xgrit} and F_{xgrit} are functions of z_c^2, z_c, θ and fixed grit parameters. Since, θ is a function of time and at different instants of time different sets of grit are in contact with the workpiece, $F_{x_{total}}$ and $F_{z_{total}}$ are functions of z_c^2, z_c and time, t. Therefore let,

$$F_{x_{total}} = f_1(z_c^2, z_c, t) \tag{4.28}$$

$$F_{z_{total}} = f_2(z_c^2, z_c, t) \tag{4.29}$$

The expressions for $f_1(z_c^2, z_c, t)$ and $f_2(z_c^2, z_c, t)$ are not required since forces F_x and F_z are determined numerically and hence, explicit expressions for these quantities are not presented in this thesis.

It is clear from the above derivation that the rake angle varies from one element of a grit to another element of the same grit. This kind of variation in rake angle within a grit has been accounted in the grinding force model developed above. Also, the rake angle of an element of a grit at a given angle α differs from the rake angle of a corresponding element at the same α but of a different grit due to the difference in the semi-cone angle between the two grits. This kind of

variation in rake angle among the grits has also been considered in the grinding force model developed above. In brief, the effect of variation in rake angle within a grit and from grit to grit has been included in the grinding force model developed in this chapter. The grinding force model developed here includes the contribution of each grit in contact with the workpiece at any instant taking into account the random variation of the individual grit geometry.

Chapter 5

Modeling of the Grinding Machining System

5.1 Introduction

Machine tool vibration adversely affects the surface quality of a machined surface. Like the vibration observed in other machining processes, the vibration observed in grinding process is also classified into two types: *forced vibration* and *self-excited vibration.* Forced vibrations are caused by unbalance or/and disturbances introduced by the spindle structure, vibration of neighbouring machine tools etc. Any self-excited vibration is mainly linked to the cutting process. The variation of the cutting force follows a dynamic pattern that excites the machine tool structure and feeds back its effect to the cutting process, forming a closed loop system. The machine tool vibration due to the cutting process itself is also called

Machine Tool Chatter. The various grits of the grinding wheel have varying geometry. Since different grits with different geometry are in contact with the workpiece at different instants, the grinding force varies with time resulting in machine tool chatter.

In order to predict surface topography generated during grinding, it is necessary to include the effects of the grinding machine vibrations in the model developed for simulating the surface topography. Such a model requires a dynamic model of the machine tool structure to take into consideration the effect of structural dynamics of the machine tool on the surface topography generated during the machining process.

Fig. 5.1 presents a typical model for a machining system. The model was developed by Merritt [13]. This model has two feedback paths one is called primary feedback path and the other regenerative feedback path. Regeneration is defined as the effect of machining performed in previous pass or previous revolution on the machining performed in current pass or current revolution. In this chapter a mathematical model for the grinding machining system is developed.

5.2 Dynamic Modeling of the Machine Tool Structure

In a machining system, the machine tool and the workpiece are susceptible to chatter. In a surface grinding process, the workpiece is held firmly on the machine

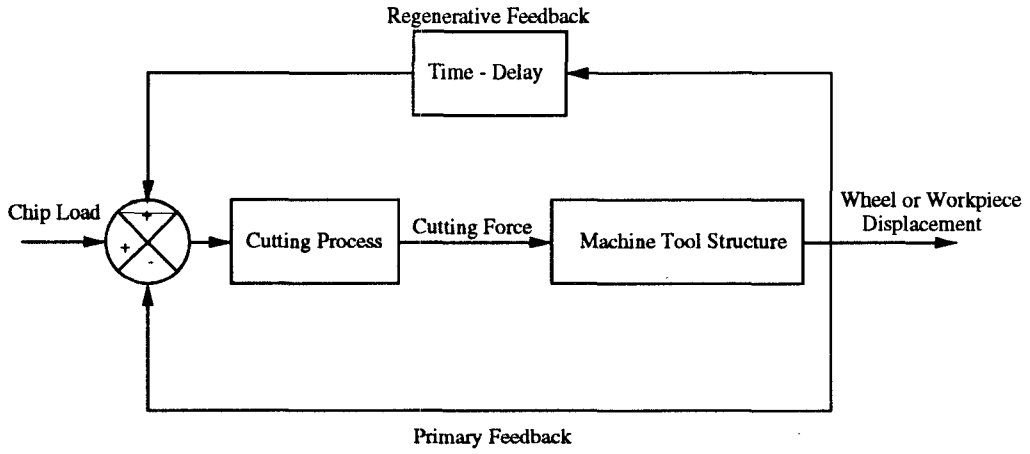

Figure 5.1: A Typical Dynamic Model for a Machining System

tool table and hence, the dynamics of the workpiece is neglected in this thesis work. Therefore, only the dynamics of the wheel is modeled, since it is considered to be more dominant factor than the dynamics of the workpiece.

In the dynamic model, the grinding wheel is treated as a discrete lumped parameter system with two degrees of freedom, each of which displays second order dynamics as shown in Fig. 5.2 .

Two differential equations can be used to describe the wheel motion during grinding.

$$m\,\frac{d^2q_1(t)}{dt^2} + c_1\,\frac{dq_1(t)}{dt} + k_1\,q_1(t) = F_1(t) \tag{5.1}$$

$$m\,\frac{d^2q_2(t)}{dt^2} + c_2\,\frac{dq_2(t)}{dt} + k_2\,q_2(t) = F_2(t) \tag{5.2}$$

or,

$$q_1(t) = \frac{F_1(t)}{m\,p^2 + c_1\,p + k_1} = \frac{F_1(t)/m}{p^2 + 2\,\zeta_1\,\omega_1\,p + \omega_1^2} \tag{5.3}$$

$$q_2(t) = \frac{F_2(t)}{m\,p^2 + c_2\,p + k_2} = \frac{F_2(t)/m}{p^2 + 2\,\zeta_2\,\omega_2\,p + \omega_2^2} \tag{5.4}$$

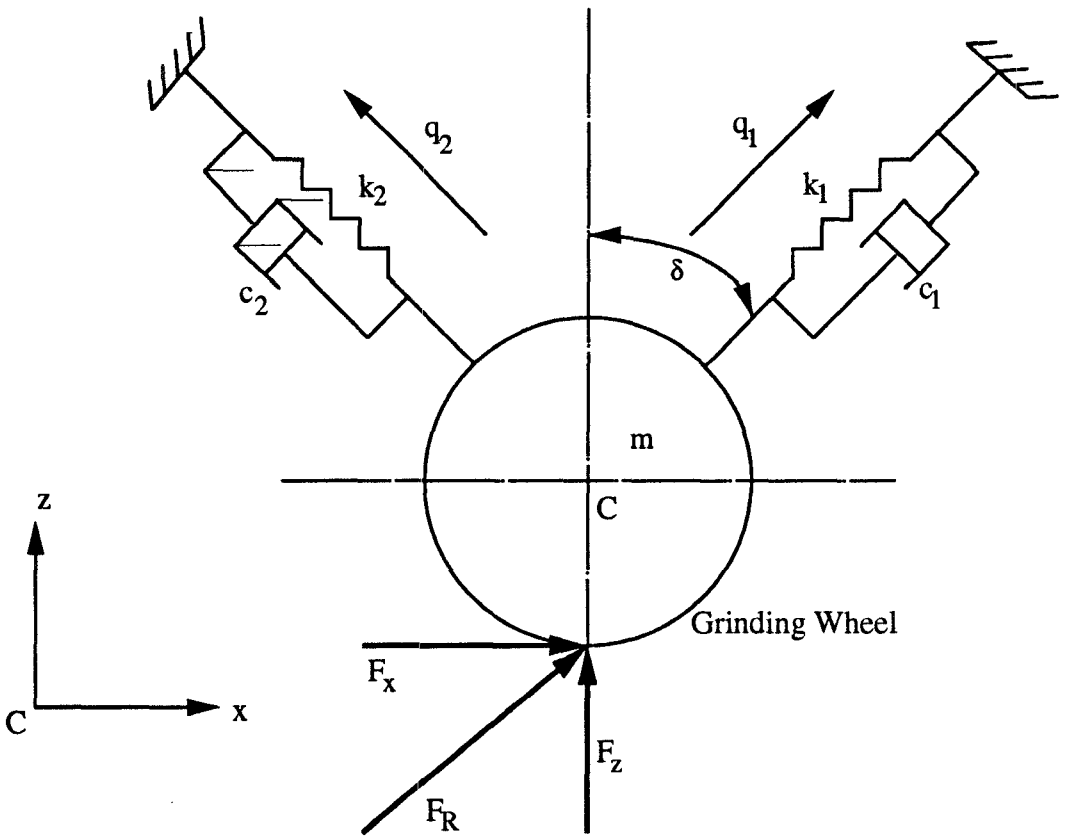

Figure 5.2: Modeling of the Grinding System Dynamics

where,

$q_1(t)$ and $q_2(t)$ are the displacements of the grinding wheel along the two principal modes.

m is the equivalent mass of the grinding wheel.

k_1 and k_2 are the stiffnesses along the two principal modes.

c_1 and c_2 are the damping factors along the two principal modes.

$F_1(t)$ and $F_2(t)$ are the resultant external forces along the principal modes.

$p \equiv \frac{d}{dt}$

$p^2 \equiv \frac{d^2}{dt^2}$

$\omega_1 = \sqrt{\frac{k_1}{m}}$

$\zeta_1 = \frac{c_1}{2\sqrt{m\,k_1}}$

$\omega_2 = \sqrt{\frac{k_2}{m}}$

$\zeta_2 = \frac{c_2}{2\sqrt{m\,k_2}}$

And,

$$F_1(t) = F_x(t)\,sin\,\delta + F_z(t)\,cos\,\delta \tag{5.5}$$

$$F_2(t) = -F_x(t)\,cos\,\delta + F_z(t)\,sin\,\delta \tag{5.6}$$

In Eqns. 5.5 and 5.6 $F_x(t)$ and $F_z(t)$ are the components of the resultant cutting force along the x and z direction respectively. As illustrated in Fig. 5.2, angle δ represents the angle between the first principal mode and the positive z-axis.

Due to the vibration of the grinding wheel, the position of the center of the grinding wheel changes. Let $(x_c(t),\ z_c(t))$ be the coordinates of the center of the grinding wheel at an instant. Let $\tilde{x}_c(t)$ and $\tilde{z}_c(t)$ be the dynamic variation of

$x_c(t)$ and $z_c(t)$ respectively. From Fig. 5.2, we have

$$\tilde{x}_c(t) = q_1(t)\, sin\, \delta - q_2(t)\, cos\, \delta \tag{5.7}$$

$$\tilde{z}_c(t) = q_1(t)\, cos\, \delta + q_2(t)\, sin\, \delta \tag{5.8}$$

And,

$$x_c(t) = x_{c_o} + \tilde{x}_c(t) \tag{5.9}$$

$$z_c(t) = z_{c_o} + \tilde{z}_c(t) \tag{5.10}$$

where,

(x_{c_o}, z_{c_o}) is the equilibrium position of the center of the grinding wheel.

The expressions for $F_x(t)$ and $F_z(t)$ are of the following forms as explained in the previous chapter.

$$F_x(t) = f_1(z_c^2, z_c, t) \tag{5.11}$$

$$F_z(t) = f_2(z_c^2, z_c, t) \tag{5.12}$$

Based on the above equations, the grinding machining system can be represented in a block diagram as illustrated in Fig. 5.3 .

Thus, the position of the center of the grinding wheel ($x_c(t)$, $z_c(t)$) for any instant t can be determined from equations 5.7 to 5.10 . Now dynamically varying $x_c(t)$ and $z_c(t)$ can be used in the grinding model instead of constants x_{c_o} and z_{c_o} in order to simulate the surface topography generated during the grinding process taking into account the machine tool chatter.

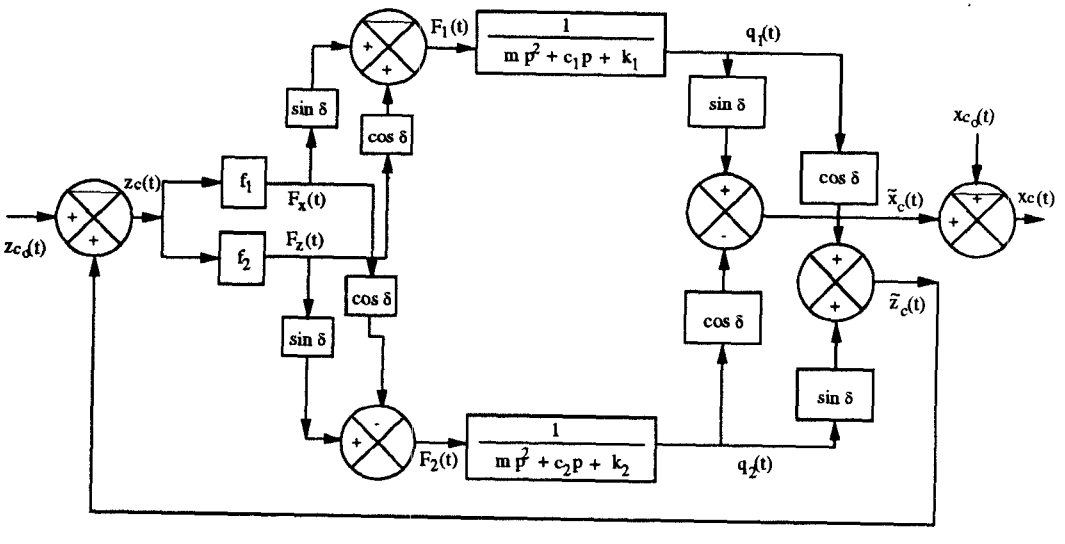

Figure 5.3: A Block Diagram Representation of the Grinding System

Chapter 6

Surface Topography Generation in Presence of Chatter

The generation of ideal ground surface topography has been discussed in detail in Chapter 3. But during the grinding process, physical phenomena like grinding wheel wear, thermal damage, machine tool vibration etc. occur. These phenomena severely affect the ground surface texture. In this thesis work, an effort is made to include the effect of machine tool chatter on the ground surface topography generation. In this regard, a grinding force model is developed in Chapter 4 and a model capable of characterizing the dynamics of the grinding machining system is developed in Chapter 5.

At any instant, the forces due to individual grits which are in contact with the workpiece are determined taking into account the variation in depth of cut of the individual grits with time. At a particular instant, forces $F_{x_{total}}$ and $F_{z_{total}}$ due

to the cutting action of the grits in contact with the workpiece are calculated. Then the vibrations along the two principal modes q_1 and q_2 are determined as discussed in Chapter 5. The sample time Δt is chosen as a fraction of the smallest of the two time periods. Knowing $q_1(t)$ and $q_2(t)$, the variations of x_c and z_c - the coordinates of the center of the grinding wheel - can be determined using Eqns. 5.7 and 5.8 . The current values of x_c and z_c are used to locate the individual grits which are in contact with the workpiece and to determine the depth of cut of these individual grits. And then the above mentioned steps are repeated as explained from the beginning of this paragraph. The dynamical analysis is performed for both upgrinding and downgrinding. The results of the dynamical analysis are stored. $F_{x_{total}}$, $F_{z_{total}}$, x_c, z_c for upgrinding and downgrinding are stored in two separate files for every time step. The ideal ground surface topography is then generated as explained in Chapter 3. Also, the time instant $t(i,j)$ when each point (i,j) on the workpiece surface is ground is determined using the following equation.

$$t(i,j) = 60\,\frac{tan^{-1}\left(\frac{x}{z}\right)}{2\,\pi\,N} + t_o \tag{6.1}$$

where,

x is the x - coordinate of point (i,j) in xyz coordinate system attached to the axis of the grinding wheel just above the center of the corresponding cavity as discussed in Chapter 3.

z is the z - coordinate of point (i,j) in xyz coordinate system attached to the axis of the grinding wheel just above the center of the corresponding cavity and

is related to workpiece Z-coordinate as $Z(i,j) = -(z - z_{c_o})$ as per the transformation rule given in Eqn. 3.40 .

t_o is found out using Eqns. 3.36 and 3.37 .

z_{c_o} is the distance between the center of the grinding wheel and the top unmachined surface of the workpiece in absence of machine tool chatter and $z_{c_o} = mean\ \ grit\ \ height + D/2 - downfeed.$

D is the diameter of the grinding wheel.

N is the rpm of the grinding wheel.

Also, whether a point (i,j) on the workpiece is ground during upgrinding or downgrinding is noted. Then, the time instant t' closest to $t(i,j)$ corresponding to the point (i,j) is found out from the file containing the results of the dynamical analysis. The appropriate file is read out depending on whether the point (i,j) on the workpiece is ground during upgrinding or downgrinding. Corresponding to time t', the quantities x_c and z_c are read out from the file. The amount of vibration that the grinding wheel undergoes is given by (Refer Eqns. 5.9 and 5.10)

$$\tilde{x}_c(t) = x_c(t) - x_{c_o} \tag{6.2}$$

$$\tilde{z}_c(t) = z_c(t) - z_{c_o} \tag{6.3}$$

where,

(x_{c_o}, z_{c_o}) is the equilibrium position of the center of the grinding wheel.

$(x_c(t), z_c(t))$ is the position of the center of the grinding wheel at any time t.

$\tilde{x}_c(t)$ and $\tilde{z}_c(t)$ is the dynamic variation of $x_c(t)$ and $z_c(t)$ respectively.

The effect of the grinding wheel vibration is then superimposed on the ideal surface topography to generate the ground surface topography in presence of machine tool chatter.

Flow chart explaining the basic methodology followed to generate the ground surface topography in presence of machine tool chatter is listed in Tables 6.1 and 6.2. Table 6.3 lists the flow chart depicting the overall methodology adopted to generate the ground surface topography in presence of machine tool chatter.

Thus the simulation package developed in this thesis can predict the ideal ground surface topography and ground surface topography in presence of machine tool chatter taking into account randomly varying grain size, random location and distribution of grits and effect of these random variations on the grinding force.

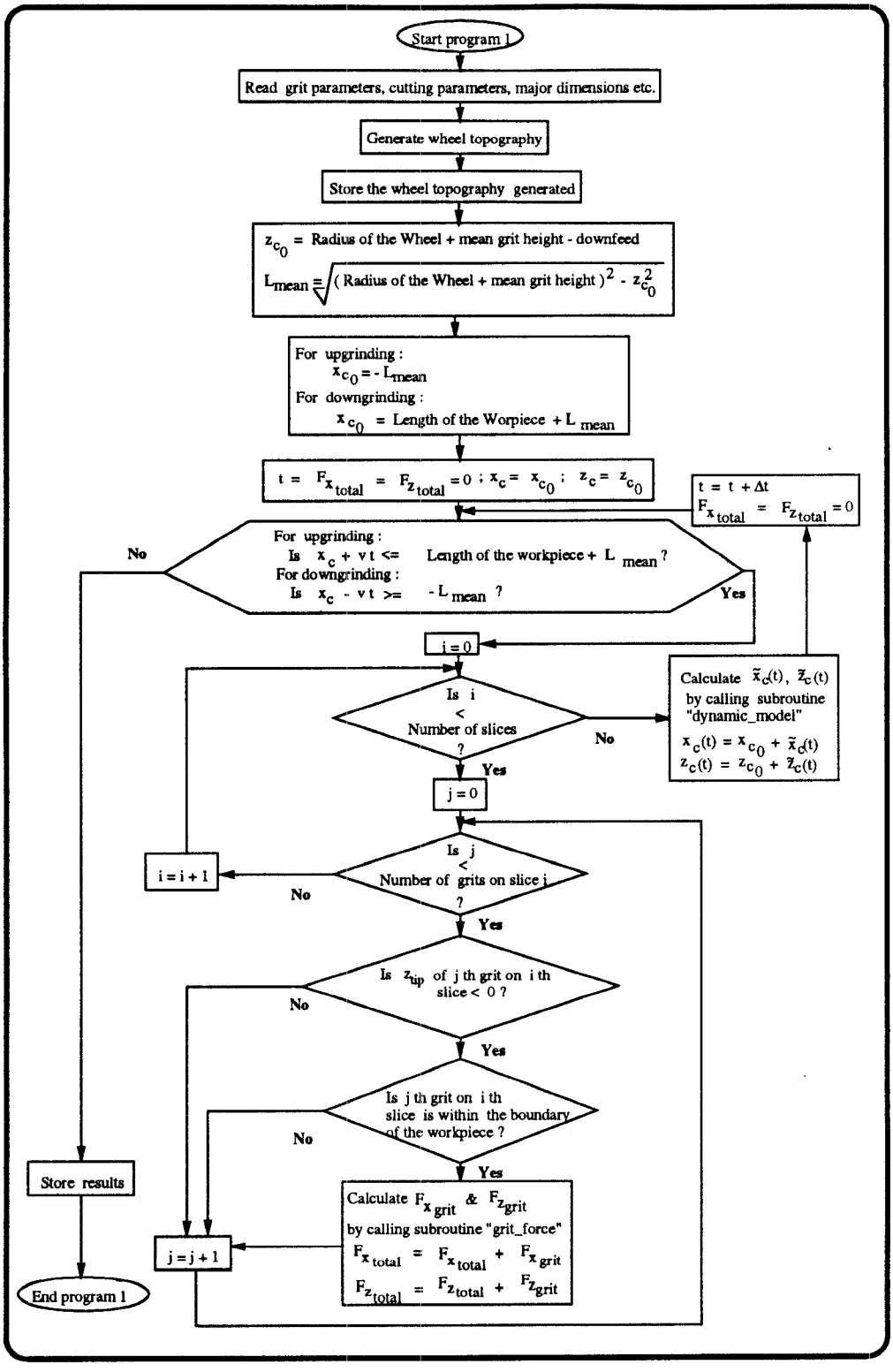

Table 6.1: Flow Chart for Dynamical Analysis

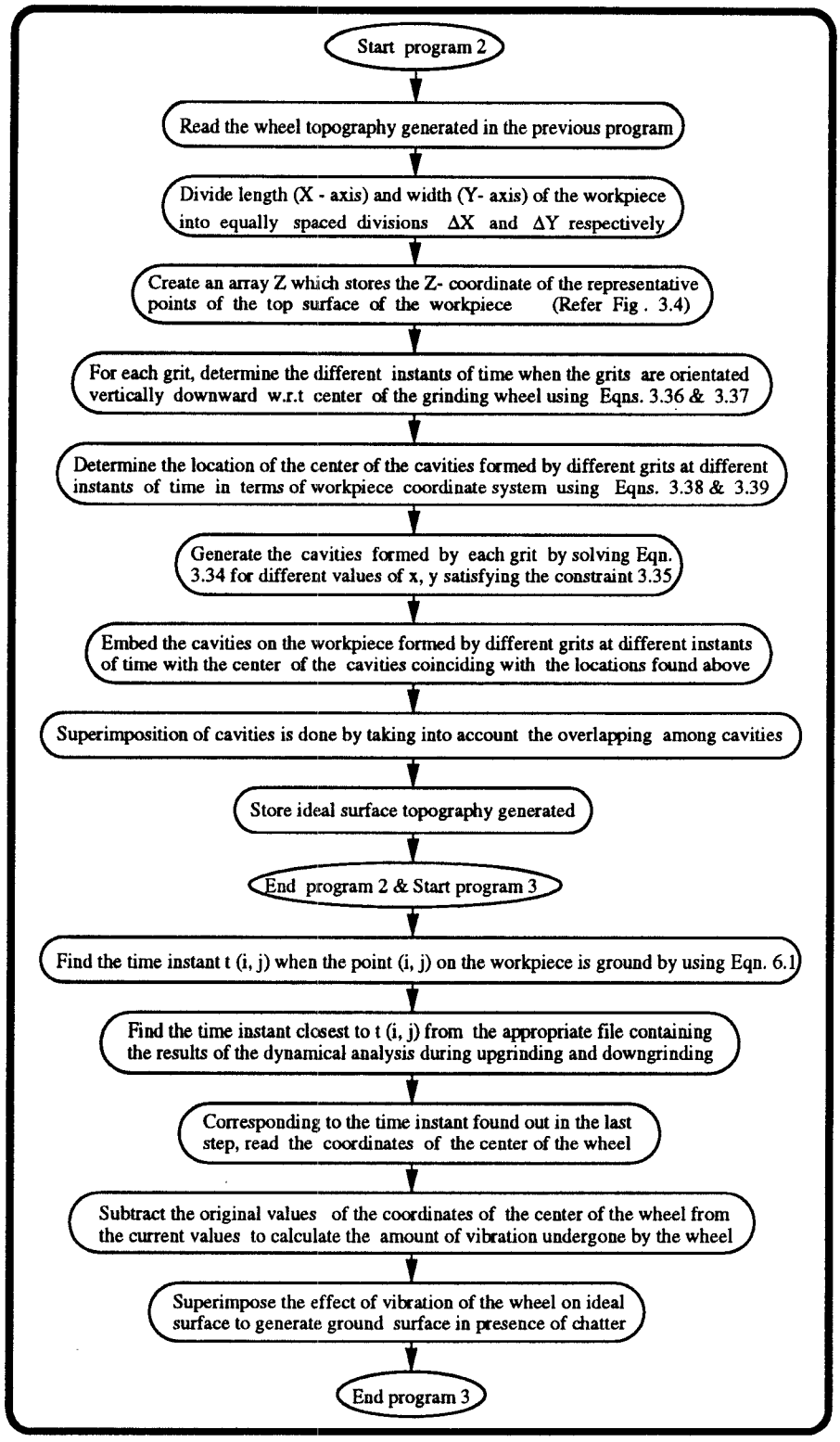

Table 6.2: Flow Chart for Surface Topography Generation in Presence of Chatter

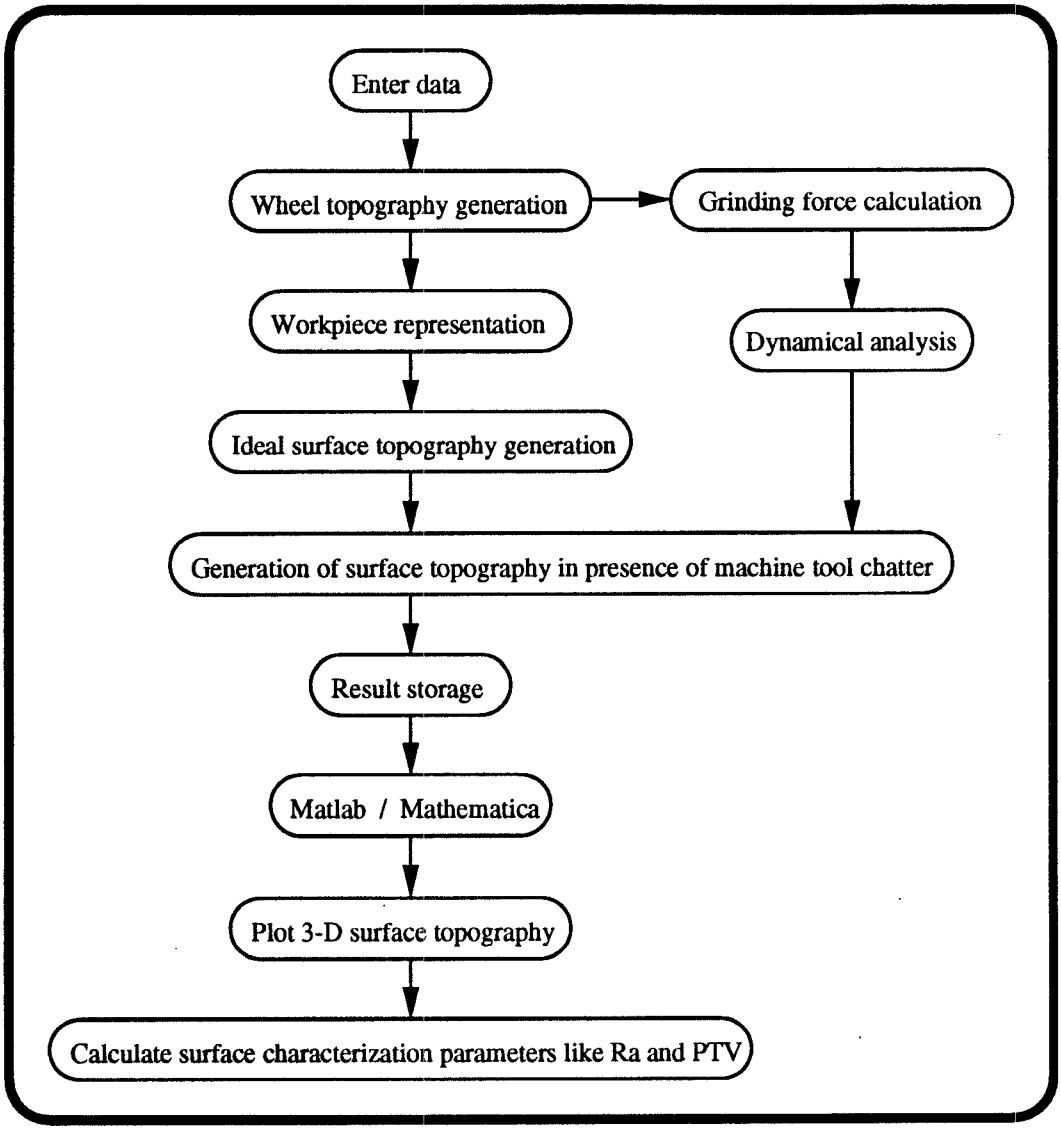

Table 6.3: Plan for Surface Topography Generation in Presence of Chatter

Chapter 7

Experimental and Simulation Results

In this chapter, the experimental work performed in this thesis work is discussed. Experimental set ups used to perform various experiments are explained and experimental results are presented. Simulation results are discussed and are compared with the experimental results.

7.1 Experimental Verification

7.1.1 Experimental Set Ups

Grinding experiments are performed in the machine shop of Stone Industrial, College Park, MD. The experimental arrangement used to perform the grinding experiments is illustrated in Fig. 7.1 . The surface grinding machine used is

Brown and Sharpe 618 Micromaster Surface Grinding Machine. An aluminium oxide grinding wheel is used. Relevant specifications of the grinding wheel are listed in Table 7.1 .

1. Abrasive Type	: Aluminium Oxide
2. Abrasive Size	: 60
3. Grade	: J
4. Bond Type	: Vitrified
5. Wheel Diameter	: $7\frac{7}{8}$ in = 200 mm
6. Wheel Width	: 0.5 in = 12.7 mm

Table 7.1: Important Specifications of the Grinding Wheel

The grinding experiments are performed based on 2^2 factorial design. 2^2 factorial design means there are two experimental parameters which vary during the course of the experiment and each of these parameters has two different levels and hence, there are four sets of experimental conditions. Therefore, four samples of steel are prepared for the grinding experiments. First, all four samples are machined simultaneously to ensure similar surface conditions prior to the experiment. During the course of the experiment, the RPM of the grinding wheel and the table speed are kept constant. The grinding wheel is rotated at a constant speed of 3450 revolutions per minute. The table speed is fixed at 100 feet per minute which is equivalent to 508 millimeters per second. Crossfeed and downfeed are the experimental parameters which are varied during the experiments.

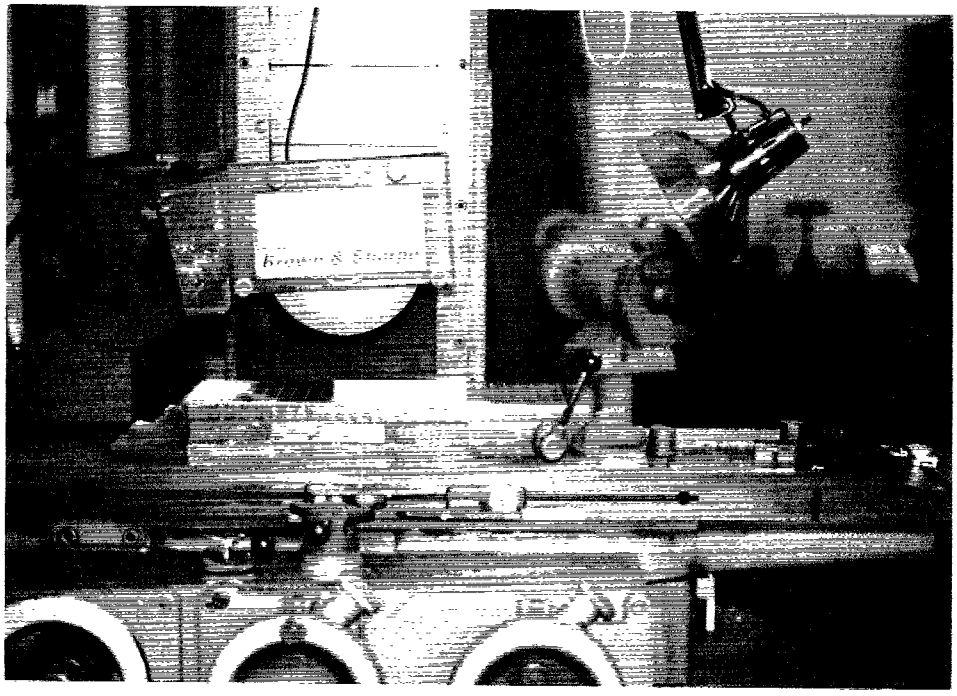

Figure 7.1: Experimental Set Up for Grinding Experiments

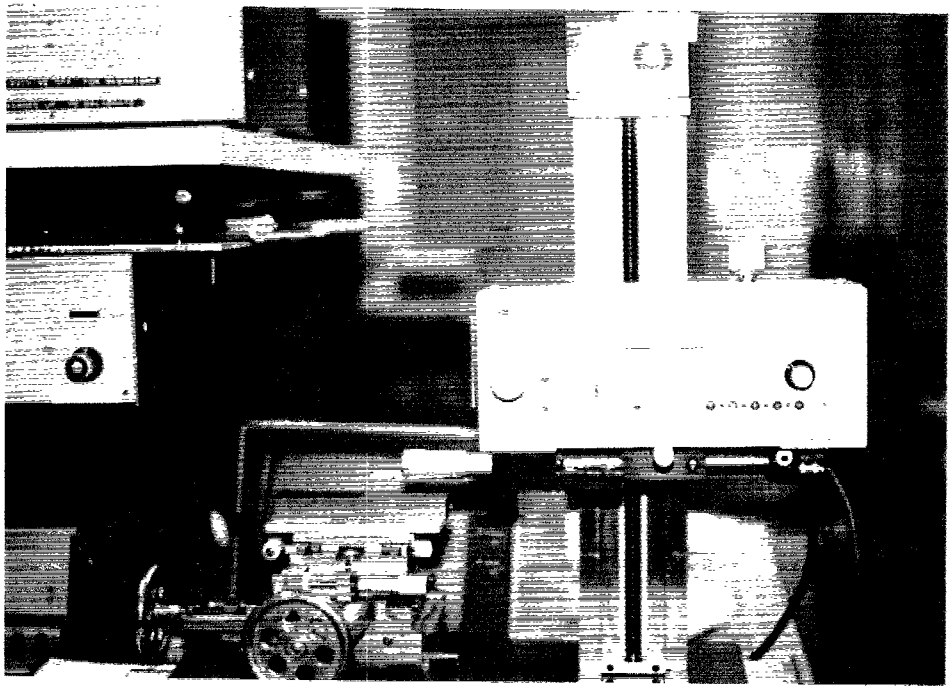

Figure 7.2: Experimental Set Up for Surface Roughness Measurements

In order to perform the factorial design, two different crossfeeds and downfeeds are chosen. The desired cutting conditions for the factorial design are listed in Table 7.2 . In Table 7.2, '+' and '−' represent high and low levels respectively of a particular experimental parameter. Then the four steel specimens are ground

Test Number	Crossfeed mm (inch)	Downfeed mm (inch)
1	0.2032 (0.008) +	0.0762 (0.003) +
2	0.2032 (0.008) +	0.0508 (0.002) −
3	0.1016 (0.004) −	0.0762 (0.003) +
4	0.1016 (0.004) −	0.0508 (0.002) −

Table 7.2: Desired Cutting Conditions for Factorial Design

at these four different sets of cutting conditions. Due to human errors or other

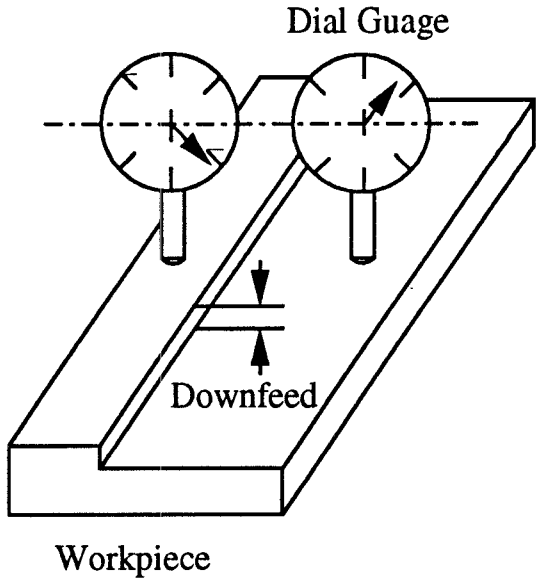

Figure 7.3: Set Up for Measurement of the Actual Downfeed

uncertainties the actual downfeed usually differs from the desired or intended downfeed. In order to measure the actual downfeed, a small portion of the workpiece is left unground. Using a dial guage, the actual downfeed is determined for each of the specimens as illustrated in Fig. 7.3 . The actual cutting conditions are listed in Table 7.3 .

The surface roughness measurements are performed at the Precision Engineering Division of the National Institute of Standards and Technology, Gaithersburg, MD. A surface profilometer is used to measure the surface characterization parameters, such as R_a, R_q and PTV as defined in Section 3.2.2 in Chapter 3. The set up used to perform surface roughness measurements is illustrated in Fig. 7.2

.

A scanning electron microscope is used to scan the ground specimens in order

Test Number	Crossfeed mm (inch)	Downfeed mm (inch)
1	0.2032 (0.008)	0.0910 (0.0035)
2	0.2032 (0.008)	0.0465 (0.0018)
3	0.1016 (0.004)	0.1058 (0.0041)
4	0.1016 (0.004)	0.0402 (0.0016)

Table 7.3: Actual Cutting Conditions

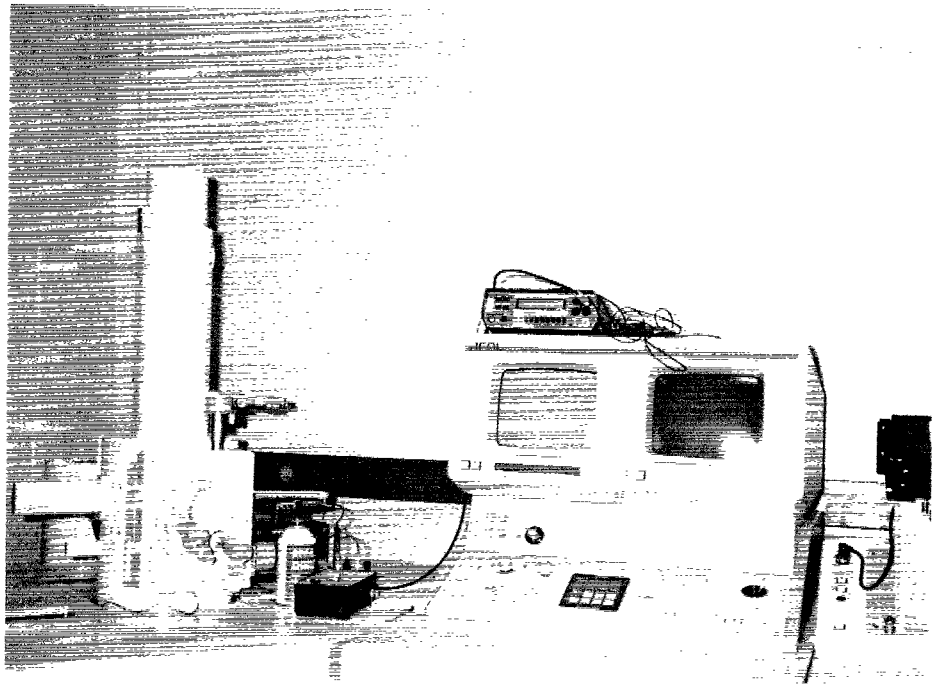

Figure 7.4: Scanning Electron Microscope

to get 3-D plots of the actual ground surfaces. The SEM set up used for this purpose is illustrated in Fig. 7.4 . The photographs taken on SEM are scanned and processed with the help of an image processing software to get three dimensional plots of the ground surfaces.

7.1.2 Experimental Results

The measured values for R_a, R_q and PTV obtained from the experiments for the aforementioned four cutting conditions are listed in Table 7.4 . From the mea-

sured values of R_a, R_q and PTV, it can be seen that the quality of the surface ground at higher crossfeed with larger downfeed is the worst and that ground at lower crossfeed with smaller downfeed is the best. Based on the experimen-

Test Number	Crossfeed Direction			Grinding Direction		
	R_a μm	R_q μm	PTV μm	R_a μm	R_q μm	PTV μm
1	0.164	0.220	1.630	0.082	0.100	0.520
2	0.111	0.154	1.380	0.091	0.109	0.610
3	0.081	0.114	1.120	0.086	0.108	0.530
4	0.069	0.096	1.190	0.091	0.125	0.730

Table 7.4: R_a, R_q, PTV from Experiment

tal data, empirical relations between various surface characterization parameters and various cutting parameters can be developed. The empirical formula relating R_a with crossfeed and downfeed is developed as follows. Let X_1 and X_2 represent the two varying experimental parameters, namely, crossfeed and downfeed respectively. The relationship between actual values of the two parameters and the variables X_1 and X_2 is given as:

$Crossfeed = 0.2032 \ \ mm \Longrightarrow X_1 = +1$

$Crossfeed = 0.1016 \ \ mm \Longrightarrow X_1 = -1$

$Downfeed = 0.1058 \ \ mm \Longrightarrow X_2 = +1$

$Downfeed = 0.0402\ \ mm \Longrightarrow X_2 = -1$

Therefore, the actual cutting conditions can be written in terms of the variables X_1 and X_2 as given in Table 7.5 (Refer to Tables 7.3 and 7.4 also). Let the

Test Number	X_1	X_2	$X_1 X_2$	R_a Crossfeed Direction μm
1	+1	+0.54878	+0.54878	0.164
2	+1	−0.80792	−0.80792	0.111
3	−1	+1	−1	0.081
4	−1	−1	1	0.069

Table 7.5: Actual Cutting Conditions in terms of X_1 and X_2

empirical formula for R_a be

$$R_a = a_0 + a_1 X_1 + a_2 X_2 + a_3 X_1 X_2 \tag{7.1}$$

where,

a_0 represents the grand average of R_a.

a_1 represents the main effect of crossfeed on R_a.

a_2 represents the main effect of downfeed on R_a.

a_3 represents the effect of interaction between crossfeed and downfeed on R_a.

Substituting the values of X_1, X_2 and R_a in Eqn. 7.1 for the aforementioned

four sets of cutting conditions, we get four equations in four unknowns. The unknowns are a_0, a_1, a_2 and a_3. The set of four equations can be written in the matrix form as

$$\vec{R}_a = \mathbf{X}\,\vec{a} \tag{7.2}$$

where,

$$\mathbf{X} = \begin{pmatrix} 1 & 1 & 0.54878 & 0.54878 \\ 1 & 1 & -0.80792 & -0.80792 \\ 1 & -1 & 1 & -1 \\ 1 & -1 & -1 & 1 \end{pmatrix} \tag{7.3}$$

$$\vec{a} = \begin{pmatrix} a_0 \\ a_1 \\ a_2 \\ a_3 \end{pmatrix} \tag{7.4}$$

$$\vec{R}_a = \begin{pmatrix} 0.164 \\ 0.111 \\ 0.081 \\ 0.069 \end{pmatrix} \tag{7.5}$$

Solving the matrix equation we get,

$$\vec{a} = \mathbf{X}^{-1}\,\vec{R}_a \tag{7.6}$$

$$\vec{a} = \begin{pmatrix} 0.1088 \\ 0.0388 \\ 0.0255 \\ 0.0165 \end{pmatrix} \tag{7.7}$$

Therefore, the empirical formula for R_a along the crossfeed direction is

$$R_a = 0.1088 + 0.0338\,X_1 + 0.0225\,X_2 + 0.0165\,X_1\,X_2 \tag{7.8}$$

Using the above empirical relation, R_a values for X_1 varying from -1 to 1 and X_2 varying from -1 to 1 can be determined.

The traces taken during the surface roughness measurements are presented in Fig. 7.5 . The three dimensional images of the actual ground surfaces and SEM pictures of the actual ground surfaces are shown in Fig. 7.6 . From the 3-D plots and SEM pictures of the actual ground surfaces similar observations can be made as made from the measured values of R_a, R_q and PTV. Surfaces ground at higher crossfeed (Test Numbers 1 and 2) have higher peaks than the surfaces ground at lower crossfeed (Test Numbers 3 and 4) as seen from the 3-D plots. From the SEM pictures of actual ground surfaces, it can be seen that the surfaces ground at lower crossfeed are smoother than the surfaces ground at higher crossfeed.

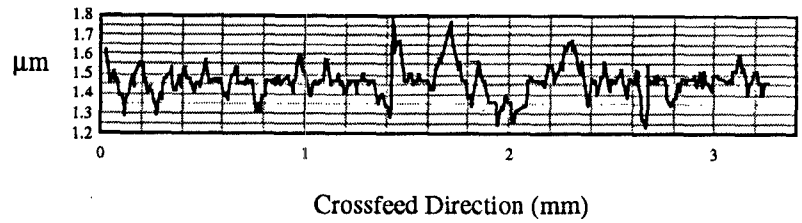

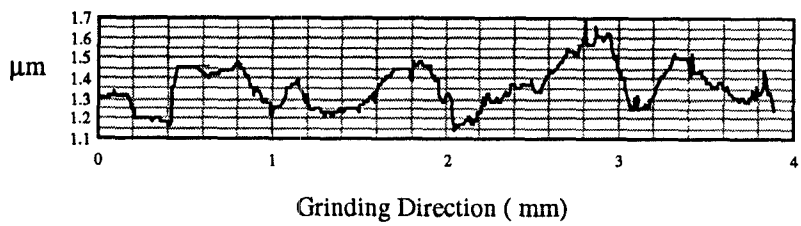

Figure 7.5 a: Test Number 1

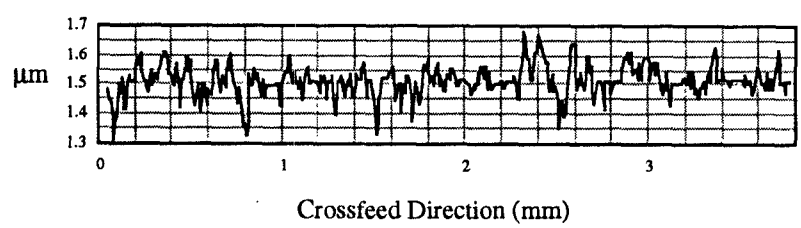

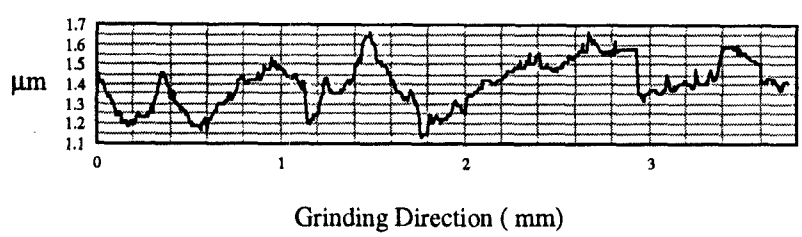

Figure 7.5 b: Test Number 2

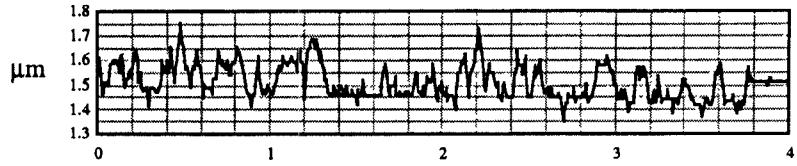

Crossfeed Direction (mm)

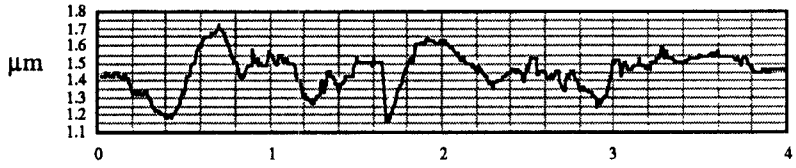

Grinding Direction (mm)

Figure 7.5 c: Test Number 3

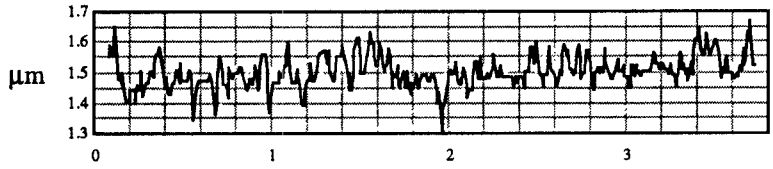

Crossfeed Direction (mm)

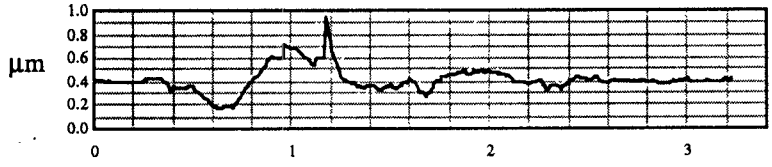

Grinding Direction (mm)

Figure 7.5 d: Test Number 4

Figure 7.5: Surface Profiles from Experiments

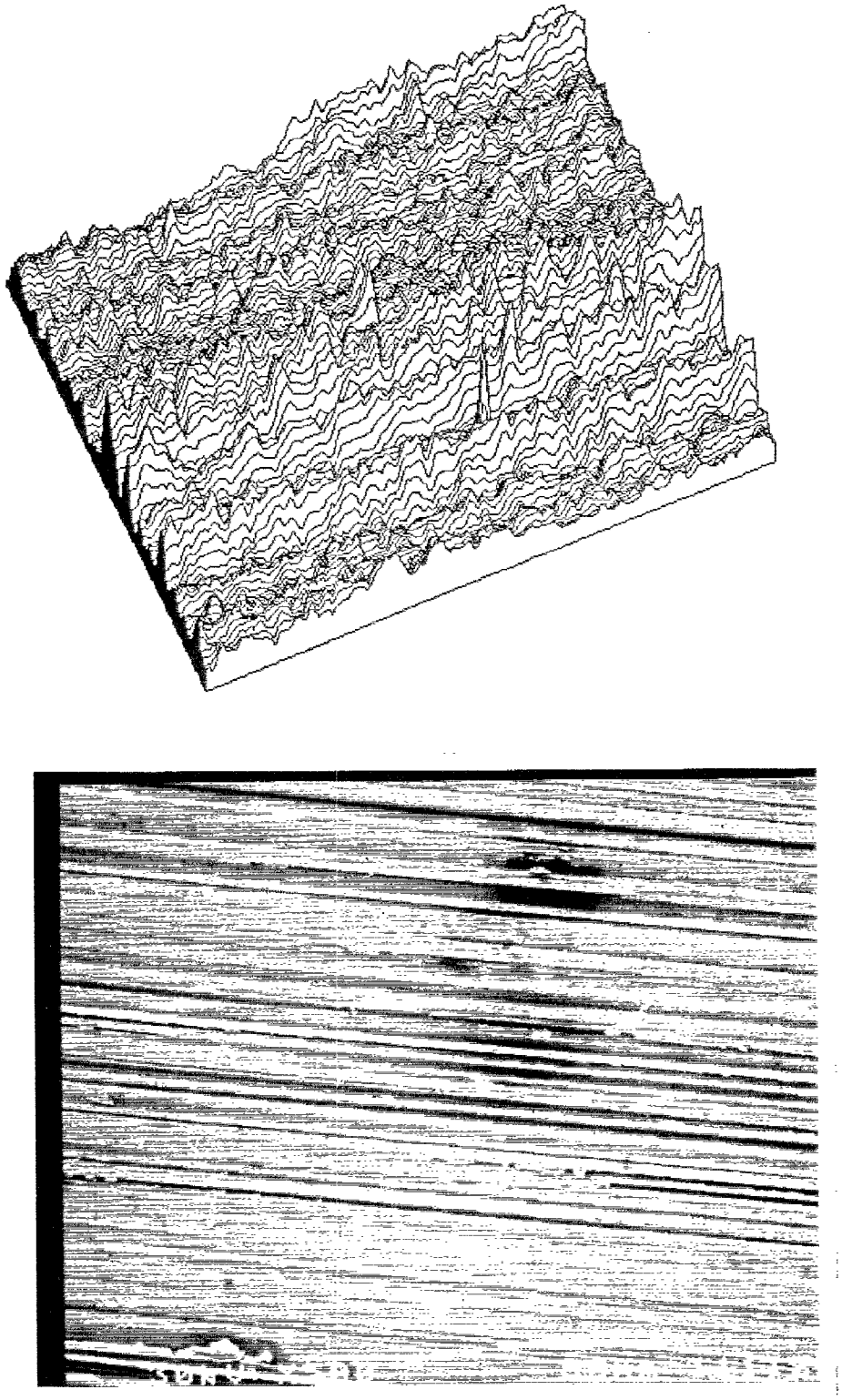

Figure 7.6 a: Test Number 1

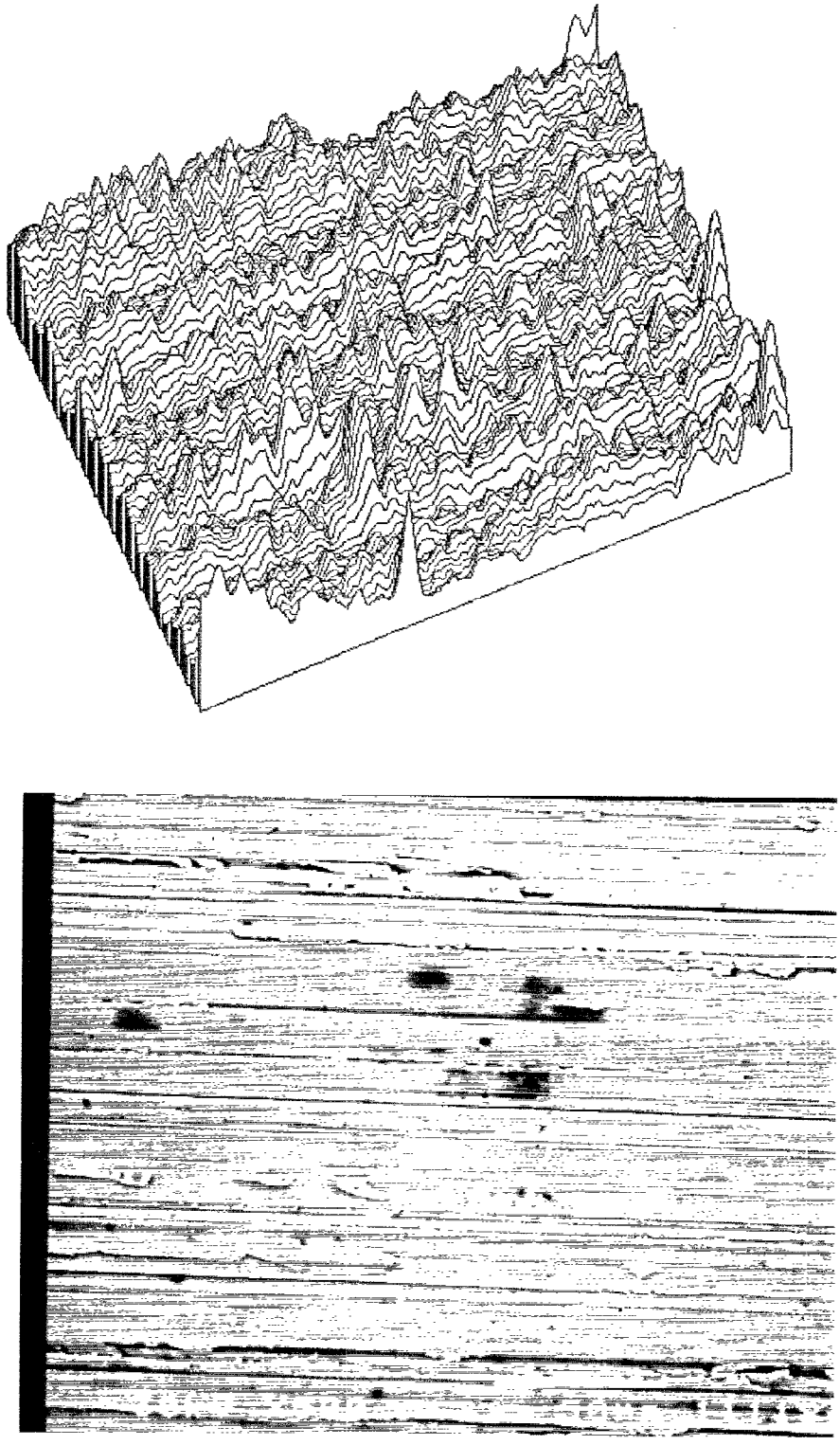

Figure 7.6 b: Test Number 2

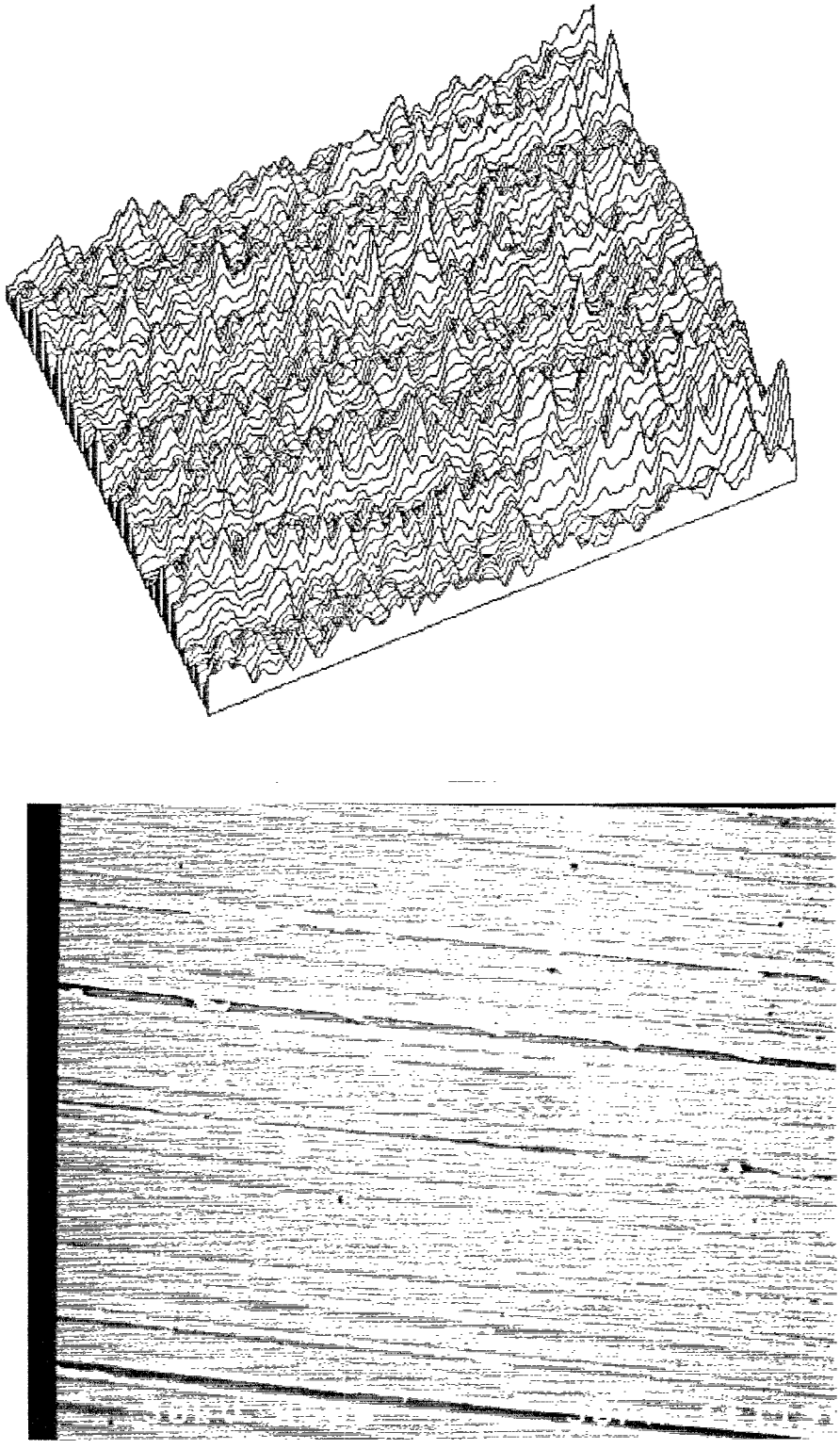

Figure 7.6 c: Test Number 3

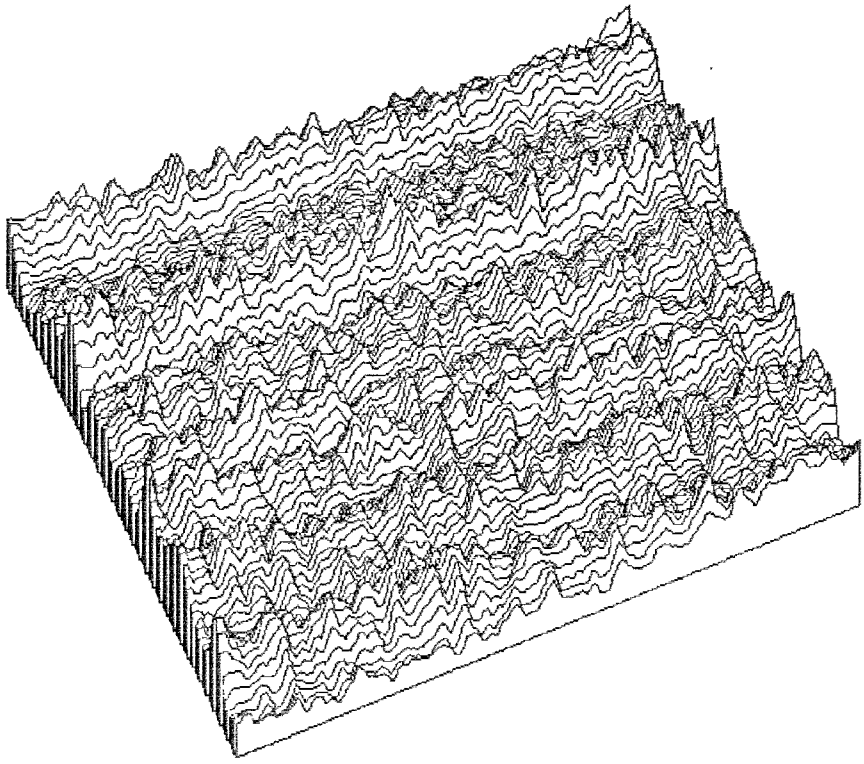

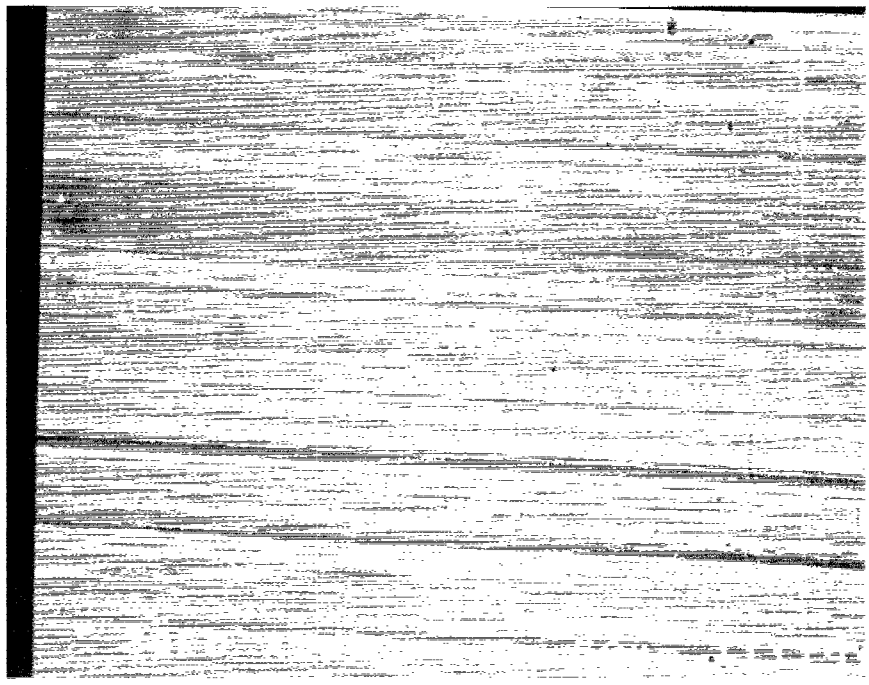

Figure 7.6 d: Test Number 4

Figure 7.6: 3-D Plots and SEM Pictures of Actual Ground Surfaces

7.2 Simulation Results

Using the simulation program developed as a part of this thesis work, the ideal ground surface topography is generated for the same four cutting conditions as used during the experiments. The important input parameters related to the abrasive grains and the grinding wheel used for performing the simulation are listed in Table 7.6 .

1. Nose radius for type 2 grit	: 0.005	mm
2. Standard deviation for grit height distribution	: 0.0001	mm
3. Standard deviation for grit diameter distribution	: 0.0001	mm
4. Standard deviation for angular spacing distribution	: 2^o	
5. Mean for distribution for number of grits on each slice	: 10	
6. Std. dev. for distribution for number of grits on each slice	: 1	

Table 7.6: Important Inputs Related to Abrasive Grains

The mean values of R_a, R_q and PTV and their standard deviations along the crossfeed and grinding directions for ideal ground surfaces obtained from simulation are listed in Tables 7.7 and 7.8 . The mean values of surface characterization parameters along the crossfeed direction is greater than that along the grinding direction for a particular set of cutting conditions. The values of R_a, R_q and PTV are maximum for the surface ground at higher crossfeed with larger downfeed and are minimum for the surface ground at lower crossfeed with smaller

downfeed. Similar observations are also made from the experimental data. In Table 7.9, the values of R_a, R_q and PTV for ideal ground surfaces ground at four different sets of cutting conditions are presented for the overall simulated area. These numbers can be used to compare the quality of the surfaces ground at different cutting conditions. Based on the simulation results, the empirical formula relating R_a with crossfeed and downfeed can be developed following the same procedure as used in Section 7.1.2 . To develop such an empirical formula, R_a values for the overall simulated area are used. Solving the matrix equation (Eqn. 7.2) where the matrix $\mathbf{X}$ and $\vec{a}$ are the same as before and $\vec{R_a} = \begin{pmatrix} 0.072 \\ 0.067 \\ 0.055 \\ 0.054 \end{pmatrix}$ (Refer to Table 7.9) we get,

$$\vec{a} = \begin{pmatrix} 0.0622 \\ 0.0077 \\ 0.0021 \\ 0.0016 \end{pmatrix} \tag{7.9}$$

Therefore, the empirical formula for R_a for ideal ground surface topography is

$$R_a = 0.0622 + 0.0077\,X_1 + 0.0021\,X_2 + 0.0016\,X_1\,X_2 \tag{7.10}$$

The surface profiles obtained from simulation in the case of ideal ground surfaces are illustrated in Fig 7.7 . The 3-D plots of ideal ground surfaces are illustrated in Fig. 7.8 .

Test Number	R_a		R_q		PTV	
	μ_{R_a} μm	σ_{R_a} μm	μ_{R_q} μm	σ_{R_q} μm	μ_{PTV} μm	σ_{PTV} μm
1	0.072	0.021	0.097	0.040	0.539	0.283
2	0.067	0.009	0.085	0.012	0.431	0.081
3	0.055	0.007	0.070	0.009	0.353	0.065
4	0.054	0.006	0.069	0.008	0.350	0.052

Table 7.7: R_a, R_q, PTV for Ideal Ground Surfaces (Crossfeed Direction)

Test Number	R_a		R_q		PTV	
	μ_{R_a} μm	σ_{R_a} μm	μ_{R_q} μm	σ_{R_q} μm	μ_{PTV} μm	σ_{PTV} μm
1	0.071	0.025	0.094	0.040	0.527	0.322
2	0.066	0.010	0.084	0.012	0.430	0.085
3	0.053	0.011	0.067	0.013	0.300	0.075
4	0.053	0.010	0.066	0.013	0.297	0.067

Table 7.8: R_a, R_q, PTV for Ideal Ground Surfaces.(Grinding Direction)

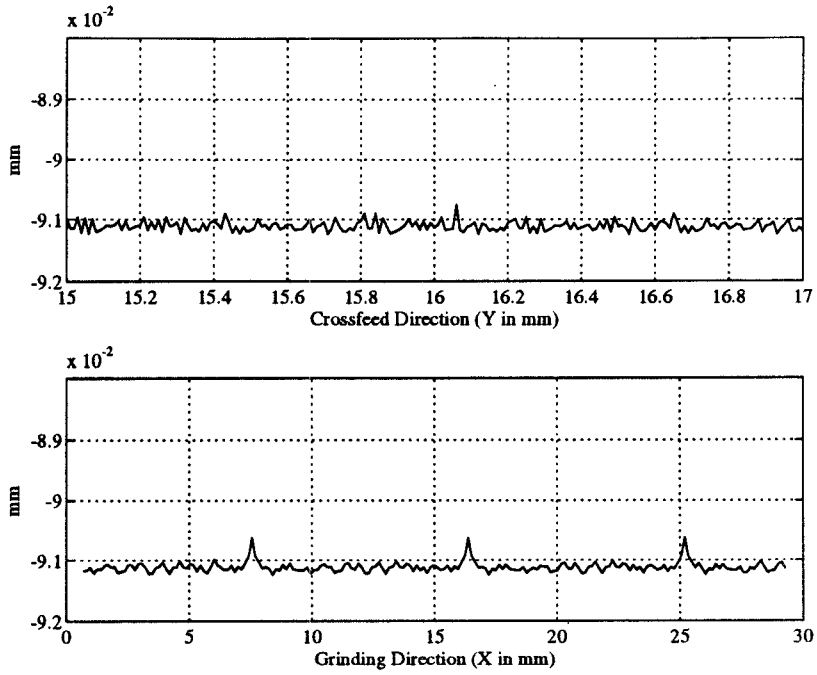

Figure 7.7 a: Test Number 1

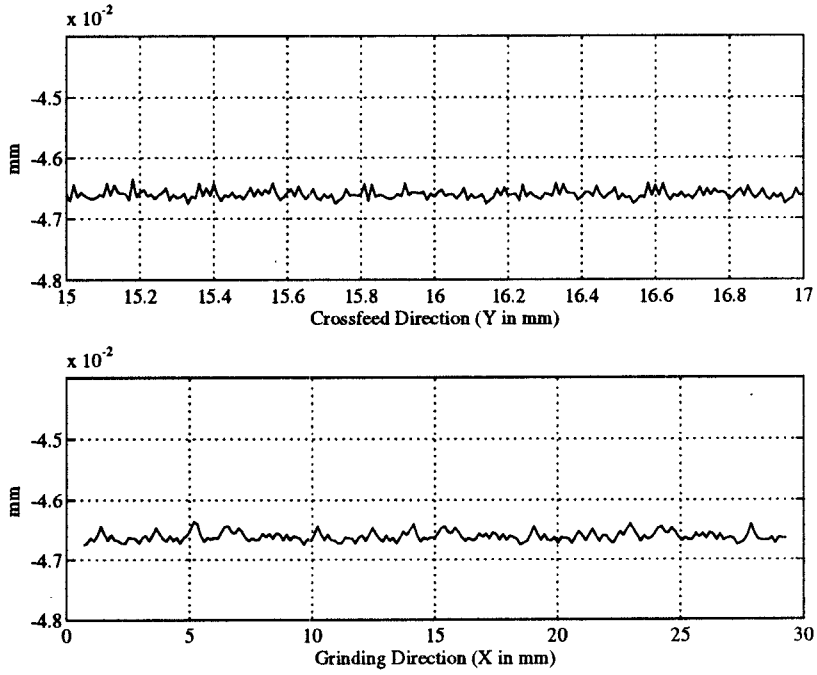

Figure 7.7 b: Test Number 2

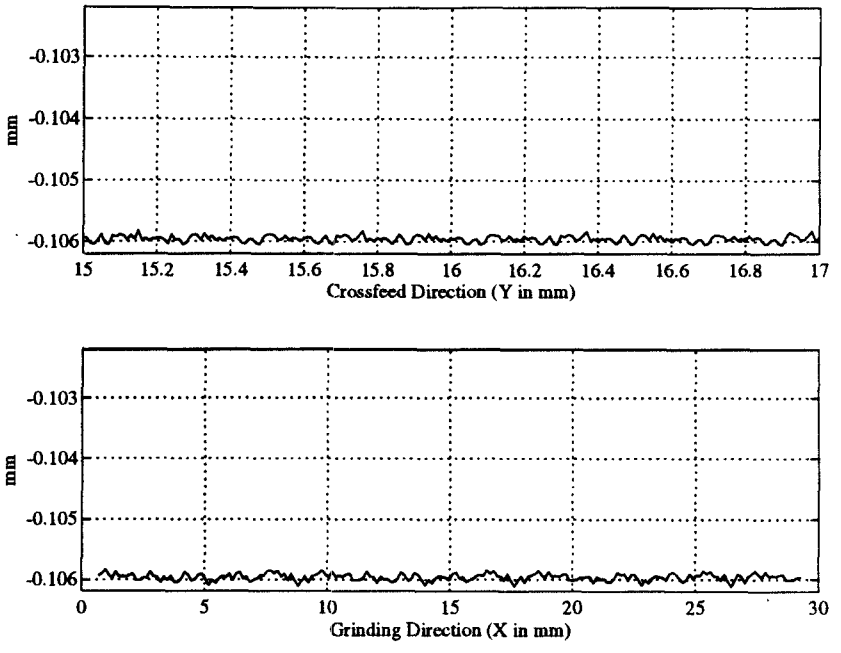

Figure 7.7 c: Test Number 3

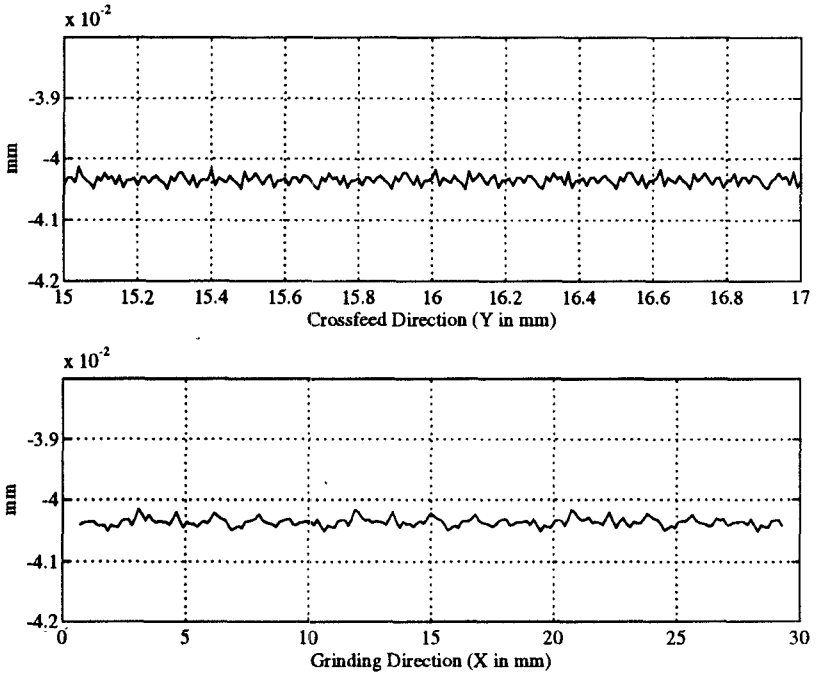

Figure 7.7 d: Test Number 4

Figure 7.7: Surface profiles in case of Ideal Ground Surfaces

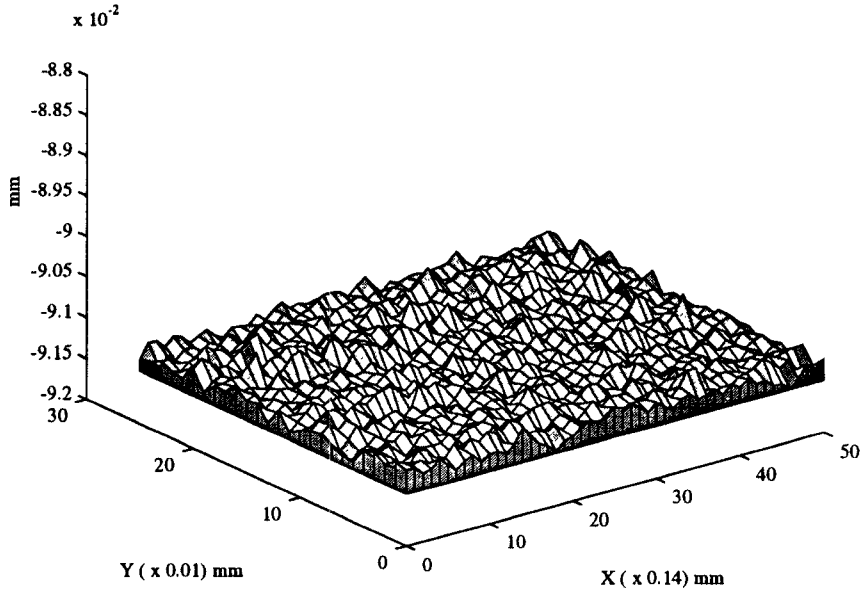

Figure 7.8 a: Test Number 1

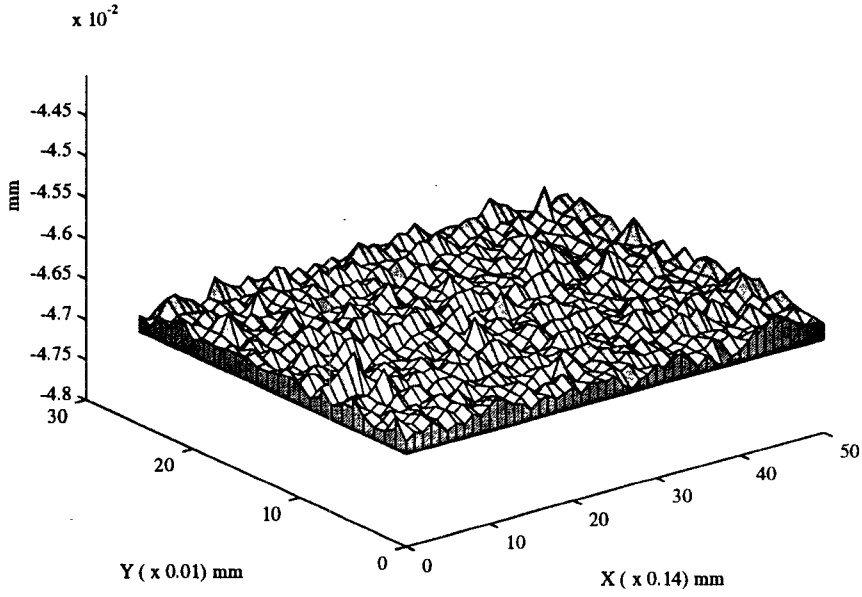

Figure 7.8 b: Test Number 2

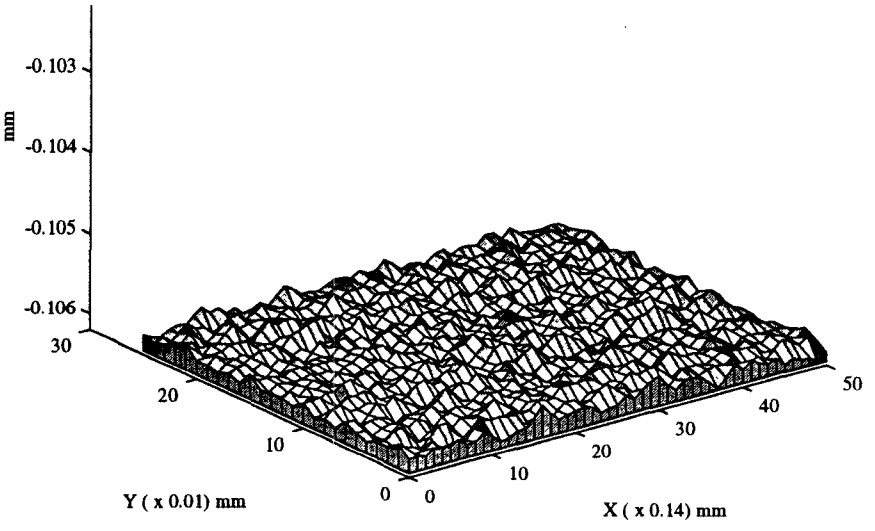

Figure 7.8 c: Test Number 3

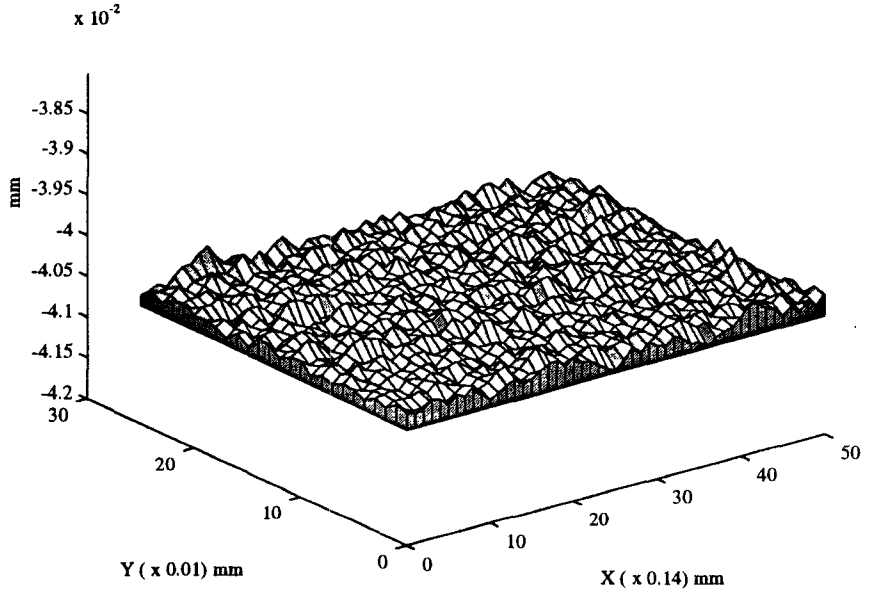

Figure 7.8 d: Test Number 4

Figure 7.8: 3-D Plots of Ideal Ground Surfaces

Test Number	R_a μm	R_q μm	PTV μm
1	0.072	0.106	1.921
2	0.067	0.087	0.731
3	0.055	0.071	0.571
4	0.054	0.070	0.535

Table 7.9: Overall R_a, R_q, PTV for Ideal Ground Surfaces

Further, the simulation is performed to consider the effect of machine tool chatter on the ground surface topography. The important input parameters related to the machine tool structure (Refer Chapter 5) used for performing the dynamical analysis are listed in Table 7.10 [16] . The unit cutting force for a

1. Equivalent mass of the grinding wheel,	m	: 2	kg
2. Stiffness along the first principal mode,	k_1	: 10^9	N/m
3. Stiffness along the second principal mode,	k_2	: 8×10^8	N/m
4. Damping factor along the first principal mode,	c_1	: 8894	N-s/m
4. Damping factor along the second principal mode,	c_2	: 8894	N-s/m
5. Angle between first principal mode and vertical axis,	δ	: 40^o	

Table 7.10: Important Inputs Related to the Machine Tool Structure

workpiece made of steel, k_s is 2482 N/sq. mm [17]. The results of the dynamical

analysis are shown in Fig. 7.9 . In this figure, variation of F_x, F_z, $\tilde{x}_c$ and $\tilde{z}_c$ (Refer Chapter 5) are shown for each of the four cutting conditions. The mean and standard deviation of F_x, F_z, $\tilde{x}_c$ and $\tilde{z}_c$ for the four sets of cutting conditions are listed in Tables 7.11 and 7.12 . The magnitude of the mean values of F_x, F_z, $\tilde{x}_c$ and $\tilde{z}_c$ increases with the downfeed. Also, it can be observed that ratio of F_z to F_x is 4.3 for all four grinding conditions.

The mean values of R_a, R_q and PTV and their standard deviations along the crossfeed and grinding directions for ground surfaces in the presence of machine tool chatter obtained from simulation are listed in Tables 7.13 and 7.14 . The mean values of surface characterization parameters along the crossfeed direction is greater than that along the grinding direction for a particular set of cutting conditions in presence of the machine tool chatter too. The surface quality of the surface ground at lower crossfeed with smaller downfeed is the best. The mean values of R_a, R_q and PTV from simulation show similar trend as shown by the measured values of R_a, R_q and PTV. In Table 7.15, the values of R_a, R_q and PTV for ground surfaces in the presence of chatter are presented for the overall simulated area. These numbers can also be used to compare the quality of the surfaces ground at different cutting conditions. Following the same procedure as used before, an empirical formula for R_a can be developed. The empirical formula for R_a in the presence of chatter based on the overall simulated area is

$$R_a = 0.3050 - 0.0205\,X_1 + 0.2259\,X_2 - 0.0136\,X_1\,X_2 \qquad (7.11)$$

The surface profiles obtained from simulation of ground surfaces in the presence

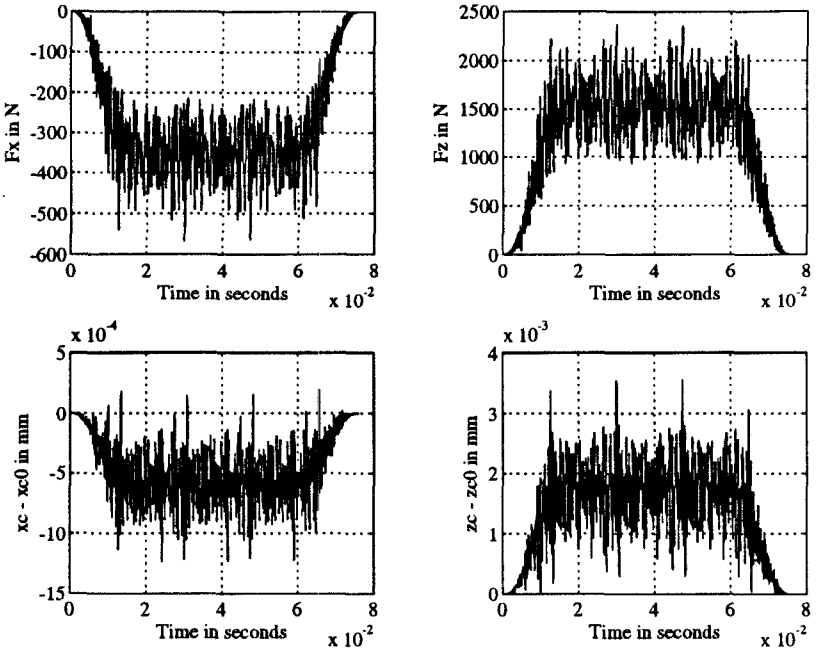

Figure 7.9 a: Test Number 1

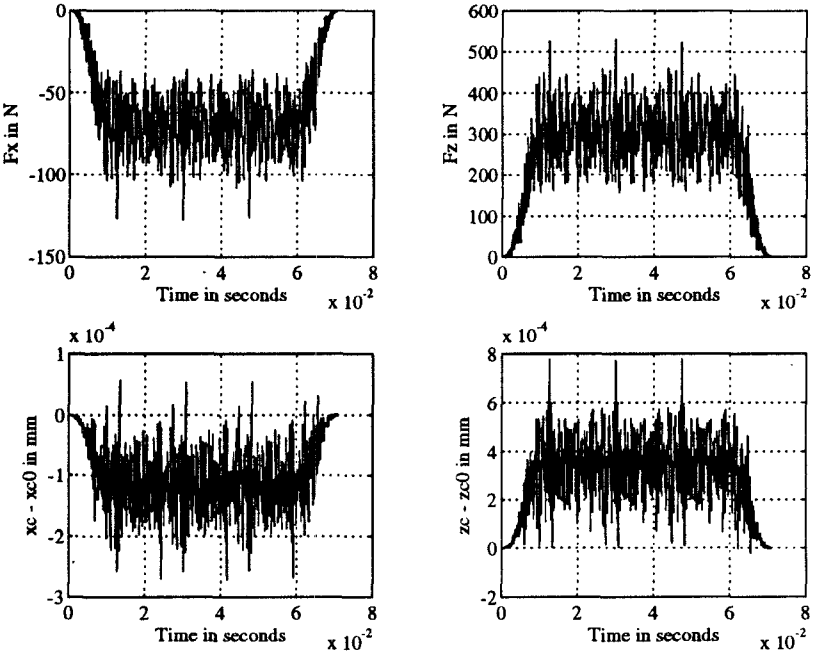

Figure 7.9 b: Test Number 2

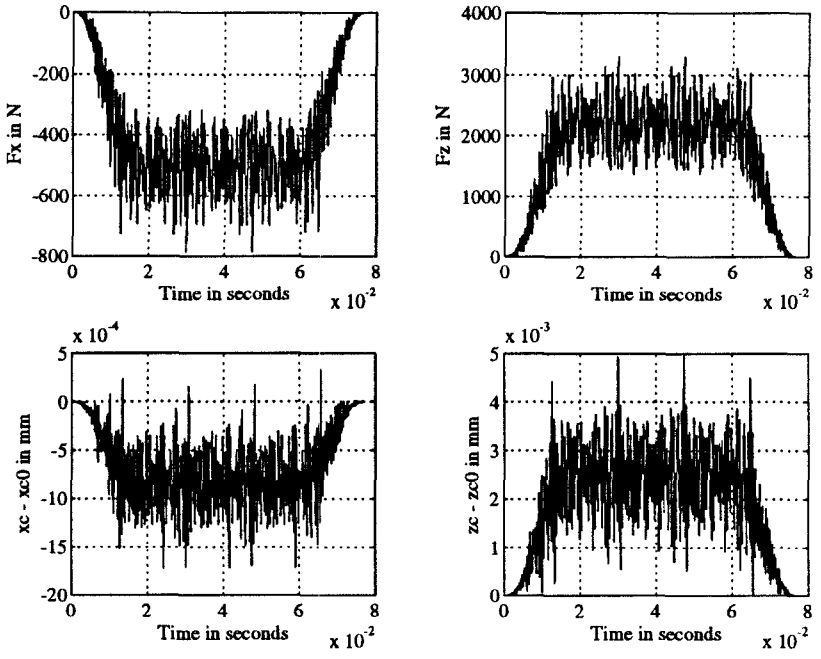

Figure 7.9 c: Test Number 3

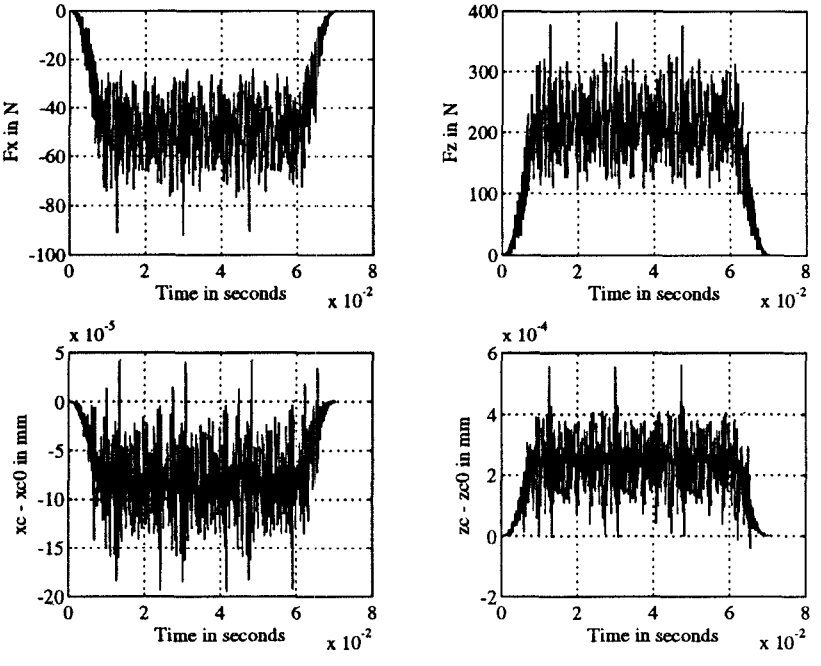

Figure 7.9 d: Test Number 4

Figure 7.9: Plots of F_x, F_z, $\tilde{x}_c$ and $\tilde{z}_c$ vs. Time

Test Number	F_x		F_z	
	μ_{F_x} N	σ_{F_x} N	μ_{F_z} N	σ_{F_z} N
1	-276.10	136.46	1189.1	585.70
2	-58.449	26.291	250.54	112.15
3	-389.30	196.70	1678.2	845.10
4	-41.704	18.359	178.50	78.170

Table 7.11: F_x and F_z from Dynamical Analysis

Test Number	$\tilde{x}_c$		$\tilde{z}_c$	
	$\mu_{\tilde{x}_c}$ μm	$\sigma_{\tilde{x}_c}$ μm	$\mu_{\tilde{z}_c}$ μm	$\sigma_{\tilde{z}_c}$ μm
1	-0.4629	0.2764	1.3000	0.7409
2	-0.0978	0.0576	0.2830	0.1490
3	-0.6540	0.3900	1.8990	1.0550
4	-0.0697	0.0488	0.2021	0.1053

Table 7.12: $\tilde{x}_c$ and $\tilde{z}_c$ from Dynamical Analysis

Test Number	R_a		R_q		PTV	
	μ_{R_a} μm	σ_{R_a} μm	μ_{R_q} μm	σ_{R_q} μm	μ_{PTV} μm	σ_{PTV} μm
1	0.395	0.038	0.482	0.050	2.359	0.376
2	0.111	0.012	0.138	0.016	0.698	0.117
3	0.557	0.054	0.680	0.071	3.347	0.453
4	0.085	0.008	0.106	0.011	0.532	0.083

Table 7.13: R_a, R_q, PTV in Presence of Chatter (Crossfeed Direction)

Test Number	R_a		R_q		PTV	
	μ_{R_a} μm	σ_{R_a} μm	μ_{R_q} μm	σ_{R_q} μm	μ_{PTV} μm	σ_{PTV} μm
1	0.376	0.076	0.458	0.088	1.964	0.488
2	0.109	0.017	0.135	0.021	0.636	0.129
3	0.499	0.141	0.608	0.162	2.402	0.597
4	0.084	0.016	0.104	0.019	0.444	0.095

Table 7.14: R_a, R_q, PTV in Presence of Chatter (Grinding Direction)

Test Number	R_a μm	R_q μm	PTV μm
1	0.401	0.491	5.053
2	0.113	0.141	1.177
3	0.565	0.693	5.048
4	0.086	0.108	0.869

Table 7.15: Overall R_a, R_q, PTV in Presence of Chatter

of machine tool chatter are illustrated in Fig 7.10 . The 3-D plots of ground surfaces in the presence of machine tool chatter are illustrated in Fig. 7.11 .

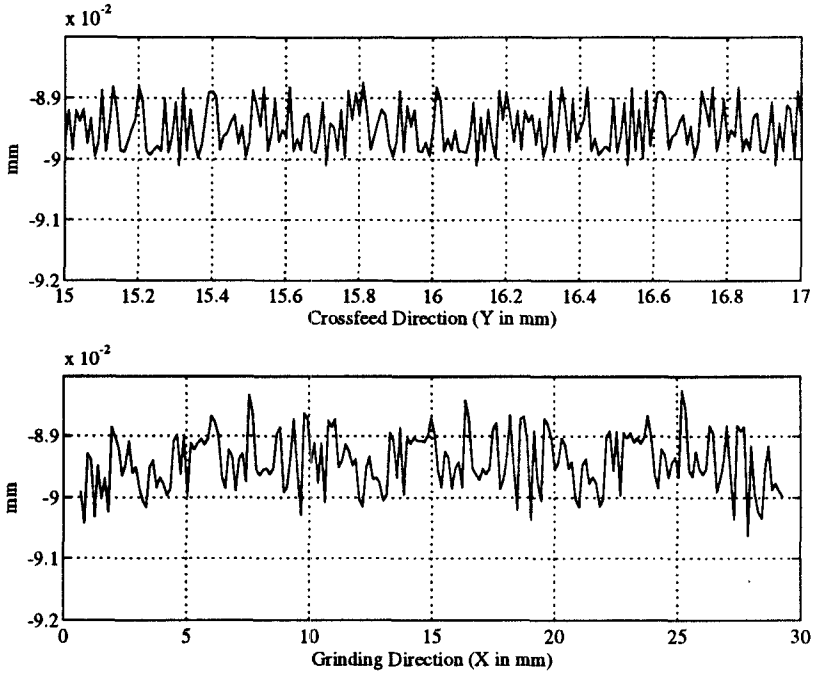

Figure 7.10 a: Test Number 1

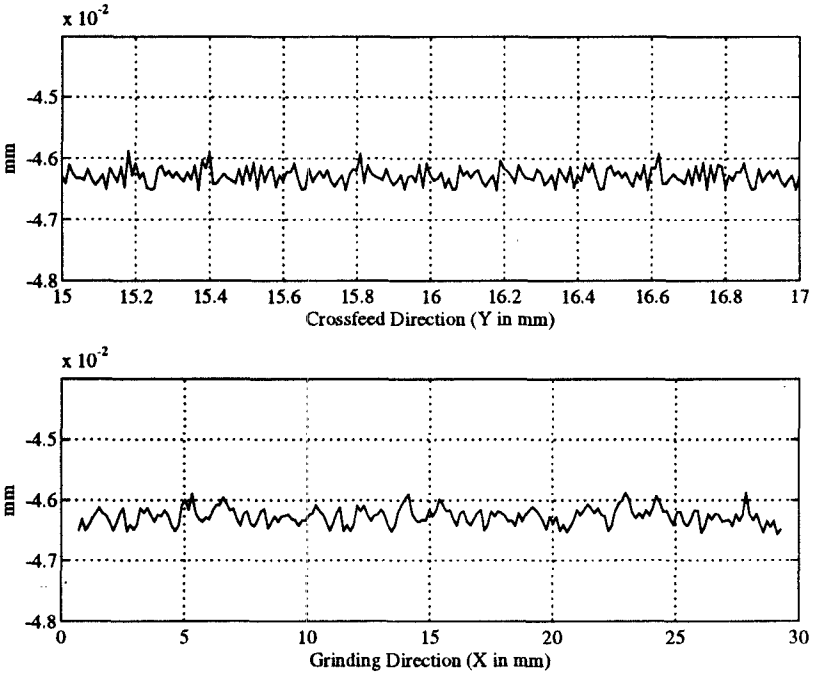

Figure 7.10 b: Test Number 2

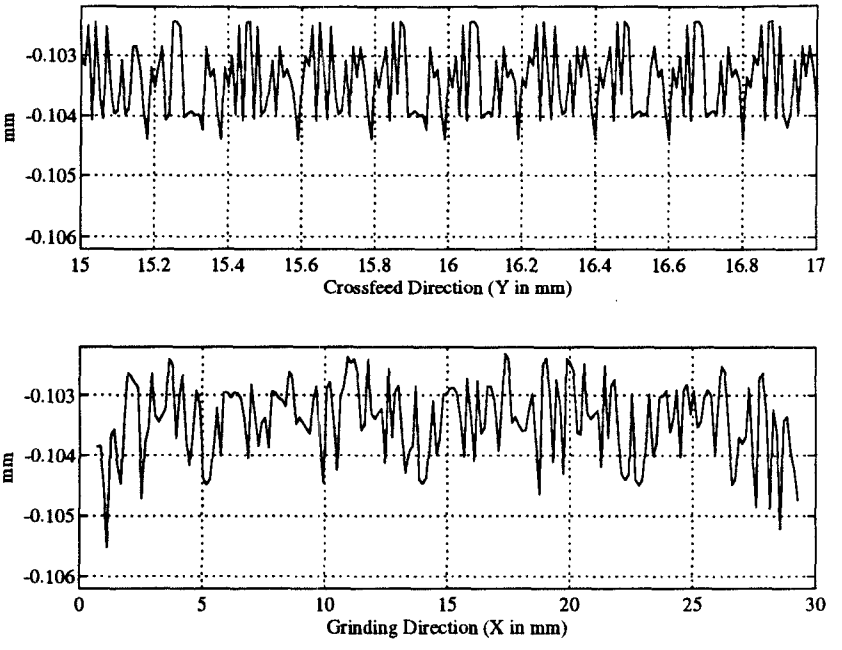

Figure 7.10 c: Test Number 3

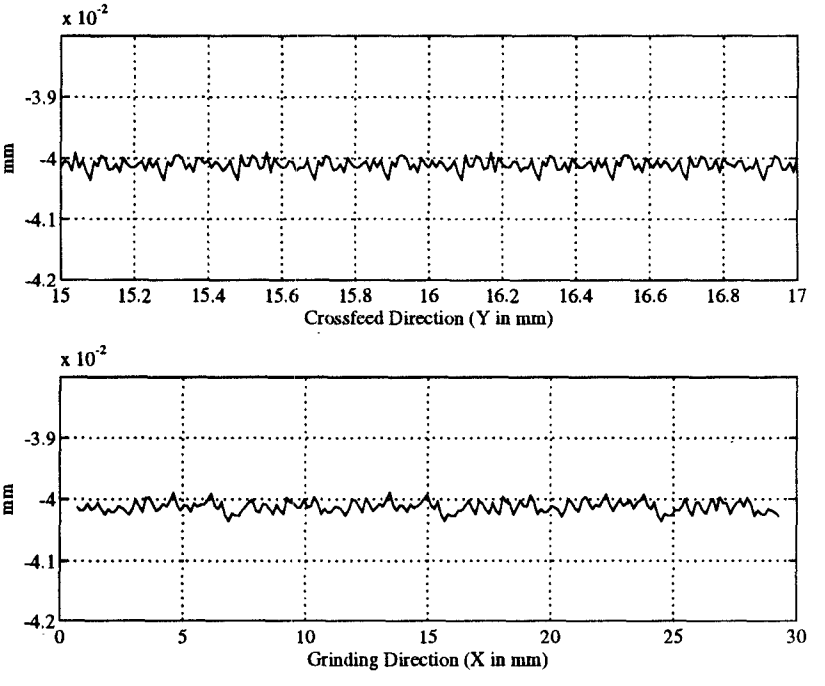

Figure 7.10 d: Test Number 4

Figure 7.10: Surface profiles of Ground Surfaces in Presence of Chatter

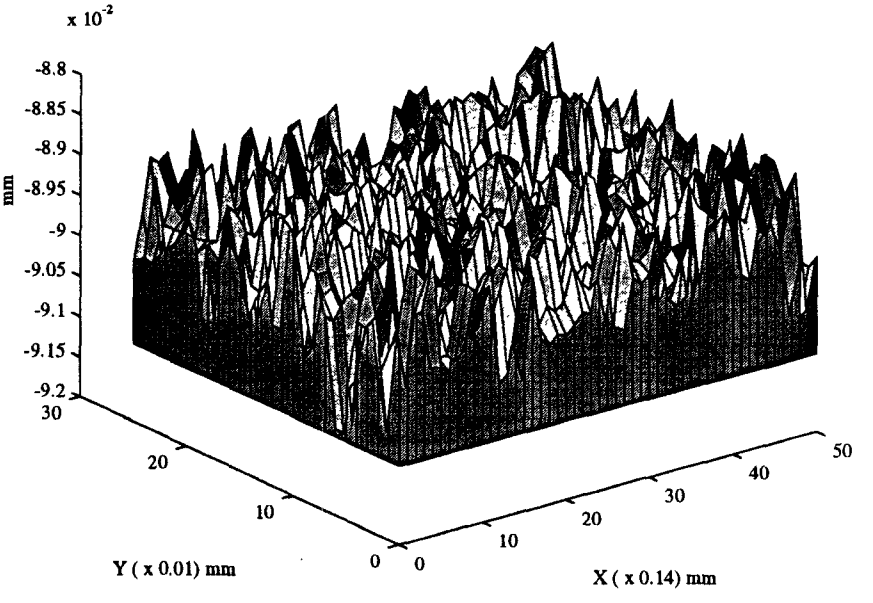

Figure 7.11 a: Test Number 1

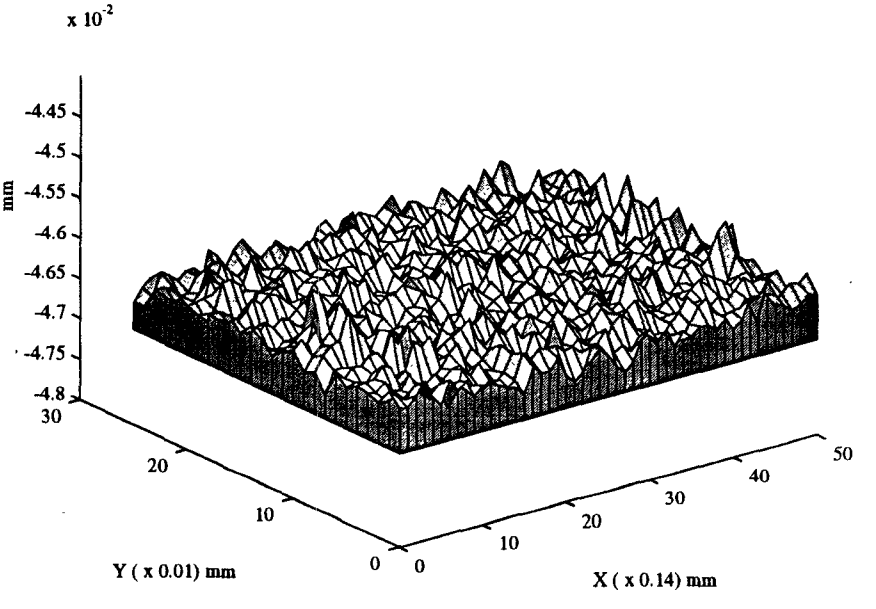

Figure 7.11 b: Test Number 2

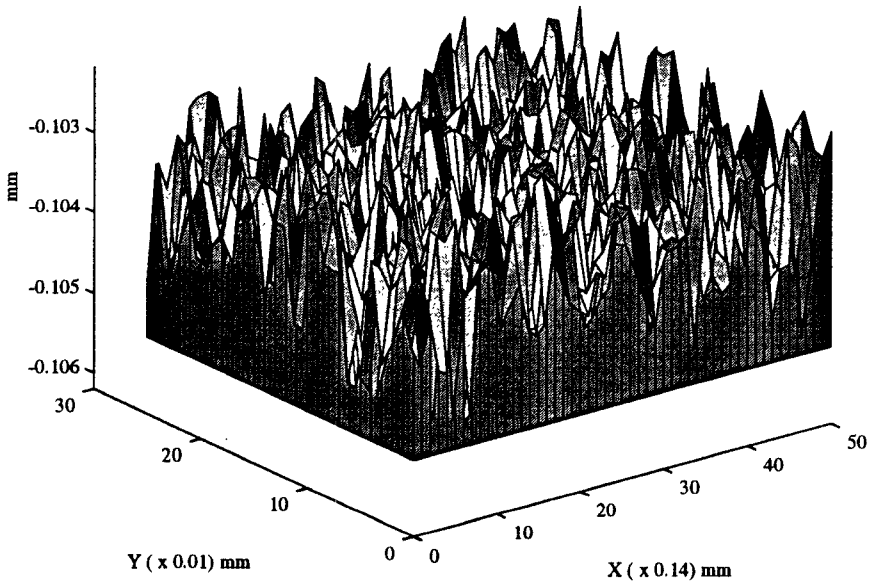

Figure 7.11 c: Test Number 3

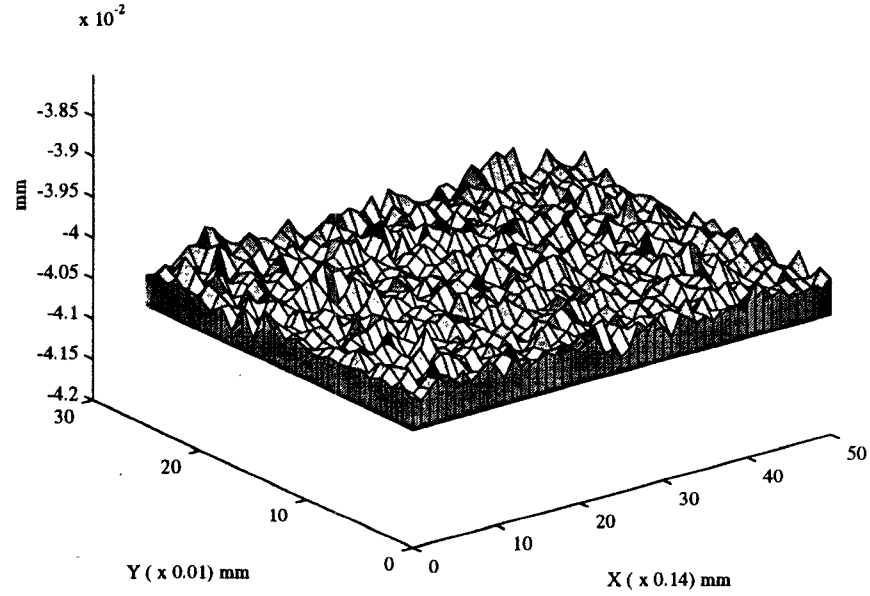

Figure 7.11 d: Test Number 4

Figure 7.11: 3-D Plots of Ground Surfaces in Presence of Chatter

Chapter 8

Conclusions and Recommendations

The main conclusions from the present study are summarized in this chapter. A few recommendations for the future work are also listed.

8.1 Conclusions

Conclusions of this thesis work are listed below:

1. In this thesis work a statistical model of the grinding wheel is developed taking into account the random variations in the grit size and the grit location. Two basic shapes of the grit are assumed, namely, cone shaped grit with a sharp tip called type 1 grit and another with a rounded tip called type 2 grit. To generate the random distribution of the grits on the

grinding wheel surface, the following assumptions are made.

- The grinding wheel is divided into thin slices along the axial direction.
- The number of grits on the slices is assumed to be normally distributed.
- The angular spacing between two consecutive grits along the circumference of a slice is assumed to be normally distributed.

To determine the randomly varying grit size, the following two assumptions are made.

- The grit diameter is assumed to be normally distributed.
- The grit height is assumed to be normally distributed.

A single grit forms a cavity on the workpiece due to the kinematic interaction between the grit and the workpiece during the grinding process. An analytical representation for the cavities formed by the different grits on the workpiece is developed. This analytical representation is in the form of a cubic equation which is solved numerically using Newton-Raphson Method. One of the three possible solutions of the cubic equation is finally used to generate the ideal ground surface topography. This work focuses on the surface grinding process. In such a grinding process, the table reverses its direction of motion during the course of the grinding process. The reversing of the table motion is taken into consideration in the generation of the ideal ground surface topography.

2. A grinding force model is formulated in this thesis work. The cone shaped grits are divided into triangular elements. The cutting action of the each of the triangular elements is treated as the cutting action of a single-point tool. A rake angle is defined for the assumed cone shaped grits. The rake angle of a triangular element of a type 1 grit is constant for the element. But, the rake angle of a triangular element of a type 2 grit varies along the rounded tip of the element. This variation of the rake angle for the type 2 grit is taken into account by introducing an effective rake angle which is defined as the average rake angle. The grinding forces F_x and F_z for a single grit are determined by integrating the grinding forces F_x and F_z for the triangular elements of the grit numerically using Simpson's Rule. The grinding forces F_x and F_z due to individual grits which are in contact with the workpiece at a particular instant are summed up to calculate the total grinding forces F_x and F_z at that instant. Thus, the total grinding forces F_x and F_z are calculated based on the exact number of abrasive grains in contact with workpiece at a particular instant of time. The variation in rake angle within a grit is taken into consideration in this model. Also, the variation in rake angle among the grits is taken into consideration in the grinding force model.

3. Machine tool chatter adversely affects the ground surface topography. The effect of grinding wheel vibration on the ground surface topography is considered in this work. For this purpose a mathematical model representing

the grinding system is developed. Only the dynamics of the grinding wheel motion is considered because the workpiece is usually rigidly held on the machine tool table during the surface grinding process. The grinding wheel is treated as a discrete lumped parameter system with a two degrees of freedom system, each of which shows second order dynamics. The total forces along the two principal modes are functions of the vertical coordinate of the center of the grinding wheel. The dynamical equations are solved numerically using fourth order Runga-Kutta Method to get the dynamic variation of the location of the center of the grinding wheel. The dynamic variation of the location of the center of the grinding wheel is then superimposed on the ideal ground surface topography to generate ground surface topography in the presence of chatter.

4. Experimental and simulation results show similar trends for surfaces ground at different sets of cutting conditions. It is observed from experimental and simulation results that the quality of the surface ground at higher crossfeed with larger downfeed is the worst and that of the surface ground at lower crossfeed with smaller downfeed is the best. Based on the empirical models relating R_a with crossfeed and downfeed, it can be concluded that the effect of crossfeed on the surface quality of the ground component is more than that of downfeed. Also, based on the grinding force model, it can be concluded that ratio of two forces F_z and F_x is constant for all four grinding conditions. With the help of the simualtion package, the quality of

the surfaces ground at different sets of the cutting conditions are compared qualitatively and quantitatively.

8.2 Recommendations

Based on the present study, the following two recommendations are made for future work in this area.

1. The grinding process requires an extremely high input of energy per unit volume of the material removed. Major part of this energy is converted to heat which is concentrated within the grinding region. The excessive high temperature near the grinding region introduces various kinds of thermal damages to the workpiece surface, namely, burning of the workpiece, tempering of the finished surface, residual stresses in the neighbourhood of the finished surface, thermal expansion of the workpiece etc. Thus, excessive grinding temperature does adversely affect the ground surface topography. Understanding the effects of thermal damages on the ground surface requires a great deal of study and experimentation. The effect of thermal damages should be modeled and included in the simulation program.

2. Other than thermal damages occurring due to excessive grinding temperature, grinding wheel wear is another important phenomenon which deserves a thorough investigation. Grinding wheel wear is a complex process. Researchers have been studying the wheel wear mechanism and have iden-

tified the prevailing wear mechanisms and the influence of various factors, including the abrasives, workpiece and the grinding fluids. Further study is necessary to develop a comprehensive model representing the grinding wheel wear mechanism so that it can be implemented in the simulation package.

Appendix A

User Manual

1. Type *grinding* in a Xterm Window.

2. Choose one of the five options echoed on the screen. Options are self explanatory. The options are
   1. Ideal Surface Topography Generation
   2. Surface Topography Generation in Presence of Chatter
   3. Results of Dynamical Analysis
   4. Surface Quality Analysis
   5. Quit

3. If option 1 or option 2 is selected, the user is required to enter a set of inputs as asked by the computer.

4. Option 1 generates wheel topography and ideal ground surface topography for given set of inputs.

5. Option 2 performs dynamical analysis of the grinding system and results of the dynamical analysis are superimposed on the ideal ground surface to get ground surface topography in the presence of machine tool chatter.

6. Option 3 plots the results of the the dynamical analysis, namely, grinding forces and grinding wheel displacement in Matlab.

7. Option 4 plots surface profiles and 3-D plots of the ground surfaces in Matlab. Surface characterization parameters like R_a, R_q and PTV can also be determined here.

8. Option 2 can be chosen only if option 1 is chosen earlier.

9. Option 3 can be chosen only if option 2 is chosen earlier.

10. Option 4 can be chosen only if either option 1 or option 2 is chosen earlier.

11. When an option is selected by the user, a lot of information is echoed on the screen. It tells the user what the particular option does and what the user is supposed to do next.

Bibliography

[1] Baul, R.M. and Shilton, R., "Mechanics of Metal Grinding with Particular Reference to Monte Carlo Simulation", *Proceedings of the Eight International Machine Tool Design and Research Conference*, 1967, pp. 923.

[2] Yoshikawa, H. and Sata, T., "Simulated Grinding Process by Monte Carlo Method", *Annals of the CIRP*, Vol. 16, 1968, pp. 297.

[3] McAdams, H.T., "Markov Chain Models of Grinding Profiles", *Trans. ASME, J. of Eng. for Ind.*, Vol. 86, 1964, pp. 383.

[4] Law, S.S, Wu, S.M. and Jogelkar, A.M., "On Building Models for the Grinding Process", *Trans. ASME, J. of Eng. for Ind.*, Vol. 95, 1973, pp. 983.

[5] Law, S.S. and Wu, S.M., "Simulation Study of the Grinding Process", *Trans. ASME, J. of Eng. for Ind.*, Vol. 95, 1973, pp. 972.

[6] Hahn, R.S., "On the Theory of Regenerative Chatter in Precision Grinding Operations", *Trans ASME*, Vol. 76, No. 1, 1954, pp. 593.

[7] Bartalucci, B. and Lisni, G.G., "Grinding Process Instability", *Trans. ASME, J. of Eng. for Ind.*, Vol. 91, No. 3, 1969, pp. 597.

[8] Thompson, R.A., "On the Doubly Regenerative Stability of a Grinder", *Trans. ASME, J. of Eng. for Ind.*, Vol. 96, No. 1, 1974, pp. 275.

[9] Thompson, R.A., "The Dynamic Behaviour of Surface Grinding, Part 1 - A Mathematical Treatment of Surafce Grinding", *Trans. ASME, J. of Eng. for Ind.*, Vol. 93, No. 2, 1971, pp. 485.

[10] Backer, W.R. and Merchant, M.E., "On the Basic Mechanics of the Grinding Process", *Trans. ASME*, Vol. 80, 1958, pp. 141.

[11] Marshall, E.R. and Shaw, M.C., "Forces in Dry Surface Grinding", *Trans. ASME*, Vol. 74, 1952, pp. 51.

[12] Nakayama, K. and Shaw,M.C., "Study of the Finish Produced in Surface Grinding, Part 2 - Analytical", *Proc. Inst. Mech. Engrs*, Vol. 182, 1966, pp. 179.

[13] Merritt, H. E., "Theory of Self-Excited Machine Tool Chatter", *Trans. ASME*, Vol. 87, 1965, pp. 447.

[14] Zhang, L., Suto, T., Noguchi, H. and Waida, T., "An Overview of Applied Mechanics in Grinding", *Manufacturing Review*, Vol. 5, No. 4, 1992, pp. 261.

[15] Bhateja, C. P., "An Enveloping Profile Approach for the Generation of Ground Surface Texture", *Annals of the CIRP*, Vol. 25, No. 1, 1977, pp. 333.

[16] Zhang, G.M., "Dynamic Modeling and Dynamic Analysis of the Boring Machining System", Ph. D. Dissertation, University of Illinois at Urbana-Champaign, 1986.

[17] Kronenberg, M., *Machining Science and Application*, Pergamon Press, London, 1966.

[18] Malkin, S., *Grinding Technology*, Ellis Horwood Limited, West Sussex, England, 1989.

[19] Lewis, Kenneth B., *The Grinding Wheel - A Textbook for Modern Grinding Practice*, The Grinding Wheel Institute, Cleveland, Ohio, 1959.

[20] Bhattacharyya, Amitabha , *Metal Cutting - Theory and Practice*, Central Book Publishers, Calcutta, India, 1984.